National Library of Canada
Bibliothèque nationale du Canada

Canadian Theses Service
Service des thèses canadiennes

Ottawa, Canada
K1A 0N4

NOTICE

The quality of this microform is heavily dependent upon the quality of the original thesis submitted for microfilming. Every effort has been made to ensure the highest quality of reproduction possible.

If pages are missing, contact the university which granted the degree.

Some pages may have indistinct print especially if the original pages were typed with a poor typewriter ribbon or if the university sent us an inferior photocopy.

Previously copyrighted materials (journal articles, published tests, etc.) are not filmed.

Reproduction in full or in part of this microform is governed by the Canadian Copyright Act, R.S.C. 1970, c. C-30.

AVIS

La qualité de cette microforme dépend grandement de la qualité de la thèse soumise au microfilmage. Nous avons tout fait pour assurer une qualité supérieure de reproduction.

S'il manque des pages, veuillez communiquer avec l'université qui a conféré le grade.

La qualité d'impression de certaines pages peut laisser à désirer, surtout si les pages originales ont été dactylographiées à l'aide d'un ruban usé ou si l'université nous a fait parvenir une photocopie de qualité inférieure.

Les documents qui font déjà l'objet d'un droit d'auteur (articles de revue, tests publiés, etc.) ne sont pas microfilmés.

La reproduction, même partielle, de cette microforme est soumise à la Loi canadienne sur le droit d'auteur, SRC 1970, c. C-30.

NL-339 (r. 86/04)

Canada

THE UNIVERSITY OF ALBERTA

SUPERCOMPUTER FINITE DIFFERENCE METHODS FOR SEISMIC WAVE PROPAGATION

by

© Antonios Vafidis

A THESIS

SUBMITTED TO THE FACULTY OF GRADUATE STUDIES AND RESEARCH

IN PARTIAL FULFILLMENT OF THE REQUIREMENTS FOR THE DEGREE OF DOCTOR OF PHILOSOPHY

IN

GEOPHYSICS

DEPARTMENT OF PHYSICS

EDMONTON, ALBERTA

Spring 1988

Permission has been granted to the National Library of Canada to microfilm this thesis and to lend or sell copies of the film.

The author (copyright owner) has reserved other publication rights, and neither the thesis nor extensive extracts from it may be printed or otherwise reproduced without his/her written permission.

L'autorisation a été accordée à la Bibliothèque nationale du Canada de microfilmer cette thèse et de prêter ou de vendre des exemplaires du film.

L'auteur (titulaire du droit d'auteur) se réserve les autres droits de publication; ni la thèse ni de longs extraits de celle-ci ne doivent être imprimés ou autrement reproduits sans son autorisation écrite.

ISBN 0-315-42845-7

THE UNIVERSITY OF ALBERTA

RELEASE FORM

NAME OF AUTHOR Antonios Vafidis

TITLE OF THESIS SUPERCOMPUTER FINITE DIFFERENCE METHODS FOR SEISMIC WAVE PROPAGATION

DEGREE FOR WHICH THESIS WAS PRESENTED Doctor of Philosophy

YEAR THIS DEGREE GRANTED Spring 1988

Permission is hereby granted to THE UNIVERSITY OF ALBERTA LIBRARY to reproduce single copies of this thesis and to lend or sell such copies for private, scholarly or scientific research purposes only. The author reserves other publication rights, and neither the thesis nor extensive extracts from it may be printed or otherwise reproduced without the author's written permission.

(SIGNED) Βαφίδης

PERMANENT ADDRESS:
ANTONIS VAFIDIS
13, G. DROSINI
THESSALONIKI, GREECE.

DATED February 15, 1988

THE UNIVERSITY OF ALBERTA

FACULTY OF GRADUATE STUDIES AND RESEARCH

The undersigned certify that they have read, and recommend to the Faculty of Graduate Studies and Research, for acceptance, a thesis entitled SUPERCOMPUTER FINITE DIFFERENCE METHODS FOR SEISMIC WAVE PROPAGATION

submitted by ANTONIOS VAFIDIS in partial fulfillment of the requirements for the degree of DOCTOR OF PHILOSOPHY in GEOPHYSICS.

E. R. Kanasewich

Supervisor

Sven Treitel

External Examiner

Date February 15, 1988

To Voula

ABSTRACT

The propagation of seismic waves in a two dimensional medium whose physical parameters are spatially variable can be described by a hyperbolic system of first order partial differential equations. Two finite difference schemes are used for solving this hyperbolic system, the first being a new modified second order accurate Lax-Wendroff scheme and the second a fourth order accurate MacCormack splitting scheme.

Very fine grids and small time steps required by finite differences for simulating realistic seismic experiments make the method computationally expensive and often intractable in a conventional computer. Vectorized finite difference algorithms, based on a matrix times vector multiplication by diagonals technique, have been implemented for supercomputers. The computational time is drastically reduced enabling us to apply the method for high resolution seismic experiments.

Algorithms for SH and elastic wave propagation have been developed for the Lax-Wendroff and MacCormack techniques. They are set up to handle SH and P-SV cases for sources of both compressional and shear energy and for receivers in any geometric configuration. Their numerical solutions have been tested against the exact solutions for simple problems. By numerically solving the equivalent first order systems instead of the second order wave equations the derivatives of the medium's parameters are avoided. Line sources of P, SH and SV waves have been implemented by means of Alterman's and Karal's technique.

A new technique for including amplitude attenuation in the time domain based on a superposition model with a logarithmic creep function expressed in terms of a recursive filter is applied at intermediate steps during the finite difference process to account for attenuation. The method effectively preserves the amplitudes but does not introduce

dispersion. Dissipation operators based on plane wave attenuation are also incorporated in the finite difference algorithms.

Two sets of data from seismic experiments conducted by ESSO Resources, Canada for monitoring steam injection projects in the Cold Lake area have been compared with realistic computer simulations using finite differences. These simulations, apart from reconstructing the full wave field, provide insight into the complicated interactions and assist in the interpretation of the real data. They strongly suggest the necessity for two component acquisition as well as the importance of S-waves. These model simulations indicate that seismic experiments, when carefully designed, can play a major role in helping to solve production and recovery problems by determining the spatial distribution of reservoir properties and their changes with time.

ACKNOWLEDGEMENTS

I would like to sincerely thank my supervisor, Dr. E. R. Kanasewich for invaluable sustained guidance and encouragement throughout this programme.

I wish to thank Dr. F. Abramovici for unstinted sharing of his time and knowledge on aspects of numerical modelling with me.

I wish to express my appreciation to the Alberta Oil Sands Technology and Research Authority, Natural Science and Engineering Research Council and ESSO Resources Canada Limited for the financial support during my Ph.D. studies.

I would like to thank Mr. C. McCloughan since on many occasions his experience with computer software matters was of benefit to me. The assistance and support of the supercomputing group at the University of Calgary is deeply appreciated. I also want to thank my colleagues Costas Macrides, Suhas Phadke, Lawrence Le and Constantine Tsingas for exchanging ideas and permitting me to use their computer programs.

I am grateful to my fiancée Voula Antoniadou for her support and encouragement and to my parents who made it all possible.

Table of Contents

Chapter		Page
1.	INTRODUCTION	1
	1.1 Introduction	1
	1.2 Finite Differences in wave propagation	2
	1.3 Outline of the thesis	4
2.	HIGH ORDER FINITE DIFFERENCE SCHEMES FOR HYPERBOLIC SYSTEMS	6
	2.1 Introduction	6
	2.2 Heterogeneous approach for first order hyperbolic systems	7
	2.3 Accuracy, convergence and stability	13
	2.3.1 Accuracy	13
	2.3.2 Convergence	14
	2.3.3 Stability	16
	2.3.4 Dispersion and dissipation	19
	2.4 Accuracy test of the numerical schemes	23
	2.5 Finite differences on a vector processor	28
	2.6 Matrix times vector by diagonals: The algorithm	30
3.	FINITE DIFFERENCES ON THE SH-WAVE EQUATION	36
	3.1 Introduction	36
	3.2 Problem formulation	37
	3.3 Lax-Wendroff scheme for the SH hyperbolic system on the CYBER 205	42
	3.4 A MacCormack type scheme for the SH hyperbolic system on the CYBER 205	46
	3.5 The source	50
	3.6 The propagating enclosure method	59

Chapter		Page
	3.7 Numerical example	62
4.	FINITE DIFFERENCES ON THE PSV-WAVE EQUATION	68
	4.1 Introduction	68
	4.2 Problem formulation	68
	4.3 Line sources of P and SV waves	76
	4.4 Numerical example	78
5.	MODELLING STEAM INJECTION PROBLEM WITH FINITE DIFFERENCES	85
	5.1 Introduction	85
	5.2 Hole to hole experiment in Cold Lake area	86
	5.3 Surface experiment	103
	5.4 Conclusion	105
6.	ATTENUATION IN TIME DOMAIN	116
	6.1 Introduction	116
	6.2 Definitions of Q	117
	6.3 Attenuation models	118
	6.4 Attenuation in time domain	123
	6.5 Assumptions	127
	6.6 Recursive filter design for Lomnitz logarithmic law	127
	6.7 Dissipation operators in time domain	132
7.	CONCLUSION	138
BIBLIOGRAPHY		141
APPENDIX A		147
APPENDIX B		154
APPENDIX C		158

List of tables

Table		Page
4.1	Numerical parameters for a homogeneous model	81
4.2	Numerical parameters for a two layer model	84
5.1	Numerical parameters - Crosshole experiment	91
5.2	Numerical parameters - Surface experiment	105

List of figures

Figure		Page
2.1	The differencing star for the modified Lax-Wendroff scheme (eq. 2.2.4)	10
2.2	The domains of dependence on the plane x-z: a square for Lax-Wendroff scheme and a circle for the simplest ($\rho(x,z)=\mu(x,z)=1$) SH wave equation.	17
2.3	The magnitude of the leading terms of the relative phase errors given from equation (2.3.19) for the second order and (2.3.20) for the fourth order as a function of the number of grid points per wavelength (G) for pa=0.25.	22
2.4	Particle velocity responses of the exact and numerical solutions at location (5.4,0.6) with h=0.1 and κ=0.001 sec.	25
2.5	Relative error of the Lax-Wendroff scheme for three different grid spacings and the same time step κ=0.001 sec.	26
2.6	The same as in figure 2.5 for the MacCormack type of scheme.	27
2.7	Graphic representation of the matrix-vector multiplication by diagonals.	33
3.1	Normalized particle velocity for a point source with Gaussian excitation function ($\sigma=3\ 10^5$).	53
3.2	Normalized frequency response of the particle velocity shown in figure 3.1.	54
3.3	Particle velocity for a line source with Gaussian excitation function ($\sigma=3\ 10^5$) and time delay 0.02 sec.	57
3.4	Alterman and Karal implementation of the source. In the inner region the residual field is calculated numerically while in the outer region the total field is calculated numerically.	58
3.5	Propagating enclosure method.	60
3.6	Flow chart for the SH finite difference algorithm.	64

Figure		Page
3.7	Source-receiver geometry in Lamb's problem.	65
3.8	Analytical and numerical solutions (Lax-Wendroff) for different number of grid points per dominant wavelength, G.	66
3.9	Analytical and numerical solutions (MacCormack) for different number of grid points per dominant wavelength, G.	67
4.1	Horizontal and vertical particle velocity components for a point P-source with a gaussian excitation function.	79
4.2	The same as in figure (4.1) for a line P-source.	80
4.3	Horizontal and vertical particle velocity responses in a homogeneous medium at a receiver 200 m away from a line P-source for the Lax-Wendroff and MacCormack schemes.	82
4.4	Exact and numerical P-wave reflection coefficients from a P-wave source.	83
5.1	Model geometry of the 1982 seismic tomography experiment.	88
5.2	Sonic log at the receiver well after sampling at 2 m sampling interval.	89
5.3	BARS plots for a steam injection experiment. The seismic signals are rectified in such a way as to allow plotting the 'before' records (blue color) entirely above the zero amplitude baseline and the 'after' records (red color) entirely below it. The original positive portions of the signals are shaded by the color. The original negative parts are unshaded.	90
5.4	BARS plots for an SH computer simulation of the 1982 crosshole experiment.	92
5.5	Ray diagrams for the 1982 crosshole experiment (a) P arrivals before steam injection and (b) converted arrivals before steam injection.	93
5.6	BARS plots for an SH computer simulation of the 1982 crosshole experiment. Velocity varies vertically according to the sonic log.	95

Figure Page

5.7 BARS plots for a P-SV computer simulation of the 1982 crosshole experiment using a P-wave line source: Vertical component of particle velocity. 96

5.8 BARS plots for a P-SV computer simulation of the 1982 crosshole experiment using a P-wave line source: Horizontal component of particle velocity. 97

5.9 BARS plots for a P-SV computer simulation of the 1982 crosshole experiment using a SV-wave line source: Vertical component of particle velocity. 99

5.10 BARS plots for a P-SV computer simulation of the 1982 crosshole experiment using a SV-wave line source: Horizontal component of particle velocity. 100

5.11 BARS plots for a P-SV computer simulation of the 1982 crosshole experiment the outcome after summing the P- and the SV-wave line source results: Vertical component of particle velocity. 101

5.12 BARS plots for a P-SV computer simulation of the 1982 crosshole experiment the outcome after summing the P- and the SV-wave line source results: Horizontal component of particle velocity. 102

5.13 Model geometry of the surface experiment. 106

5.14 Common shot gather surface data over a steam injected area. 107

5.15 SH computer simulation of the surface experiment: Section before steam injection. 108

5.16 SH computer simulation of the surface experiment: Section with a steam zone of elliptical shape whose major semiaxis is 36 m. 109

5.17 The same as in figure 5.16 with major semiaxis is 78 m. 110

5.18 SH computer simulation of the surface experiment: Section with a steam zone inside and a condensation zone outside both of elliptical shape. 111

Figure		Page
5.19	P-SV computer simulation of the surface experiment: Section before steam injection for the vertical component of the particle velocity.	112
5.20	The same as in figure 5.19 for the horizontal component.	113
5.21	P-SV computer simulation of the surface experiment: Section after steam injection for the vertical component of the particle velocity.	114
5.22	The same as in figure 5.21 for the horizontal component.	115
6.1	The constant Q creep function as given by (6.3.5) in units of $1/M_u$ plotted versus time in units of 1/a.	122
6.2	Comparison of the exact impulse response of $\ddot{\phi}_t$ and the one given by the recursive relation (the value at zero is missing).	130
6.3	Impulse response of the dissipation operator d_t resulting from sources at distances of .5, 1, 2, 4 and 8 times c_0, Q=30.	134
6.4	Comparison of the plane waveforms with attenuation (Q=30 or 1000) from finite differences (a) and from the convolution of the wavelet with dissipation operators (b).	136
6.5	Comparison of the plane waveforms with attenuation (Q=30) from finite differences after the elastic response is convolved with dissipation operators at distinct locations (numerical) and from the convolution of the wavelet with a dissipation operator (exact).	137

CHAPTER 1
INTRODUCTION

1.1 Introduction

A basic tool in exploration seismology is the synthetic seismogram which is generated by solving an elastic wave equation. The analytical solution is not always known. Therefore, various approximation methods have been suggested for the computation of synthetic seismograms.

In a series method, the solution of the propagation problem is represented by an infinite series (Asymptotic Ray Theory). The coefficients of a finite number of terms (most often the leading term only) are then determined numerically to yield an approximation to the true solution. One of the disadvantages of ART is that a large number of rays is necessary to generate a synthetic seismogram.

In transform methods, if the independent variables in the wave equation are separable by applying transforms, the partial differential equations can be reduced to ordinary differential equations which can be solved analytically or numerically. Having found the solution of the ordinary differential equations, the inverse transforms must be evaluated.

In segmentation methods, the given interval is segmented into subintervals and the differential equation is approximated with reference to those segments. Depending on the size of the segments and the approximation procedure for the solution, there are several methods. One subgroup consists of the finite difference and finite element methods.

1.2 Finite Differences in wave propagation

In finite differences (FD), both the spatial and time variables are discretized by superimposing a rectangular grid on the model. Finite difference approximations to the differential equations that describe the wave propagation, give rise to difference equations. Numerical solutions are obtained from the difference equations solved on the discrete grid subject to some initial condition.

Kelly et al.(1976) pointed out that two formulations can be distinguished: The *homogeneous* approach solves the wave equation in each homogeneous layer separately. Boundary conditions must be explicitly imposed on the interfaces between different layers. The *heterogeneous* formulation directly solves the wave equation for the whole model. The wave equation in this case allows the physical properties to vary both laterally and vertically. In the *heterogeneous* approach, boundary conditions are satisfied implicitly and more complicated geometries can be accommodated with no extra effort.

Alterman et al.(1968) applied the *homogeneous* approach to P-SV wave propagation in horizontally layered structures. They also proposed also a technique for handling the source in the grid. This technique removes the singularity at the source location by imposing the source contribution on a rectangle around the source location. Alterman and Loewenthal (1972) confirmed the accuracy of the solutions for an elastic half space and two welded elastic half spaces by comparison to the exact solution. Alford et al (1974) calculated synthetic seismograms using second and fourth order approximations to the homogeneous acoustic wave equation. They implemented a line source whose excitation is the first derivative of a Gaussian function. In their paper the numerical dispersion, also called grid dispersion, is shown to be more pronounced in the second order scheme than in the fourth order. Grid dispersion depends highly on the number of grid points per wavelength and imposes restrictions on the applicability of the finite differences in wave propagation. They

compared the numerical results to the analytical solutions for scattering from a 90^0 wedge.

The *heterogeneous* approach is based on a single wave equation which has continuously variable coefficients. When applying FD techniques to this equation, additional approximations of the derivatives of the elastic parameters are necessary (Kelly et al, 1976). Boore (1972) applied an averaging on the physical parameters based on the ideas of Tikhonov and Samarskii (Mitchell, 1969). Boore also compared wavenumber spectra of finite difference results for horizontally polarized shear waves and Love waves in layered elastic half spaces with analytical results. Stephen (1983) has compared the finite difference method with the reflectivity method (Fuchs and Muller, 1971, Kennett, 1974) for an acoustic half space separated from an elastic half space by a layer with constant velocity and density gradients. Recently Virieux (1984,1986, also Bayliss et al , 1986) presented a finite difference method for modelling SH and P-SV wave propagation in heterogeneous media using equivalent first order hyperbolic systems instead of second order wave equations. This formulation does not require numerical differentiation of the medium parameters.

FD schemes can be classified in two broad categories: *explicit* and *implicit*. In *explicit* schemes the response is evaluated at an advanced time exclusively from the response already determined at previous times. In *implicit* schemes the response is evaluated *simultaneously at all space locations* at an advanced time from known values at previous times through a matrix inversion technique.

A number of different finite difference schemes have been applied to hyperbolic systems (Clifton, 1967, Santosa and Pao, 1986). One of the most well known difference approximations to first order hyperbolic systems is the Lax-Wendroff method (Mitchell, 1969). Another group of schemes is based on the dimensional splitting technique (Strang, 1968) which, when combined with two-step operators in the spirit of MacCormack (Turkel, 1980), result in multistage operators they can be efficiently implemented on multi-processor computers.

The usefulness of any scheme greatly depends on the problem being solved; one must

choose that method which gives reasonable answers with the least amount of storage space and computer time. Of the categories, the explicit scheme is computationally simpler. In common with most explicit finite difference approximations to PDE, a condition relating the time and space grid intervals must be satisfied if the solution to the difference equations is to be stable. In wave propagation the stability condition of the finite difference schemes is not as restrictive as in the heat flow problems (Boore, 1972).

1.3 Outline of the thesis

The thesis consists of six chapters and three appendices.

Chapter 1 contains a short review of the finite difference method in wave propagation and the outline of the thesis.

In Chapter 2 a new modified Lax-Wendroff scheme is proposed for the first order hyperbolic system in two dimensions whose coefficients are space dependent and it is compared with a MacCormack one dimensional scheme in terms of accuracy, stability, convergence, numerical dispersion and dissipation. Also the vectorization of finite difference operators is described through a simple example using the matrix by vector multiplication by diagonals algorithm. This vectorization technique is used in the implementation of both schemes on a CDC 205 supercomputer as configured at the University of Calgary. These methods decrease computation time by several decades and increase, in this way, the range of applicability of finite differences. Finally, the numerical schemes are tested by comparing the numerical solutions against the exact one for a simple SH wave propagation problem.

In Chapter 3 a first order hyperbolic system for the SH wave equation in two dimensions is obtained and apply the Lax-Wendroff and MacCormack schemes, described in chapter 2, are applied to this system. Next, the operators are expressed in matrix form so

that they may be fully vectorized. Both point and line sources are implemented using Alterman's and Karal's technique. Finally, a comparison of the numerical solutions with the exact one is given for the known problem of two half spaces separated by an interface.

In Chapter 4 both schemes are applied to the more complex P-SV elastic wave equations following similar steps as in Chapter 3. A comparison of the two schemes is described through some examples.

In Chapter 5 synthetic seismograms are generated for two models applicable to a steam injection project in heavy oil extraction near Cold Lake, Alberta. The results are compared with real data.

In Chapter 6 a new technique for including attenuation in the time domain is presented. A superposition model with a logarithmic creep function expressed in terms of a recursive filter is applied at intermediate steps during the finite difference process to account for attenuation.

Chapter 7 contains the conclusions, discusses the original contribution in the thesis and makes suggestions for future work.

CHAPTER 2

HIGH ORDER FINITE DIFFERENCES FOR HYPERBOLIC SYSTEMS

2.1 Introduction

Various numerical schemes have been applied to the wave propagation problem. Most of them are applied to a second order differential equation. In designing a finite difference operator the first concern is the accuracy. A new modified Lax-Wendroff second order scheme for first order hyperbolic systems whose coefficients are space dependent is proposed. The heterogeneous approach gives certain advantages since it is not necessary to impose the continuity equations on the interfaces but it suffers from the fact that there is no control of error generated by the model's discontinuities. Detailed mathematical treatment on the accuracy results in a nine point operator.

In this chapter, the Lax-Wendroff scheme and a one dimensional MacCormack (1971) scheme are compared in terms of accuracy, stability, convergence, numerical dispersion and dissipation. The methods have been checked by comparing the numerical solutions with a given known exact solution. In this comparison the medium's parametres as well as the initial conditions of the velocity and stress components are known analytic expressions dependent on the space coordinates and they have been utilized in order to generate the numerical solution. Finally the vectorization procedure of FD schemes is discussed using a simple difference operator and the algorithm for matrix multiplications by diagonals is illustrated.

2.2 Heterogeneous approach for first order hyperbolic systems

The heterogeneous approach has certain advantages over the homogeneous since it can be applied to any model geometry without requiring major changes in the program code. In approximating the second order wave equation, numerical differentiation of the elastic parameters is necessary. Here, the equivalent first order hyperbolic system will be approximated instead.

A first order system in two dimensions can be expressed as

$$\partial_t \, \mathbf{U}(x,z,t) = \mathbf{A} \, \partial_x \, \mathbf{U}(x,z,t) + \mathbf{B} \, \partial_z \, \mathbf{U}(x,z,t) \tag{2.2.1}$$

where **U** defines a vector function of x, z and t; **A**, **B** are matrices, functions of x and z with $0 < x < H_x$, $0 < z < H_z$, $t > 0$ and ∂_s denotes a partial derivative with respect to a spatial or temporal coordinate s. This system will be solved numerically, subject to some initial conditions: $\mathbf{U}(x, z, t = 0)$.

A system is called hyperbolic if, for all real α, β with $\alpha^2+\beta^2=1$, there exists a nonsingular transformation matrix **Q**, such that

$$\mathbf{Q} (\alpha \mathbf{A} + \beta \mathbf{B}) \mathbf{Q}^{-1} = \mathbf{D} \tag{2.2.2}$$

where **D** is a diagonal matrix with real elements. All of these conditions are satisfied if the matrices **A** and **B** are real and symmetric. In chapters 3 and 4 hyperbolicity will be verified for the wave equations through the symmetry of the coefficient matrices.

To set up the finite difference method I select two integers $J > 0$, $M > 0$ and the time step $\kappa > 0$. If H_x and H_z are the endpoints of the grid with $h = H_x/J = H_z/M$, the mesh points (x_j, z_m, t_n) are defined by

$$x_j = j\,h \text{ for each } j = 0, 1, \ldots J$$

$$z_m = m\,h \text{ for each } m = 0, 1, \ldots M$$

$$t_n = n\,\kappa \text{ for each } n = 0, 1, \ldots$$

Various difference approximations for hyperbolic systems are well established and have been applied in different fields. The best known method for first-order hyperbolic systems is the Lax-Wendroff method (Lax and Wendroff, 1964, Mitchell, 1981) where a difference equation is determined so that it has accuracy of second order. A Lax-Wendroff scheme for a first order hyperbolic system in two space dimensions with the matrices of coefficients **A** and **B** varying both in space and time given by Mitchell (1981) has been modified so that it maintains second order accuracy where the matrices **A** and **B** depend on the space variables. The modified Lax-Wendroff scheme is based on the Taylor expansion of **U** at time $t+\kappa$ for $\kappa>0$ carried to second order

$$\mathbf{U}(x, z, t+\kappa) = \mathbf{U}(x, z, t) + \kappa \frac{\partial \mathbf{U}}{\partial t} + \frac{1}{2}\kappa^2 \frac{\partial^2 \mathbf{U}}{\partial t^2} + O(\kappa^3) .$$

which becomes, after replacing the time derivatives by space derivatives from equation (2.2.1) and keeping up to second order terms in κ,

$$\mathbf{U}(x,z,t+\kappa) \approx \mathbf{U}(x,z,t)+\kappa\left(\mathbf{A}\frac{\partial \mathbf{U}}{\partial x}+\mathbf{B}\frac{\partial \mathbf{U}}{\partial z}\right)+\frac{\kappa^2}{2}\left[\mathbf{A}\frac{\partial}{\partial x}\left(\mathbf{A}\frac{\partial \mathbf{U}}{\partial x}+\mathbf{B}\frac{\partial \mathbf{U}}{\partial z}\right)+\mathbf{B}\frac{\partial}{\partial z}\left(\mathbf{A}\frac{\partial \mathbf{U}}{\partial x}+\mathbf{B}\frac{\partial \mathbf{U}}{\partial z}\right)\right]$$

(see also section (2.3.1) for the proof of accuracy). This explicit Lax-Wendroff scheme is given by:

$$\begin{aligned}\mathbf{U}_{j,m}^{n+1} = \Big\{ \mathbf{I} &+ \frac{p}{2}\mathbf{A}_{j,m}(\Delta_x+\nabla_x) + \frac{p}{2}\mathbf{B}_{j,m}(\Delta_z+\nabla_z) + \frac{p^2}{4}(\mathbf{A}_{j,m}\Delta_x\mathbf{A}_{j,m}\nabla_x+\mathbf{A}_{j,m}\nabla_x\mathbf{A}_{j,m}\Delta_x) \\ &+ \frac{p^2}{4}(\mathbf{B}_{j,m}\Delta_z\mathbf{B}_{j,m}\nabla_z+\mathbf{B}_{j,m}\nabla_z\mathbf{B}_{j,m}\Delta_z) + \frac{p^2}{4}[\mathbf{A}_{j,m}(\nabla_x\mathbf{B}_{j,m})\Delta_z+\mathbf{A}_{j,m}(\Delta_x\mathbf{B}_{j,m})\nabla_z] \\ &+ \frac{p^2}{4}[\mathbf{B}_{j,m}(\nabla_z\mathbf{A}_{j,m})\Delta_x+\mathbf{B}_{j,m}(\Delta_z\mathbf{A}_{j,m})\nabla_x] + \frac{p^2}{8}(\mathbf{A}_{j,m}\mathbf{B}_{j,m}+\mathbf{B}_{j,m}\mathbf{A}_{j,m})(\Delta_x+\nabla_x)(\Delta_z+\nabla_z)\Big\}\,\mathbf{U}_{j,m}^{n}\end{aligned} \qquad (2.2.3)$$

where the forward and the backward difference operators Δ_s and ∇_s ($s = x$ or z) are

$\Delta U_s = U_{s+1} - U_s$, $\nabla U_s = U_s - U_{s-1}$ and $p = \kappa/h$. It can be shown that equation (2.2.3) can be written as:

$$
\begin{aligned}
U_{j,m}^{n+1} = \Big\{ I - \frac{p^2}{4}\big[A_{j,m}(A_{j+1,m}+2A_{j,m}+A_{j-1,m}) + B_{j,m}(B_{j,m+1}+2B_{j,m}+B_{j,m-1})\big] \\
+ \frac{p^2}{4}\big[A_{j,m}(B_{j+1,m}-2B_{j,m}+B_{j-1,m}) + B_{j,m}(A_{j,m+1}-2A_{j,m}+A_{j,m-1})\big]\Big\}\, U_{j,m}^{n} \\
+ \frac{p}{2}\big\{A_{j,m}\big[I + \frac{p}{2}(A_{j+1,m}+A_{j,m})\big] + \frac{p}{2}\, B_{j,m}(A_{j,m}-A_{j,m-1})\big\} U_{j+1,m}^{n} \\
+ \frac{p}{2}\big\{B_{j,m}\big[I + \frac{p}{2}(B_{j,m+1}+B_{j,m})\big] + \frac{p}{2}\, A_{j,m}(B_{j,m}-B_{j-1,m})\big\} U_{j,m+1}^{n} \\
- \frac{p}{2}\big\{A_{j,m}\big[I - \frac{p}{2}(A_{j,m}+A_{j-1,m})\big] + \frac{p}{2}\, B_{j,m}(A_{j,m+1}-A_{j,m})\big\} U_{j-1,m}^{n} \\
- \frac{p}{2}\big\{B_{j,m}\big[I - \frac{p}{2}(B_{j,m}+B_{j,m-1})\big] + \frac{p}{2}\, A_{j,m}(B_{j+1,m}-B_{j,m})\big\} U_{j,m-1}^{n} \\
+ \frac{p^2}{8}\,(A_{j,m}B_{j,m}+B_{j,m}A_{j,m})\big\{U_{j+1,m+1}^{n} - U_{j-1,m+1}^{n} - U_{j+1,m-1}^{n} + U_{j-1,m-1}^{n}\big\}
\end{aligned}
\qquad (2.2.4)
$$

The differencing star of this scheme is shown in figure (2.1). It is a nine point numerical scheme explicit in the vector U. Given the initial values of vector U at one time it is a simple matter to compute the values of the vector at any other time by a forward time marching process.

If a typical Fourier harmonic component $U = U_0 \exp(i\beta x + i\gamma z)$ where U_0 is a constant vector, is substituted into the difference equation for U^n, it is found that U^{n+1} is of the same form but with GU_0 replacing U_0. The matrix G is called the amplification matrix. The amplification matrix for equation (2.2.4) is:

$$
G = I - \frac{p^2}{2}\big[G_1 e^{-i\xi} + G_2 e^{i\xi} + G_3 e^{-i\eta} + G_4 e^{i\eta} + (AB+BA)\sin\xi\sin\eta\big] + ip[A\sin\xi + B\sin\eta]
\qquad (2.2.5)
$$

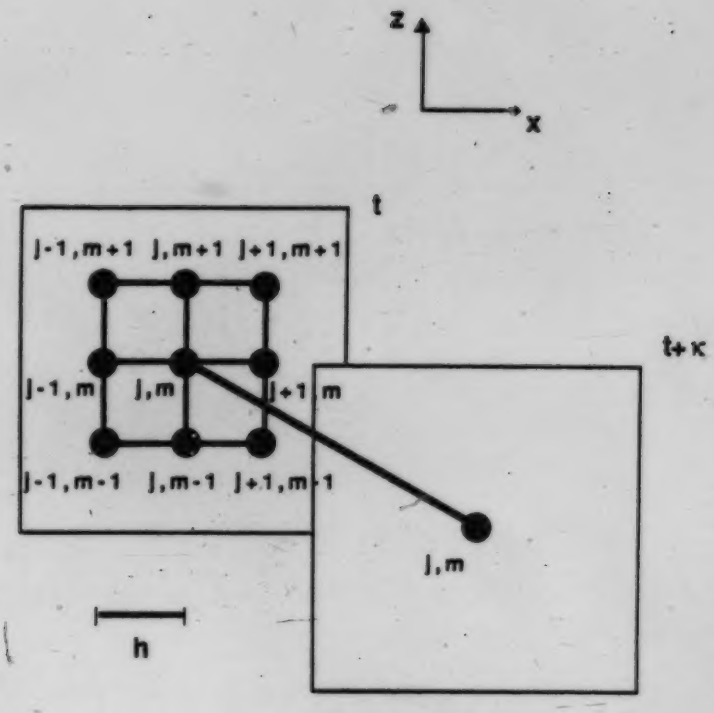

Figure 2.1 The differencing star for the modified Lax-Wendroff scheme (eq. 2.2.4)

where $\xi=\beta h$, $\eta=\gamma h$ and

$$G_1 = \frac{1}{2}\left[A_{j,m}\left(A_{j-1,m} + A_{j,m}\right) + B_{j,m}\left(A_{j,m} - A_{j,m+1}\right)\right]$$

$$G_2 = \frac{1}{2}\left[A_{j,m}\left(A_{j+1,m} + A_{j,m}\right) + B_{j,m}\left(A_{j,m} - A_{j,m-1}\right)\right]$$

$$G_3 = \frac{1}{2}\left[B_{j,m}\left(B_{j,m-1} + B_{j,m}\right) + A_{j,m}\left(B_{j,m} - B_{j+1,m}\right)\right]$$

$$G_4 = \frac{1}{2}\left[B_{j,m}\left(B_{j,m+1} + B_{j,m}\right) + A_{j,m}\left(B_{j,m} - B_{j-1,m}\right)\right]$$

(2.2.6).

The other method is based on the concept of splitting in time (Strang, 1968). Equation (2.2.1) can be written in a linearized version as

$$\partial_t U(x, z, t) = A\,\partial_x U(x, z, t) + B\,\partial_z U(x, z, t) = (L_x + L_z)\,U(x, z, t)$$

(2.2.7).

From Taylor's theorem

$$U(x, z, t+\kappa) = \left(1 + \kappa\frac{\partial}{\partial t} + \frac{1}{2}\kappa^2\frac{\partial^2}{\partial t^2} + \ldots\right) U(x, z, t) = \exp\left(\kappa\frac{\partial}{\partial t}\right) U(x, z, t)$$

or

$$U(x, z, t+\kappa) = \exp\left[\kappa\left(L_x + L_z\right)\right]\; U(x, z, t)$$

but

$$\exp\left[\kappa\left(L_x + L_z\right)\right] = \exp\left[\frac{\kappa L_x}{2}\right]\exp\left[\kappa L_z\right]\exp\left[\frac{\kappa L_x}{2}\right]$$

is accurate up to $O(\kappa^2)$ and the corresponding difference approximation is described by

$$U^{n+2} = F_x F_z F_z^{\dagger} F_x^{\dagger} U^n$$

(2.2.8)

where F_x, $F_x^{\dagger}$, F_z, $F_z^{\dagger}$ are one dimensional difference operators. One advantage of splitting methods is that stability properties are governed by the one dimensional (1D)

schemes since we apply 1D approximations. Also splitting methods have smaller phase error than a wide class of unsplit schemes (Turkel, 1974).

A (2,4) version of the MacCormack scheme (Gottlieb and Turkel, 1976), which is called in this thesis simply MacCormack scheme, applied to the one dimensional system,

$$\partial_t U(x, z, t) = A \partial_x U(x, z, t) \tag{2.2.9}$$

consists (see Appendix A for complete derivation) of the predictor:

$$U^{(1)}_{j,m} = U^n_{j,m} - \frac{p}{6} A_{j,m}(7U^n_{j,m} - 8U^n_{j+1,m} + U^n_{j+2,m})$$

and the corrector

$$U^{n+1}_{j,m} = \frac{1}{2}(U^{(1)}_{j,m} + U^n_{j,m}) + \frac{p}{12} A_{j,m}(7U^{(1)}_{j,m} - 8U^{(1)}_{j-1,m} + U^{(1)}_{j-2,m}) \tag{2.2.10}$$

where the superscript (1) denotes an intermediate step. This is used in alternate time steps with

$$U^{(1)}_{j,m} = U^n_{j,m} + \frac{p}{6} A_{j,m}(7U^n_{j,m} - 8U^n_{j-1,m} + U^n_{j-2,m})$$

$$U^{n+1}_{j,m} = \frac{1}{2}(U^{(1)}_{j,m} + U^n_{j,m}) - \frac{p}{12} A_{j,m}(7U^{(1)}_{j,m} - 8U^{(1)}_{j+1,m} + U^{(1)}_{j+2,m}) \tag{2.2.11}.$$

In both two step schemes described by equations (2.2.10) and (2.2.11) the updated vector U at the location (j, m) depends on the neighboring grid points in the x-direction only. The amplification matrix associated with this approximation is

$$G = I - ipA\frac{\sin\xi}{12-3\cos\xi} - \frac{1}{2}p^2A^2(1-\cos\xi)(2+\sigma-\sigma\cos\xi) \tag{2.2.12}$$

where $\sigma = 7/9$ for equation (2.2.10) and $\sigma = 55/9$ for equation (2.2.11). Equations (2.2.10) and (2.2.11) correspond to the operators F_x and $F_x^{\dagger}$ respectively. Similar predictor-corrector equations can describe operators F_z and $F_z^{\dagger}$. The amplification matrices will be used later in stability and dispersion analysis.

2.3 Accuracy, convergence and stability

To guarantee that solutions to the difference equations remain bounded as the computations proceed, and that as the grid spacing becomes smaller and smaller those solutions approach the solution of the differential equation, the accuracy, the convergence and stability must be checked.

2.3.1 Accuracy

A criterion for the local accuracy of a finite difference formula is defined by the difference, **E**, between the exact solutions of the differential, **W**, and the difference, **U**, equations at a grid point (jh, mh, (n+1)κ) as

$$E^n_{j,m} = W^n_{j,m} - U^n_{j,m} \qquad (2.3.1).$$

The Taylor series of W^n is

$$W^{n+1} = W^n + \kappa W^n_t + \frac{\kappa^2}{2} W^n_{tt} + O[\kappa^3] \qquad (2.3.2).$$

Replacing the time derivatives from the differential system (2.2.1) we get

$$W^{n+1} = W^n + \kappa(AW_x + BW_z)^n + \frac{\kappa^2}{2}[A(AW_x+BW_z)^n_x + B(AW_x+BW_z)^n_z] + O(\kappa^3) \qquad (2.3.3).$$

The Lax-Wendroff scheme (eq. 2.2.3) after approximating the difference operators by

(keeping the leading terms only)

$$(\Delta_x+\nabla_x)\,U^n \approx 2hU_x{}^n,\quad (\Delta_z+\nabla_z)\,U^n \approx 2hU_z{}^n,\quad (\Delta_x A\nabla_x+\nabla_x A\Delta_x)U^n \approx 2h^2(AU_x{}^n)_x$$

$$(\Delta_z B\nabla_z+\nabla_z B\Delta_z)U^n \approx 2h^2(BU_z{}^n)_z,\quad (\Delta_x+\nabla_x)(\Delta_z+\nabla_z)U^n \approx 4h^2U_{xz}{}^n$$

$$[(\Delta_z A)\nabla_x+(\nabla_z A)\Delta_x]U^n \approx 2h^2A_zU_x{}^n,\quad [(\Delta_x B)\nabla_z+(\nabla_x B)\Delta_z]U^n \approx 2h^2B_xU_z{}^n \tag{2.3.4}$$

gives

$$U^{n+1}=U^n+ph(AU_x+BU_z)^n+\frac{p^2h^2}{2}[A(AU_x)_x{}^n+A(BU_{xz}+B_xU_z)^n$$

$$+B(AU_{xz}+A_zU_x)^n+B(BU_z)_z{}^n] \tag{2.3.5}$$

Substituting the equations (2.3.2) and (2.3.5) in equation (2.3.1), the truncation error is of third order in time. Similarly, by expanding the Taylor series in the space domain, one can obtain accuracy of the order (h^2, κ^2) or (2, 2).

The truncation error of MacCormack schemes (2.2.10) and (2.2.11) has the form (see appendix A for complete derivation)

$$E = \kappa\left[\pm\frac{1}{6}A_0\ (A_xU_x)_x\kappa h + O(h^4) + O(\kappa h^2) + O(\kappa^2)\ \right] \tag{2.3.6}$$

By alternating (2.2.10) and (2.2.11) at successive time steps the first error term will cancel and will yield a (2, 4) scheme.

2.3.2 Convergence

The various difference schemes are only for useful for solving PDE if they are convergent and stable. Convergence exists if the theoretical solution to a difference equation approaches the solution of the corresponding differential equation as the mesh is

refined.

The Courant-Friedrichs-Lewy (1928) (CFL) condition must be satisfied for explicit difference replacements to the hyperbolic differential equations for the systems to be convergent. The CFL condition states that the domain of dependence of the difference equation must include the domain of dependence of the differential equation. If the CFL condition is not satisfied the solution of the difference equation is independent of the initial data of the problem which lies outside the domain of dependence of the difference equation but lies inside the domain of dependence of the differential equation. Alteration of this initial data modifies the solution of the differential equation but leaves the solution of the difference equation unaltered. The domain of dependence of a hyperbolic system can be found by the method of characteristics (Mitchell, 1981). The domain of dependence of an explicit difference system is confined by the grid points which influence the value of U at a certain point and depends on the mesh ratio p.

As an example the simple SH wave equation with $\mu(x,z)=\rho(x,z)=1$ will be considered. The domains of dependence of the system (3.2.4) and the explicit difference system (2.2.4) will be examined with respect to the Cauchy initial value problem where the initial conditions are

$$U(x, z, 0) = C(x, z), \qquad -\infty < x, z < \infty \tag{2.3.7}$$

The domain of dependence for the equivalent wave equation (3.2.1) with constant coefficients is calculated by using the method of characteristics (Hilbert and Courant, 1962). The domain of dependence in the (x,z) plane of the differential system for a point P(X,Z,T) is the circle

$$(x - X)^2 + (z - Z)^2 \leq T^2 \tag{2.3.8}$$

which is cut from the (x, z) plane by the circular (characteristic) cone (Mitchell, 1981) with

apex $\pi/4$, vertex at P and axis parallel to the t-axis. The explicit difference formula (2.2.4) allows the value of the vector **U** at the grid point P(X, Z, T) to be expressed uniquely in terms of the values of **C** at certain points of the initial plane t=0, $\mathbf{U}^0_{j,m} = \mathbf{C}(jh, mh)$. The grid points which influence the value of **U** at P lie inside a pyramid which cuts out from the initial plane t = 0 one square as the domain of dependence. The CFL condition for the difference scheme (2.2.4) to be convergent for all initial smooth data is that the square of dependence of this difference scheme must contain the circle of dependence of the corresponding differential equation in its interior. The domain of dependence will be given without loss of generality for a point lying on the t-axis. Then the domain of dependence for the differential equation is a circle of radius $T=n\kappa$ and the square of dependence for the difference equation with sides $2nh$ (figure 2.2) must satisfy the CFL condition,

$$n\kappa \leq nh \qquad \text{or} \qquad p = \kappa / h \leq 1$$

(2.3.9).

In two dimensions the convergence condition is less restrictive than the stability condition (see next section). Convergence analysis for the more general hyperbolic wave system with **A**, **B** not constant becomes cumbersome. Convergence can also be guaranteed when a scheme is stable and the truncation error tends to zero with h, $\kappa \rightarrow 0$ (consistent scheme, Boore, 1972).

2.3.3 Stability

The problem of stability consists of finding conditions under which the difference between the theoretical and numerical solutions of the difference equation remains bounded as time progresses. A finite difference scheme is unstable when its error grows without a bound. The easiest way of investigating stability is to use the Fourier series approach pioneered by von Neumann. In this discussion boundary or initial conditions are not going to be taken into consideration.

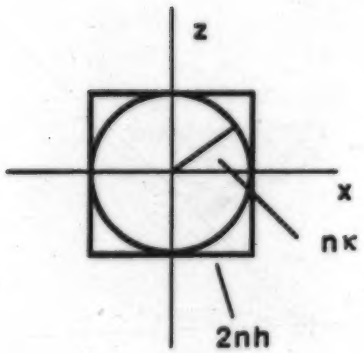

Figure 2.2 The domains of dependence on the plane x-z: a square for Lax-Wendroff scheme and a circle for the simplest ($\rho(x,z)=\mu(x,z)=1$) SH wave equation.

A stability analysis of a hyperbolic system in two space dimensions is difficult, even with **A** and **B** constant. The stability of a difference scheme at a grid point in the field will be the same as the stability of the corresponding difference equation where the values of the coefficients have been 'frozen' to the values attained at that grid point. This local stability condition, usually a limitation on the size of the mesh ratio p, will vary from point to point in the field and the overall stability condition must be the largest mesh ratio which satisfies the local stability condition at every grid point in the region. The von Neumann necessary condition for the stability of a system requires the magnitude of the maximum eigenvalue of the amplification matrix to be less than one. The amplification matrix for the Lax-Wendroff scheme (2.2.5) with **A**, **B** constant

$$\mathbf{G} = \mathbf{I} - p^2[\mathbf{A}^2(1-\cos\xi)+\mathbf{B}^2(1-\cos\eta)+\frac{1}{2}(\mathbf{AB}+\mathbf{BA})\sin\xi\sin\eta]+ip[\mathbf{A}\sin\xi+\mathbf{B}\sin\eta] \tag{2.3.10}$$

is used to evaluate the eigenvalues. Lax and Wendroff(1964) proved that if

$$|a_m| = \max_{A,B}(|a_A|, |a_B|) \tag{2.3.11}$$

where a_A, a_B the eigenvalues of the matrices **A**,**B** respectively, then the Lax-Wendroff scheme with **A**,**B** constant is stable if

$$p\,|a_m| \le \frac{1}{2\sqrt{2}} \tag{2.3.12}$$

For the MacCormack scheme, since the matrix **A** (or **B**) can be diagonalized, the von Neumann condition is both necessary and sufficient for stability. If a is an eigenvalue of **A** the stability condition for this scheme (Gottlieb and Turkel, 1976) is given by

$$p|a_m| \leq \frac{2}{3}$$

(2.3.13).

The MacCormack scheme stability condition is almost half as restrictive than the Lax-Wendroff. The number of time steps required for the generation of a synthetic trace of a given duration is therefore halved so that the method becomes less expensive.

2.3.4 Dispersion and dissipation

The dispersion properties of difference approximations relate to the speed of propagation of the numerical solution. A measure of dispersion is the phase error. Phase errors occur due to replacement of the differential equation by a difference equation. Phase errors produce a variation of phase velocity with frequency (time dispersion) or wavenumber (spatial dispersion). Waves propagating on a discrete grid become progressively dispersed with increasing travel time.

The numerical phase is defined as

$$P(\xi,\eta) = \arctan\left[\frac{Im(G)}{Re(G)}\right]$$

(2.3.14).

In any discretization, only the long waves are well approximated. Thus, the numerical phase of the higher frequency components is of little significance. The true phase can be reasonably well approximated for long wave components of the solution. Thus $P(\xi, \eta)$ is of importance only for small Fourier variables ξ and η. If $P_a(\xi, \eta)$ the analytic phase

$$P_a(\xi,\eta) = p(A\xi+B\eta)$$

(2.3.15)

the numerical phase error is given by:

$$P_e(\xi,\eta) = P(\xi,\eta) - P_a(\xi,\eta)$$

(2.3.16).

The phase error is only evaluated for the case where **A** and **B** are constant and commute (see appendix A for the derivation), though the results seem to be applicable to more general systems. For the modified Lax-Wendroff method, the following new equation holds:

$$P_e(\xi,\eta) = -\frac{1}{6}[p\mathbf{A}\xi^3+p\mathbf{B}\eta^3-(p\mathbf{A}\xi+p\mathbf{B}\eta)^3] + O(\xi^4+\eta^4)$$

(2.3.17).

If $p\rho(\mathbf{A})+p\rho(\mathbf{B}) << 1$ where $\rho(\,)$ denotes spectral radius, and ξ, η are positive then P_e is positive i.e. there is a phase lag.

The relative phase error is also defined by

$$P_r(\xi) = \frac{P_e(\xi)}{P_a(\xi)}$$

(2.3.18).

For the one-dimensional problem the relative phase error of the Lax-Wendroff method is (Gottlieb and Turkel, 1976),

$$P_r(\xi) = -\frac{1}{6}(1-p^2a^2)\xi^2 + \frac{1}{120}(1+5p^2a^2-6p^4a^4)\xi^4 + O(\xi^6)$$

(2.3.19)

where *a* is an eigenvalue of matrix **A**. For the one dimensional MacCormack schemes the relative error is

$$P_r(\xi) = \frac{1}{6}p^2a^2\xi^2 - \frac{1}{120}(4-15(\sigma-1/3)p^2a^2+6p^4a^4)\xi^4 + O(\xi^6)$$

(2.3.20).

The leading terms in equations (2.3.19) and (2.3.20) are of the same order. The Lax-Wendroff scheme has a lagging phase, while the MacCormack scheme has a leading phase. For small p $\rho(A)$ this term is negligible and the phase error of the MacCormack scheme can be much smaller for sufficiently small p. This is the major advantage of the higher order accurate (in space) scheme.

The phase error is directly related to the grid dispersion. Defining the ratio of the wavelength over the grid spacing as $G = \lambda/h$ and knowing that the Fourier variable for a plane wave is $\xi = kh$, where k is the wavenumber, then G and ξ are inversely proportional: $\xi = 2\pi/G$. Since the phase error is small for ξ small, it is also small for G large. In figure (2.3) the leading terms of the phase error for both schemes is displayed for $pa = 0.25$. As a rule of thumb one can say that for second order schemes the phase error is negligible when $G > 10$ and for fourth order when $G > 5$ (Alford et al, 1974). The grid dispersion imposes constraints on the application of the finite difference methods making them more useful for finding the wavefield in the vicinity of the seismic source or inhomogeneity.

A difference scheme is dissipative of order $2r$ if there is a positive constant δ and a positive integer r such that

$$|a_m| \leq 1 - \delta\,|\xi|^{2r} \qquad (2.3.21)$$

for all ξ. The solutions of dissipative schemes decay to zero as $n \to \infty$. Also the decay of high frequency modes is much greater than that of low frequencies. Both Lax-Wendroff and MacCormack schemes are dissipative of second order (Gottlieb and Turkel,1976). Dissipative schemes minimize dispersion effects particularly at high frequency modes.

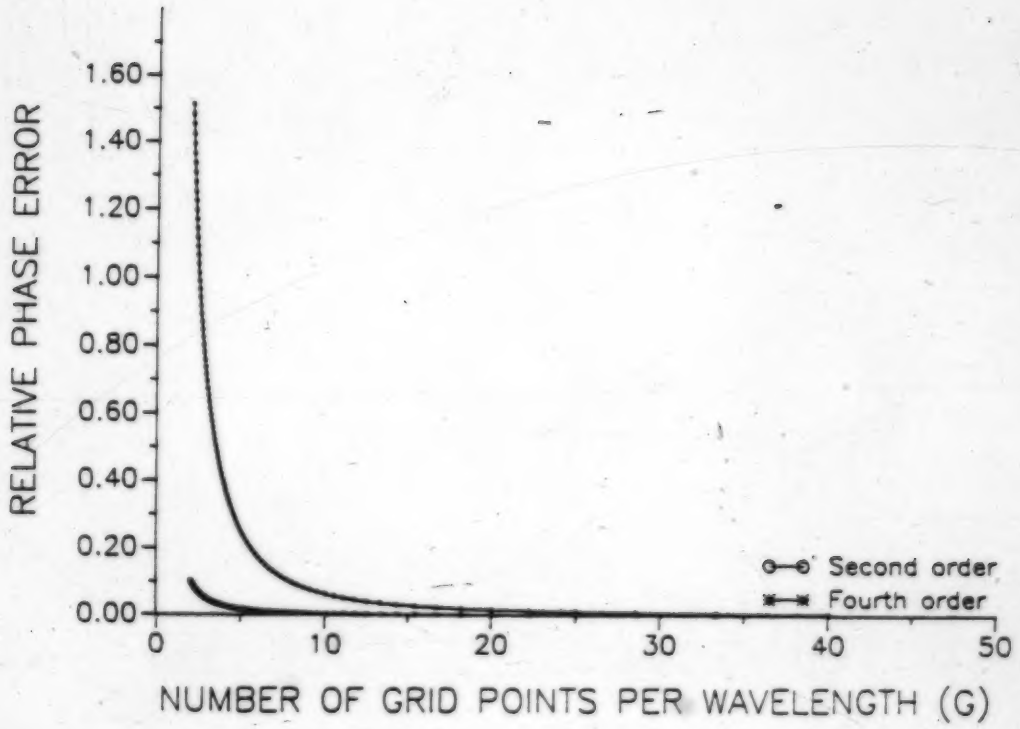

Figure 2.3 The magnitude of the leading terms of the relative phase errors given from equation (2.3.19) for the second order and (2.3.20) for the fourth order as a function of the number of grid points per wavelength (G) for pa=0.25.

2.4 Accuracy test of the numerical schemes

It is a common practice to verify the accuracy of a numerical solution by comparing it with a known exact solution. The local error of the numerical solution can be examined by changing the numerical parameters, i.e. grid spacing, time step etc. It was found earlier that the local error of the numerical scheme (2.2.3) must be a third order function in both the time step and the grid spacing. In this comparison one of the parameters, i.e. the time step, is kept constant while the grid spacing varies. By doubling the number of grid points successively, the grid spacing is halved while the local error must be reduced to one eighth for the second order scheme and to 1/32nd for the fourth order scheme.

The exact solution is constructed for the system (3.2.4) which describes the SH-wave propagation problem in two dimensions. Let the parameters for the medium be the following given functions of x and z:

$$\rho = \frac{3z^2 - x^2}{z^3}, \qquad \mu = -\frac{x^2 + z^2}{z}$$

(2.4.1).

The physical parameters as well as the variables in this case are taken dimensionless. This particular example was chosen because the exact solution can be calculated analytically. The exact particle velocity and the stress components are given by

$$\dot{v} = x\,z \sin t\,, \quad \sigma_{xy} = (x^2 + z^2)\cos t, \quad \sigma_{zy} = \frac{x(x^2 + z^2)}{z}\cos t$$

(2.4.2).

The stress component in the z-direction has a singularity at z = 0. Also the velocity of propagation given by

$$v_s = \sqrt{\frac{\mu}{\rho}} = \sqrt{\frac{z^2(x^2+z^2)}{x^2-3z^2}} \qquad (2.4.3)$$

is singular along the lines $z = \pm x/\sqrt{3}$. Velocity values are real when $x^2-3z^2 \geq 0$.

The considerations above put constraints on the range when numerically solving the problem since near the singularities the local error is affected by the misrepresentation of the singularity in a digital computer. For values of the velocity of propagation near a singularity the stability condition is never satisfied and the numerical procedure is unconditionally unstable. The range $5.0 \leq x \leq 5.9, 0.1 \leq z \leq 1.0$ satisfies the conditions above.

Taking discrete equivalents of the density and the rigidity on a rectangular grid in the region above one can numerically solve this problem using the initial conditions

$$\dot{v} = 0, \quad \sigma_{xy} = (x^2+z^2), \quad \sigma_{zy} = \frac{x(x^2+z^2)}{z} \qquad (2.4.4).$$

For the sake of comparison, the numerical and the exact solutions recorded at a specific location are displayed as functions of time (figure 2.4). Also the relative local error is displayed as a function of time at the same location for three different grid spacings. For the Lax-Wendroff scheme, halving the grid spacing decreases the relative error proportionally to the third power of the grid spacing i.e. it becomes one eighth of the previous error (figure 2.5). For the MacCormack fourth order scheme the relative error becomes 1/32nd of the previous one (figure 2.6).

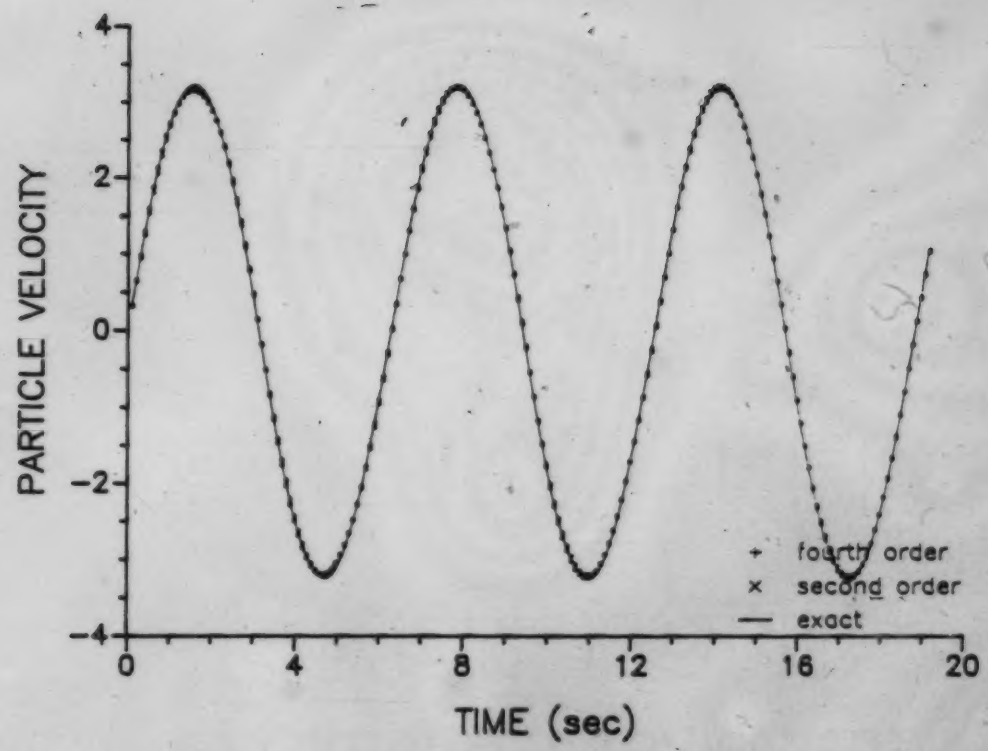

Figure 2.4 Particle velocity responses of the exact and numerical solutions at location (5.4,0.6) with h=0.1 and κ=0.001 sec.

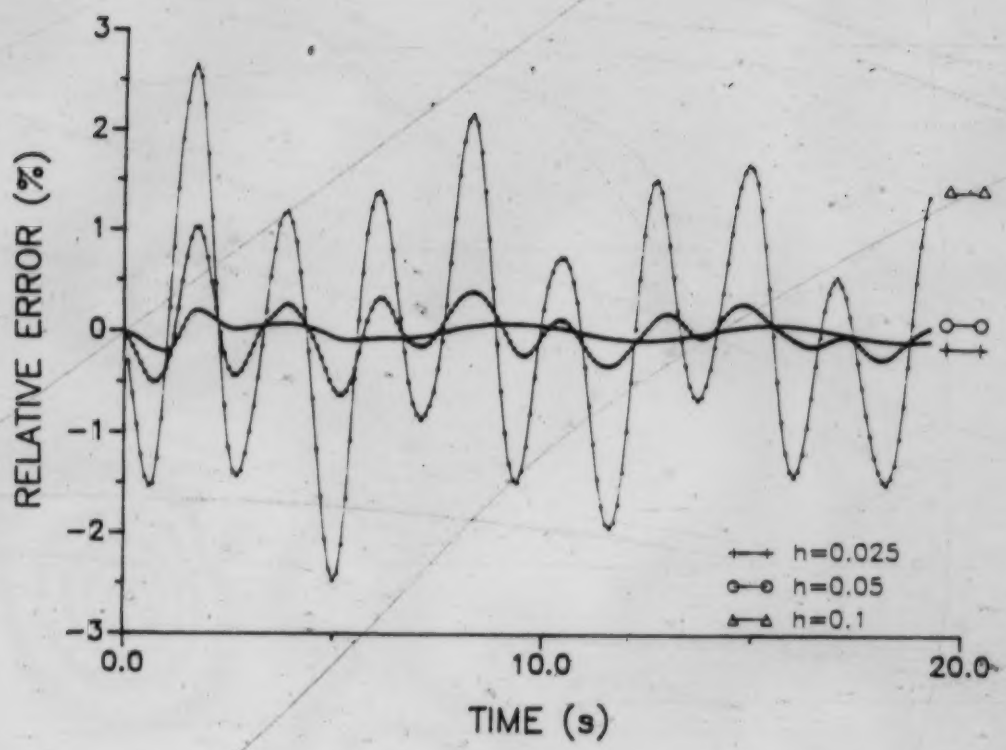

Figure 2.5 Relative error of the Lax-Wendroff scheme for three different grid spacings and the same time step κ=0.001 sec.

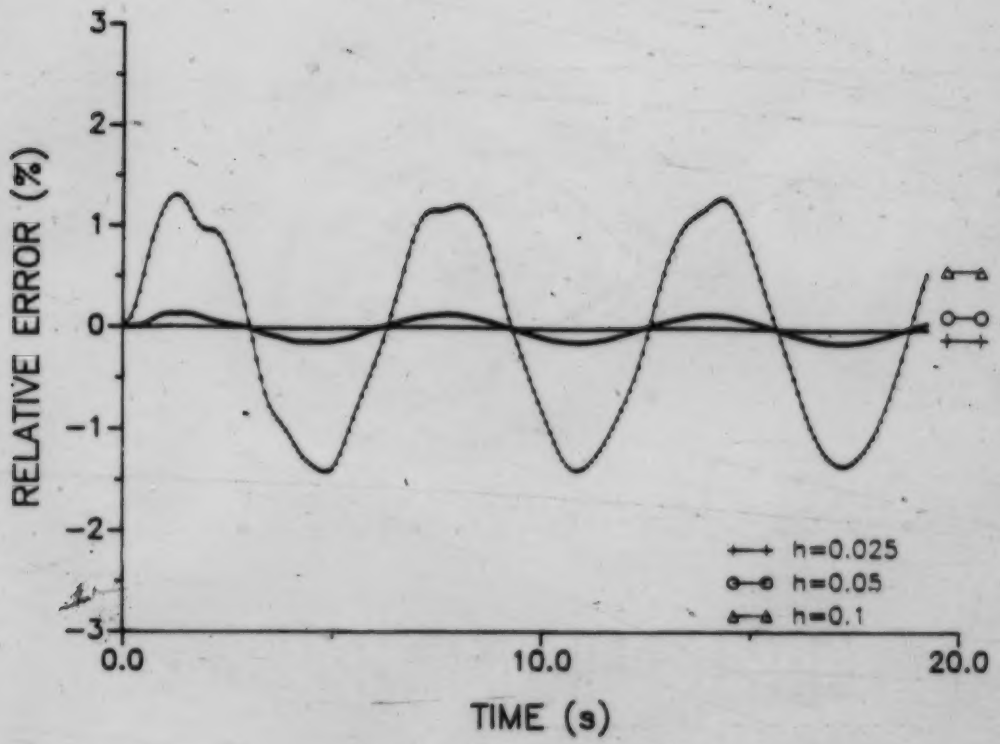

Figure 2.6 The same as in figure 2.5 for the MacCormack type of scheme.

2.5 Finite differences on a vector processor

Finite difference (F.D.) methods have been used successfully to solve the seismic wave equation numerically. Explicit schemes are more popular in two or three dimensional problems since their solution is straightforward. Limitations are set on the spatial interval so that the number of calculations per time step and the memory storage requirement do not make the method excessively expensive. The spatial interval also must be chosen carefully so that spatial aliasing is minimum.

Once the spatial interval has been chosen, the stability condition specifies the maximum time step allowed to avoid instabilities. A major factor in this choice is the model's maximum velocity.

Finite differences can be computationally expensive especially when the spatial resolution is high and/or the velocities in the model are quite large. So the efficiency of the method greatly depends on the technique of calculating the amplitudes per time step.

The advent of supercomputers opens new horizons in the applications of finite differences. Here a new concept of vector operations will be described for a difference equation which corresponds to the simplest heat flow equation in one space dimension

$$\partial_t T(x,t) = \partial_{xx} T(x,t) \qquad (2.5.1)$$

where T(x,t) is the temperature. A second order explicit difference approximation

$$\frac{1}{\kappa} \left(T_x^{t+1} - T_x^t \right) = \frac{1}{h^2} \left(T_{x+1}^t - 2\,T_x^t + T_{x-1}^t \right)$$

can also be written as

$$T_x^{t+1} = q\,T_{x+1}^t + (1-2q)\,T_x^t + q\,T_{x-1}^t$$

$$\text{where } q = \frac{\kappa}{h^2} .$$

(2.5.2).

Suppose that the model consists of four grid points, that is

$$T^t : (T_1, T_2, T_3, T_4) .$$

A differencing star is used to illustrate how the amplitudes in the next step are calculated. By moving the differencing star

$$(q, 1-2q, q)$$

along the vector **T** at the current time step, the amplitudes at the next time step, T^{t+1} are evaluated. Here the amplitudes at different locations are calculated one at a time.

The new generation of vector computers can work faster and more efficiently only if calculations can be done simultaneously at different places. So one has to consider whether equation (2.5.2) can be rewritten to take advantage of vector computation. Equation (2.5.2) can be written as a system of simultaneous equations in matrix form:

$$\begin{bmatrix} T_1 \\ T_2 \\ T_3 \\ T_4 \end{bmatrix}^{t+1} = \begin{bmatrix} 1-2q & q & 0 & 0 \\ q & 1-2q & q & 0 \\ 0 & q & 1-2q & q \\ 0 & 0 & q & 1-2q \end{bmatrix} \begin{bmatrix} T_1 \\ T_2 \\ T_3 \\ T_4 \end{bmatrix}^t$$

(2.5.3)

Instead of evaluating the amplitudes one at a time, one can calculate the vector of amplitudes, **T** , simultaneously.

Matrix-vector multiplication by rows on the right-hand side of equation (2.5.3) makes

use of all the elements of the matrix in the calculation of the product even in cases where this is a sparse matrix. Another method which uses the diagonals of the matrix was developed by Madsen et al (1976). In equation (2.5.3) calculations are performed in three steps:

$$\mathbf{T}^{t+1} = (1-2q)\ \mathbf{T}^{t}$$

$$\mathbf{T}^{t+1}(1;3) = \mathbf{T}^{t}(1;3) + q\,\mathbf{T}^{t}(2;3)$$

$$\mathbf{T}^{t+1}(2;3) = \mathbf{T}^{t}(2;3) + q\,\mathbf{T}^{t}(1;3) \qquad (2.5.4)$$

where $\mathbf{T}(i;j)$ denotes j elements in contiguous locations starting at the ith element; i.e.

$$\mathbf{T}(1;3) \equiv (T_1, T_2, T_3) \quad \text{and } \mathbf{T}(2;3) \equiv (T_2, T_3, T_4)\ . \qquad (2.5.5)$$

This algorithm has two advantages:

1. All calculations are done in contiguous locations of the vectors.

2. Only the necessary calculations are performed in the case of sparse (diagonal) matrices.

This algorithm increases the efficiency of the method on a parallel computer by making it fully vectorized. A similar method can be generated for two dimensional problems where instead of a tridiagonal system there is a set of sparse diagonal matrices whose number of diagonals is equal to the number of elements in the differencing star.

2.6 Matrix times vector by diagonals: The algorithm

The key to the success of this algorithm is the way in which matrices are stored. Previously matrices have been viewed in terms of rows and columns. In most of the scientific programming languages a row or column type storage is assumed. However, storage by diagonals for banded matrices is a very efficient way of minimizing storage

requirements.

In a vector computer every diagonal is considered to be a vector. This type of storage has another advantage when using vector processors. It is easier to do matrix manipulations like transposition etc. The main disadvantage is that the matrix algorithms are more difficult and less intuitive to describe and understand. Also the diagonals have different lengths and there are more diagonals than there are rows and columns.

Madsen, et al (1976) give a description of the matrix multiplication by diagonals both for full and banded matrices. The basic conceptual difference of this method is that instead of forming a row or a column of the product matrix one forms a diagonal. Before proceeding with the description of the algorithm some definitions are necessary. Any matrix $\mathbf{A}$ can be expressed as:

$$\mathbf{A} = \begin{bmatrix} a_0 & a_1 & . & . & a_{k_u} \\ a_{-1} & . & . & . & . \\ . & . & . & . & . \\ a_{-k_l} & . & . & . & . \end{bmatrix} = (a_k),\ k = -k_l, \ldots, 0, \ldots, k_u$$

(2.6.1)

where k_l, k_u the number of lower and upper diagonals respectively and the kth diagonal is defined as

$$a_k = \begin{cases} (a_{i,i+k}) & k \geq 0 \\ (a_{i-k,i}) & k < 0 \end{cases} \qquad i = 1, 2, 3, \ldots..$$

(2.6.2)

Also the element by element product and sumation operations for two vectors α, β are defined by (Abramovici et al, 1987)

$$(\alpha \otimes \beta)_i = \alpha_i \beta_i \quad \text{and} \quad (\alpha \oplus \beta)_i = \alpha_i + \beta_i$$

(2.6.3).

Here the version for the multiplication of a diagonal banded matrix **A** with a vector **x** by diagonals will be described. The algorithm will be illustrated using the graphic representation in figure (2.7) where an intermediate matrix **D** is used. To evaluate the product vector **b** one multiplies each diagonal of **A** by the vector **x**. In case that the matrix **A** is square, **x** has the same length as the main diagonal $\mathbf{a}_0$ in **A**. One performs the product operation (element by element) of the main diagonal $\mathbf{a}_0$ with **x** and stores the result on the main diagonal of **D**, $\mathbf{d}_0 = \mathbf{a}_0\mathbf{x}$. The rest of the diagonals of **A** have less elements than **x**. Thus, the kth upper diagonal of **A** is multiplied with the part of **x** which does not include the upper k elements. Similarly, the kth lower diagonal of **A** is multiplied with the part of **x** which does not include the lower k elements. The results are again stored on the corresponding diagonals of **D**. Finally the elements of **D** are added by rows to form the final result on vector **b** whose mth element is the sum of all the elements in the mth row of **D**. The method can be performed in a similar manner for non-square matrices.

Let **A** be a 3 by 3 matrix, **x**, a 3-vector and **D**, an intermediate 3 by 3 matrix, while **b** is the product 3-vector which can be evaluated conventionally using the row by column multiplication i.e.

$$\mathbf{b} = \mathbf{A}\,\mathbf{x} = \begin{bmatrix} a_{11} & a_{12} & a_{13} \\ a_{21} & a_{22} & a_{23} \\ a_{31} & a_{32} & a_{33} \end{bmatrix} \begin{bmatrix} x_1 \\ x_2 \\ x_3 \end{bmatrix} = \begin{bmatrix} a_{11}x_1 + a_{12}x_2 + a_{13}x_3 \\ a_{21}x_1 + a_{22}x_2 + a_{23}x_3 \\ a_{31}x_1 + a_{32}x_2 + a_{33}x_3 \end{bmatrix}$$

(2.6.4).

The matrix- vector multiplication by diagonals for this example is illustrated by

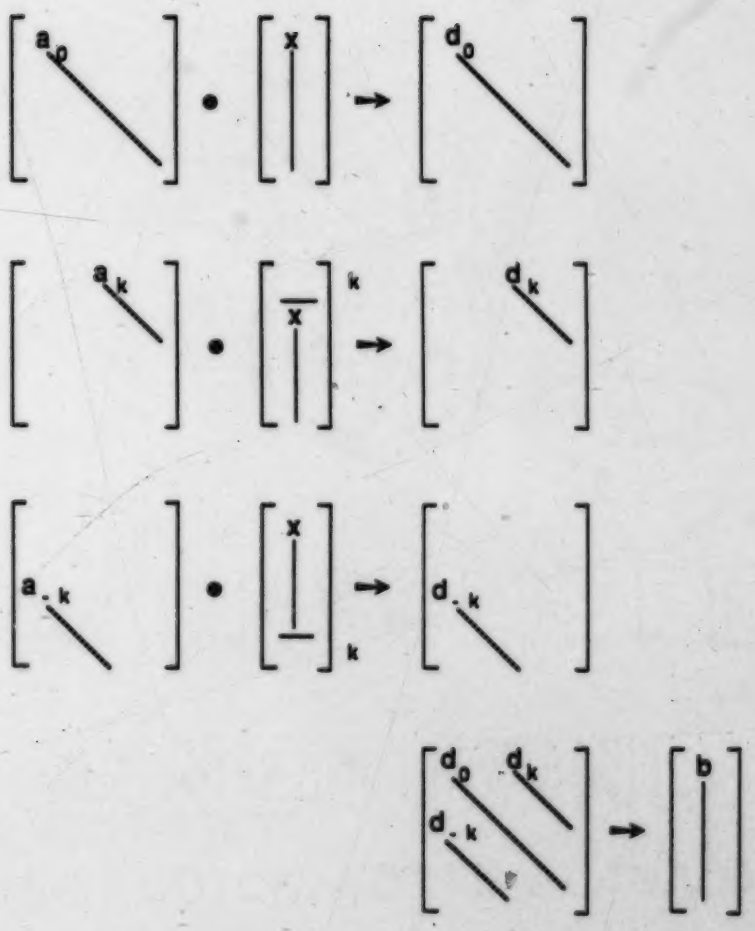

Figure 2.7 Graphic representation of the matrix-vector multiplication by diagonals.

$$\begin{bmatrix} a_{11} & a_{12} & a_{13} \\ a_{21} & a_{22} & a_{23} \\ a_{31} & a_{32} & a_{33} \end{bmatrix} \cdot \begin{bmatrix} x_1 \\ x_2 \\ x_3 \end{bmatrix} \rightarrow \begin{bmatrix} d_{11} & d_{12} & d_{13} \\ d_{21} & d_{22} & d_{23} \\ d_{31} & d_{32} & d_{33} \end{bmatrix} \rightarrow \begin{bmatrix} b_1 \\ b_2 \\ b_3 \end{bmatrix}$$

(2.6.5).

The diagonals of **A** are explicitly denoted by vectors

$$\mathbf{a}_0 : (a_{11}, a_{22}, a_{33}),\ \mathbf{a}_1 : (a_{12}, a_{23}),\ \mathbf{a}_2 : (a_{13}),$$
$$\mathbf{a}_{-1} : (a_{21}, a_{32}),\ \mathbf{a}_{-2} : (a_{31})$$

(2.6.6)

and similarly for the intermediate matrix **D**

$$\mathbf{d}_0 : (d_{11}, d_{22}, d_{33}),\ \mathbf{d}_1 : (d_{12}, d_{23}),\ \mathbf{d}_2 : (d_{13}),$$
$$\mathbf{d}_{-1} : (d_{21}, d_{32}),\ \mathbf{d}_{-2} : (d_{31})$$

(2.6.7).

The product vectors of the diagonals of **A** with the vector **x** are computed using equation (2.6.3) and are stored on the diagonals of **D**

$$\mathbf{d}_0 : (a_{11}x_1, a_{22}x_2, a_{33}x_3)$$
$$\mathbf{d}_1 : (a_{12}x_2, a_{23}x_3)$$
$$\mathbf{d}_2 : (a_{13}x_3)$$
$$\mathbf{d}_{-1} : (a_{21}x_1, a_{32}x_2)$$
$$\mathbf{d}_{-2} : (a_{31}x_1)\ .$$

(2.6.8).

Then the elements of every row of **D** are added and the result is stored on the vector **b**.

$$b_1 = d_{11} + d_{12} + d_{13}$$
$$b_2 = d_{21} + d_{22} + d_{23}$$
$$b_3 = d_{31} + d_{32} + d_{33}$$

(2.6.9).

The following algorithm for multiplication of a square matrix with a vector will be utilized in the finite difference method. Let $\mathbf{b} = 0$,

1) For $k = 0, 1, \ldots k_u$ compute

$$\mathbf{b}(;k) = \mathbf{b}(;k) \oplus \mathbf{a}_k \otimes \mathbf{x}(k;)$$

2) For $k = 1, \ldots k_l$ compute

$$\mathbf{b}(k;) = \mathbf{b}(k;) \oplus \mathbf{a}_{-k} \otimes \mathbf{x}(;k)$$

where the quantities inside parentheses are used to denote selected elements of the vectors as:

$$\mathbf{x}(k;) : (x_{k+1}, \ldots x_n) \text{ and } \mathbf{x}(;k) : (x_1, \ldots x_{n-k}) .$$

Since only vector operations (i.e. one vector multiplication and one vector addition) are involved in this algorithm, it is suitable for vector computers. Comparison of execution times for sufficient size narrow banded matrices, has shown that this algorithm is more efficient than the row by vector multiplication. Since all of the matrices involved in finite differences are banded matrices, matrix times vector by diagonals is preferable.

CHAPTER 3

FINITE DIFFERENCES ON THE SH WAVE EQUATION

3.1 Introduction

The advent of the new generation of supercomputers motivated this work towards simulations of wave propagation with higher accuracy in two dimensional inhomogeneous media. Programs written for conventional computersthey do not take advantage of vector computation. It is difficult to fully vectorize an existing program without changing the algorithm while the benefits from the automatic vectorization are limited. We follow the semantic vectorization (see Appendix B for a description of vectorization techiques) approach in which the numerical parts of the program are fully vectorized. The result is pronounced in both execution time and in handling quite large models. In this way a breakthrough in the limits of effectiveness of the finite differences is accomplished. The larger virtual memory of the supercomputers results in finer grids which dramatically minimize the dispersion effects even for the popular second order schemes. The low cost of the method suggests that extension to three dimensions is possible.

The basic equations of motion as well as the stress-strain relations have been implemented instead of the actual wave equation in order to avoid numerical derivatives for the medium's parameters (Virieux, 1984, 1986). One of the key factors in forward modelling is the implementation of the source. Since we are working with the two dimensional problem, an axial symmetry is implied and it is more natural to use a line

source. The solution of the two dimensional SH wave equation in an homogeneous infinitely extended medium with a line source is well known (Aki and Richards, 1980). Convolving the impulse response with the source excitation results in an integral which can be numerically evaluated (Romberg or Gauss integration). A Gaussian function whose frequency response is band limited with a known peak frequency describes the source excitation.

In order to simulate spherical spreading a point source has also been implemented for the same model. The shape of this source function is changed in a minor fashion by the finite difference operator since this source does not satisfy the two dimensional wave equation.

Finally the flow chart of the finite difference algorithm is described and numerical results are compared and tested with the exact solution for the problem of two half spaces separated by an interface.

3.2 Problem formulation

The basic equation for two dimensional SH-wave propagation in a heterogeneous isotropic medium is:

$$\rho(x,z)\frac{\partial^2 v(x,z,t)}{\partial t^2} = \frac{\partial}{\partial x}\left(\mu(x,z)\frac{\partial v(x,z,t)}{\partial x}\right) + \frac{\partial}{\partial z}\left(\mu(x,z)\frac{\partial v(x,z,t)}{\partial z}\right) \qquad (3.2.1)$$

where $v(x, z, t)$ is the displacement, $\mu(x, z)$ is the shear modulus, $\rho(x, z)$ is the density and ∂ denotes partial derivative. Body forces have been neglected.

Instead of approximating the second order hyperbolic wave equation one can use an equivalent first order system (Virieux, 1984, 1986, Bayliss et al, 1986). This can be derived from the equation of motion

$$\partial_t \dot{v}\,(x,z,t) = \rho^{-1}\,(x,z)\;[\partial_x \sigma_{xy}(x,z,t) + \partial_z \sigma_{zy}(x,z,t)]$$

(3.2.2)

and the stress-strain relations after taking derivatives with respect to time

$$\partial_t \sigma_{xy}(x,z,t) = \mu(x,z)\;\partial_x \dot{v}\,(x,z,t)$$

$$\partial_t \sigma_{zy}(x,z,t) = \mu(x,z)\;\partial_z \dot{v}(x,z,t)$$

(3.2.3)

where the dot denotes time derivative and $\sigma_{xy}(x, z, t)$ and $\sigma_{zy}(x, z, t)$ are the stress components. In this formulation the space derivatives of $\mu(x,z)$ are avoided.

In matrix form we get

$$\partial_t \begin{bmatrix} \dot{v} \\ \sigma_{xy} \\ \sigma_{zy} \end{bmatrix} = \begin{bmatrix} 0 & \rho^{-1} & 0 \\ \mu & 0 & 0 \\ 0 & 0 & 0 \end{bmatrix} \partial_x \begin{bmatrix} \dot{v} \\ \sigma_{xy} \\ \sigma_{zy} \end{bmatrix} + \begin{bmatrix} 0 & 0 & \rho^{-1} \\ 0 & 0 & 0 \\ \mu & 0 & 0 \end{bmatrix} \partial_z \begin{bmatrix} \dot{v} \\ \sigma_{xy} \\ \sigma_{zy} \end{bmatrix}$$

or

$$\partial_t \mathbf{U} = \mathbf{A}\,\partial_x \mathbf{U} + \mathbf{B}\,\partial_z \mathbf{U}$$

(3.2.4).

Since the system in equation (3.2.4) can also be written in the form

$$\begin{bmatrix} \rho & 0 & 0 \\ 0 & \mu^{-1} & 0 \\ 0 & 0 & \mu^{-1} \end{bmatrix} \partial_t \begin{bmatrix} \dot{v} \\ \dot{\sigma}_{xy} \\ \dot{\sigma}_{zy} \end{bmatrix} = \begin{bmatrix} 0 & 1 & 0 \\ 1 & 0 & 0 \\ 0 & 0 & 0 \end{bmatrix} \partial_x \begin{bmatrix} \dot{v} \\ \sigma_{xy} \\ \sigma_{zy} \end{bmatrix} + \begin{bmatrix} 0 & 0 & 1 \\ 0 & 0 & 0 \\ 1 & 0 & 0 \end{bmatrix} \partial_z \begin{bmatrix} \dot{v} \\ \sigma_{xy} \\ \sigma_{zy} \end{bmatrix}$$

or

$$\mathbf{E}_0\,\partial_t\,\mathbf{U} = \mathbf{A}_0\,\partial_x\,\mathbf{U} + \mathbf{B}_0\,\partial_z\,\mathbf{U} \qquad (3.2.5)$$

where $\mathbf{A}_0$, $\mathbf{B}_0$, $\mathbf{E}_0$ are real symmetric matrices, this system is hyperbolic (see section 2.2).

Formulation (3.2.4) maintains a certain symmetry between velocity and stress so that density and shear modulus are concentrated at the nodes. In contrast, when the formulation (3.2.1) is approximated with the method of Tikhonov and Samarskii (Boore, 1972) the averaged shear modulus is used over a grid mesh. Formulation (3.2.5) is divergence free and it will be used in the MacCormack type scheme.

The Lax-Wendroff scheme (2.2.4), when applied to the SH wave equation, gives rise to the following difference equations after some straightforward algebraic manipulations :

$$\begin{aligned}
\dot{v}^{\,n+1}_{j,m} = {} & \Big[\, 1 - \frac{p^2}{4}\rho^{-1}_{j,m}\left(\mu_{j+1,m} + \mu_{j-1,m} + \mu_{j,m+1} + \mu_{j,m-1} + 4\,\mu_{j,m}\right)\Big]\,\dot{v}^{\,n}_{j,m} \\
& + \frac{p^2}{4}\rho^{-1}_{j,m}\left(\mu_{j+1,m} + \mu_{j,m}\right)\,\dot{v}^{\,n}_{j+1,m} + \frac{p}{2}\rho^{-1}_{j,m}(\sigma_{xy})^n_{j+1,m} \\
& + \frac{p^2}{4}\rho^{-1}_{j,m}\left(\mu_{j-1,m} + \mu_{j,m}\right)\,\dot{v}^{\,n}_{j-1,m} - \frac{p}{2}\rho^{-1}_{j,m}\,(\sigma_{xy})^n_{j-1,m} \\
& + \frac{p^2}{4}\rho^{-1}_{j,m}\left(\mu_{j,m+1} + \mu_{j,m}\right)\,\dot{v}^{\,n}_{j,m+1} + \frac{p}{2}\rho^{-1}_{j,m}\,(\sigma_{zy})^n_{j,m+1} \\
& + \frac{p^2}{4}\rho^{-1}_{j,m}\left(\mu_{j,m-1} + \mu_{j,m}\right)\,\dot{v}^{\,n}_{j,m-1} - \frac{p}{2}\rho^{-1}_{j,m}\,(\sigma_{zy})^n_{j,m-1}
\end{aligned} \qquad (3.2.6)$$

$$(\sigma_{xy})^{n+1}_{j,m} = \left[1 - \frac{p^2}{4} \mu_{j,m} (\rho^{-1}_{j+1,m} + \rho^{-1}_{j-1,m} + 2\rho^{-1}_{j,m}) \right] (\sigma_{xy})^{n}_{j,m}$$

$$+ \frac{p^2}{4} \mu_{j,m} (\rho^{-1}_{j+1,m} - 2\rho^{-1}_{j,m} + \rho^{-1}_{j-1,m}) (\sigma_{zy})^{n}_{j,m}$$

$$+ \frac{p^2}{4} \mu_{j,m} (\rho^{-1}_{j+1,m} + \rho^{-1}_{j,m}) (\sigma_{xy})^{n}_{j+1,m} + \frac{p^2}{4} \mu_{j,m} (\rho^{-1}_{j,m} + \rho^{-1}_{j-1,m}) (\sigma_{xy})^{n}_{j-1,m}$$

$$+ \frac{p^2}{4} \mu_{j,m} (\rho^{-1}_{j,m} - \rho^{-1}_{j-1,m}) (\sigma_{zy})^{n}_{j,m+1} - \frac{p^2}{4} \mu_{j,m} (\rho^{-1}_{j+1,m} - \rho^{-1}_{j,m}) (\sigma_{zy})^{n}_{j,m-1}$$

$$+ \frac{p}{2} \mu_{j,m} (\dot{v}^{n}_{j+1,m} - \dot{v}^{n}_{j-1,m})$$

$$+ \frac{p^2}{8} \mu_{j,m} \rho^{-1}_{j,m} \left[(\sigma_{zy})^{n}_{j+1,m+1} - (\sigma_{zy})^{n}_{j-1,m+1} - (\sigma_{zy})^{n}_{j+1,m-1} + (\sigma_{zy})^{n}_{j-1,m-1} \right]$$

(3.2.7)

$$(\sigma_{zy})^{n+1}_{j,m} = \left[1 - \frac{p^2}{4} \mu_{j,m} (\rho^{-1}_{j,m+1} + \rho^{-1}_{j,m-1} + 2\rho^{-1}_{j,m}) \right] (\sigma_{zy})^{n}_{j,m}$$

$$+ \frac{p^2}{4} \mu_{j,m} (\rho^{-1}_{j,m+1} - 2\rho^{-1}_{j,m} + \rho^{-1}_{j,m-1}) (\sigma_{xy})^{n}_{j,m}$$

$$+ \frac{p^2}{4} \mu_{j,m} (\rho^{-1}_{j,m+1} + \rho^{-1}_{j,m}) (\sigma_{zy})^{n}_{j,m+1} + \frac{p^2}{4} \mu_{j,m} (\rho^{-1}_{j,m} + \rho^{-1}_{j,m-1}) (\sigma_{zy})^{n}_{j,m-1}$$

$$+ \frac{p^2}{4} \mu_{j,m} (\rho^{-1}_{j,m} - \rho^{-1}_{j,m-1}) (\sigma_{xy})^{n}_{j+1,m} - \frac{p^2}{4} \mu_{j,m} (\rho^{-1}_{j,m+1} - \rho^{-1}_{j,m}) (\sigma_{xy})^{n}_{j-1,m}$$

$$+ \frac{p}{2} \mu_{j,m} (\dot{v}^{n}_{j,m+1} - \dot{v}^{n}_{j,m-1})$$

$$+ \frac{p^2}{8} \mu_{j,m} \rho^{-1}_{j,m} \left[(\sigma_{xy})^{n}_{j+1,m+1} - (\sigma_{xy})^{n}_{j-1,m+1} - (\sigma_{xy})^{n}_{j+1,m-1} + (\sigma_{xy})^{n}_{j-1,m-1} \right]$$

(3.2.8).

Given the values of the particle velocity and the stress components at time n equations (3.2.6) to (3.2.8) calculate the values at n+1.

The MacCormack type of scheme described by equations (2.2.10) can also be similarly written for the one dimensional systems which describe SH wave propagation. The predictor and the corrector equations for the particle velocity in the x-direction are :

$$\dot{v}^{(1)}_{j,m} = \dot{v}^{n}_{j,m} - \frac{p}{6}\,\rho^{-1}_{j,m}\,(7\,(\sigma_{xy})^{n}_{j,m} - 8\,(\sigma_{xy})^{n}_{j+1,m} + (\sigma_{xy})^{n}_{j+2,m})$$

$$\dot{v}^{n+1}_{j,m} = \frac{1}{2}(\dot{v}^{(1)}_{j,m} + \dot{v}^{n}_{j,m}) + \frac{p}{12}\,\rho^{-1}_{j,m}\,(7\,(\sigma_{xy})^{(1)}_{j,m} - 8\,(\sigma_{xy})^{(1)}_{j-1,m} + (\sigma_{xy})^{(1)}_{j-2,m}) \qquad (3.2.9)$$

while in the z-direction

$$\dot{v}^{(1)}_{j,m} = \dot{v}^{n}_{j,m} - \frac{p}{6}\,\rho^{-1}_{j,m}\,(7\,(\sigma_{zy})^{n}_{j,m} - 8\,(\sigma_{zy})^{n}_{j,m+1} + (\sigma_{zy})^{n}_{j,m+2})$$

$$\dot{v}^{n+1}_{j,m} = \frac{1}{2}(\dot{v}^{(1)}_{j,m} + \dot{v}^{n}_{j,m}) + \frac{p}{12}\,\rho^{-1}_{j,m}\,(7\,(\sigma_{zy})^{(1)}_{j,m} - 8\,(\sigma_{zy})^{(1)}_{j,m-1} + (\sigma_{zy})^{(1)}_{j,m-2}) \qquad (3.2.10).$$

Similar expressions can be derived for the stress components (see Appendix C). The splitting technique described by equation (2.2.8) can be performed in the following steps:

(1) the vector of displacements is calculated at time step n+1/2 taking into account wave propagation in the x-direction only (for particle velocity equation (3.2.9) is applied to the vector at time n);

(2) the same vector is evaluated at time step n+1 taking into account wave propagation in the z-direction only (for particle velocity equation (3.2.10) is applied to the vector at time n+1/2);

(3) alternate expressions to equation(3.2.10) in the spirit of equation (2.2.11) are applied for the particle velocity at time n+3/2 for wave propagation in the z-direction (similarly for

the stress components) ;

(4) the vector of displacements is calculated at time n+2 from alternate equations to the ones applied in step (1).

The maximum eigenvalue of the matrices **A**, **B** can be found $a_m=\sqrt{\mu\,\rho^{-1}} = v_s$ and the stability conditions are $pv_s \le \frac{1}{2\sqrt{2}}$ and $pv_s \le \frac{2}{3}$ where v_s is the S-velocity.

3.3 Lax-Wendroff scheme for the SH hyperbolic system on the CYBER 205

We have already mentioned that a difference equation can be written in a matrix form. This formulation has the advantage of vectorizing the finite difference algorithms. Defining the columns of a matrix

$$(\dot{v}_{jm}) \quad j = 1, \ldots J \;), m = 1, \ldots M$$

as :

$$\mathbf{V}_m = (\dot{v}_{jm}) \quad j = 1, \ldots J$$

where M,J denote the number of columns and rows respectively, then a vector is constructed by setting the columns in subsequent locations as:

$$\mathbf{V} = (\mathbf{V}_m^T) \;\; m = 1, \ldots, M \qquad (3.3.1)$$

where T denotes transpose. This vector notation will be used for representing the displacement components as well as the medium parameters.

For the Lax-Wendroff scheme the particle velocity response at the next time step is

calculated at a particular grid point (x_j, z_m) from equation (3.2.6). In order to calculate the particle velocity response at the next time for the entire model, a system of difference equations has to be solved. This system can be written in matrix form :

$$V^{n+1} = A\, V^n \oplus B\, \Phi^n \oplus C\, \Psi^n \qquad (3.3.2)$$

where the vectors V, Φ, Ψ denote the particle velocity and the stress component vectors, σ_{xy}, σ_{zy} according to definition (3.3.1) and A, B, C are sparse coefficient matrices. Equation (2.6.3) defines the $\oplus$ summation operator. The elements of the kth row in these matrices correspond to the coefficients of the kth equation in the system. In fact the structure of these matrices is such that they can be stored in diagonals,

$$A = (a_{-J}, a_{-1}, a_0, a_1, a_J), \quad B = (b_{-1}, b_1) \quad \text{and} \quad C = (c_{-J}, c_J) \qquad (3.3.3).$$

Since every diagonal corresponds to one point of the computational star, the number of diagonals is equal to the number of points involved in the difference operator. The main diagonal a_0 can be described by a vector

$$a_0 : (a_0)_m \quad m = 1, \ldots, M$$

$$\text{with} \quad (a_0)_m : \quad 1 - \frac{p^2}{4} \rho_{j,m}^{-1} (\mu_{j+1,m} + \mu_{j,m+1} + 4\mu_{j,m} + \mu_{j,m-1} + \mu_{j-1,m}), \quad j = 1, \ldots, J. \qquad (3.3.4).$$

The diagonals that correspond to the points shifted once in the x-direction, have the following structure:

$$a_1 : (a_1)_m \qquad m = 1, \ldots, M$$

$$\text{with} \quad (a_1)_m : \quad \frac{p^2}{4} \rho_{j,m}^{-1} (\mu_{j+1,m} + \mu_{j,m}) \qquad j = 1, \ldots, J-1$$

$$: \quad 0 \qquad j = J, \; m \neq M$$

$$: \quad \text{no elements} \qquad j = J, \; m = M \qquad (3.3.5)$$

and

$$\begin{aligned} &\mathbf{a}_{-1} : (\mathbf{a}_{-1})_m \qquad m = 1, ..., M \\ &\text{with} \quad (\mathbf{a}_{-1})_m : \frac{p^2}{4} \rho_{j,m}^{-1} (\mu_{j-1,m}+\mu_{j,m}) \qquad j = 2, ..., J \\ &\qquad\qquad\quad : 0 \qquad\qquad\qquad\qquad\quad j = 1, \ m\neq 1 \\ &\qquad\qquad\quad : \text{no elements} \qquad\qquad j = 1, \ m=1 \end{aligned}$$

(3.3.6)

for the matrix **A**. In this notation, the intermediate vectors denoted by $(\mathbf{a})_m$ show the relation between the structure of the diagonal and the model indices. Also for matrix $\mathbb{B}$, the corresponding diagonals are given by:

$$\begin{aligned} &\mathbf{b}_1 : (\mathbf{b}_1)_m \qquad m = 1, ..., M \\ &\text{with} \quad (\mathbf{b}_1)_m : \frac{p}{2} \rho_{j,m}^{-1} \qquad\qquad j = 1, ..., J-1 \\ &\qquad\qquad\quad : 0 \qquad\qquad\qquad\quad j = J, \ m\neq M \\ &\qquad\qquad\quad : \text{no elements} \qquad j = J, \ m=M \end{aligned}$$

(3.3.7)

and

$$\begin{aligned} &\mathbf{b}_{-1} : (\mathbf{b}_{-1})_m \qquad m = 1, ..., M \\ &\text{with} \quad (\mathbf{b}_{-1})_m : -\frac{p}{2} \rho_{j,m}^{-1} \qquad\qquad j = 2, ..., J \\ &\qquad\qquad\quad : 0 \qquad\qquad\qquad\quad j = 1, \ m\neq 1 \\ &\qquad\qquad\quad : \text{no elements} \qquad j = 1, \ m=1 \end{aligned}$$

(3.3.8).

Similarly the diagonals for **A** shifted to the z-direction are described by:

$$\begin{aligned} &\mathbf{a}_J : (\mathbf{a}_J)_m \qquad m = 1, ..., M-1 \\ &\text{where} \quad (\mathbf{a}_J)_m : \frac{p^2}{4} \rho_{j,m}^{-1} (\mu_{j,m+1}+\mu_{j,m}) \qquad j = 1, ..., J \end{aligned}$$

(3.3.9)

and

$$a_{-J}: (a_{-J})_m \qquad m = 2, \ldots, M$$
$$\text{where } (a_{-J})_m : \frac{p^2}{4} \rho_{j,m}^{-1}(\mu_{j,m-1}+\mu_{j,m}) \qquad j = 1, \ldots, J$$

(3.3.10)

while for $\mathbb{C}$

$$c_J: (c_J)_m \qquad m = 1, \ldots, M-1$$
$$\text{where } (c_J)_m : \frac{p}{2} \rho_{j,m}^{-1} \qquad j = 1, \ldots, J$$

(3.3.11)

and

$$c_{-J}: (c_{-J})_m \qquad m = 2, \ldots, M$$
$$\text{where } (c_{-J})_m : -\frac{p}{2} \rho_{j,m}^{-1} \qquad j = 1, \ldots, J$$

(3.3.12).

Similarly the diagonals shifted in both x-and z-direction are described. Also matrix form expressions exist for the difference systems that correspond to the stress components

$$\Phi^{n+1} = D\, V^n \oplus E\, \Phi^n \oplus F\, \Psi^n$$

(3.3.13)

$$\Psi^{n+1} = G\, V^n \oplus H\, \Phi^n \oplus J\, \Psi^n$$

(3.3.14).

Since expressions (3.3.2), (3.3.13) and (3.3.14) consist of vector operations they can be implemented efficiently in a vector computer. Matrix-vector multiplications are performed using the technique of multiplication by diagonals which is fully vectorizable and more efficient for banded matrices. The total number of vector operations during one time step in the Lax-Wendroff scheme is 33 additions and 33 multiplications.

Since the coefficient matrices are time independent, they do not have to be evaluated at every time step. So given the physical parameters, one can evaluate the elements of these

matrices and store them by diagonals.This kind of storage is economic for sparse banded matrices because a limited number of diagonal vectors are required for storing the non-zero elements instead of storing all elements. Still, for a typical model of 240X240 (one large page on a CYBER 205) grid points, a large amount of memory is required (around 11 large pages for the coefficient matrices). The large virtual memory of a CYBER 205 supercomputer can handle this problem but a lot of time is spent in moving these matrices in and out of the 2M-word real memoryof the CYBER 205 as it is configured at the University of Calgary.

The particle velocity and the stress components are stored in vectors by columns according to definition (3.3.1). Then they are evaluated at the next time step using the vectorized equations. For 3000 time steps this implementation takes about 3 minutes decreasing the execution time by a factor of ten with respect to the non-vectorized one.

3.4 A MacCormack type scheme for the SH hyperbolic system on the CYBER 205

Following the same procedure as for the Lax-Wendroff scheme the systems for the McCormack type of scheme which correspond to equations (3.2.9) can be written in matrix form as

$$V^{(1)} = V^n \oplus \frac{p}{6}\ \rho^{-1} \otimes (\mathbb{Q}\ \Phi^n)$$

$$V^{n+1} = \frac{1}{2}\ (V^{(1)} \oplus V^n) \oplus \frac{p}{12}\ \rho^{-1} \otimes (\mathbb{S}\ \Phi^{(1)}) \qquad (3.4.1)$$

and to equations (3.2.10),

$$V^{(1)} = V^n \oplus \frac{p}{6}\ \rho^{-1} \otimes (\mathbb{R}\ \Psi^n)$$

$$V^{n+1} = \frac{1}{2}\ (V^{(1)} \oplus V^n) \oplus \frac{p}{12}\ \rho^{-1} \otimes (\mathbb{Y}\ \Psi^{(1)})$$

(3.4.2)

where ρ, μ are the density and rigidity vectors and Q, S, R, Y are constant sparse matrices described in terms of their diagonals as

$$Q = (Q_0, Q_1, Q_2),\quad S = (S_{-2}, S_{-1}, S_0),\quad R = (R_0, R_J, R_{2J}) \text{ and } Y = (Y_{-2J}, Y_{-J}, Y_0)$$

(3.4.3).

Define a bit vector of k elements as I(i, j; k), it consists of a pattern of 0's and 1's. Begining with a 1 bit, a pattern of i, 1 bits followed by j, 0 bits is repeated until the vector is filled. For example the vector I(2, 1; 9) = (1, 1, 0, 1, 1, 0, 1, 1, 0). Therefore the diagonals can be expressed as

$$Q_0 = -S_0 = R_0 = -Y_0 = -7\ I\ (J, 0; JxM)$$
$$Q_1 = -S_{-1} = 8\ I\ (J-1, 1; (JxM) - 1)$$
$$Q_2 = -S_{-2} = -I\ (J-2, 2; (JxM) - 2)$$
$$R_J = -Y_{-J} = 8\ I\ (J, 0; Jx(M - 1))$$
$$R_{2J} = -Y_{-2J} = -I\ (J, 0; Jx(M - 2))$$

(3.4.4).

Similar expressions can be derived for the equations of the stress components as well as the equations at alternate steps (see Appendix C). This formulation is also vectorizable consisting of nine vector additions and nine vector multiplications. There are four predictor-corrector pairs per component per two iterations. The total number of vector operations per iteration is 54.

Comparing with the Lax-Wendroff algorithm the number of operations per time step is almost double while the memory requirement is three times less. In this algorithm there is

no need to store a priori the matrices while the matrix multiplications involved can be implemented using successive WHILE statements and linked triads (see appendix B). The medium's parameters are involved in a straigthforward manner. The simplicity of the algorithm makes it sufficiently flexible to include anisotropy or to extend it to three dimensions.

As an example we consider the predictor equation in (3.4.1)

$$V^{(1)} = V^n \oplus \frac{p}{6}\ \rho^{-1} \otimes (\mathbb{Q}\ \Phi^n)$$

For the one dimensional problem with m=1 and j=1, 2, 3, 4 this equation can be written explicitly as

$$\begin{bmatrix} \dot{v}_1 \\ \dot{v}_2 \\ \dot{v}_3 \\ \dot{v}_4 \end{bmatrix}^{(1)} = \begin{bmatrix} \dot{v}_1 \\ \dot{v}_2 \\ \dot{v}_3 \\ \dot{v}_4 \end{bmatrix}^n \oplus \frac{p}{6} \begin{bmatrix} \rho_1^{-1} \\ \rho_2^{-1} \\ \rho_3^{-1} \\ \rho_4^{-1} \end{bmatrix} \otimes \left(\begin{bmatrix} -7 & 8 & -1 & 0 \\ 0 & -7 & 8 & -1 \\ 0 & 0 & -7 & 8 \\ 0 & 0 & 0 & -7 \end{bmatrix} \begin{bmatrix} (\sigma_{xy})_1 \\ (\sigma_{xy})_2 \\ (\sigma_{xy})_3 \\ (\sigma_{xy})_4 \end{bmatrix}^n \right) \tag{3.4.5}$$

Hence, the 3-point operator corresponds to a tridiagonal matrix. This form can be obtained by writing explicitly all the equations for j = 1, 2, 3, 4.

For a two dimensional model with m = 1, 2 and j = 1, 2, 3, the results are quite similar. Then, instead of a vector V, we have a matrix of particle velocities ,

$$\begin{bmatrix} \dot{v}_{11} & \dot{v}_{12} \\ \dot{v}_{21} & \dot{v}_{22} \\ \dot{v}_{31} & \dot{v}_{32} \end{bmatrix} \tag{3.4.6}$$

This matrix is mapped into a vector by associating the locations in equation (3.4.6) with vector components in a column arrangement

$$\begin{bmatrix} 1 & 4 \\ 2 & 5 \\ 3 & 6 \end{bmatrix}$$

So the vector of particle velocities is: $\mathbf{V} = \left[\dot{v}_{11}, \dot{v}_{21}, \dot{v}_{31}, \dot{v}_{12}, \dot{v}_{22}, \dot{v}_{32} \right]^T$

(3.4.7)

and the equations in matrix form are

$$\begin{bmatrix} \dot{v}_{11} \\ \dot{v}_{21} \\ \dot{v}_{31} \\ \dot{v}_{12} \\ \dot{v}_{22} \\ \dot{v}_{32} \end{bmatrix}^{(1)} = \begin{bmatrix} \dot{v}_{11} \\ \dot{v}_{21} \\ \dot{v}_{31} \\ \dot{v}_{12} \\ \dot{v}_{22} \\ \dot{v}_{32} \end{bmatrix}^{n} \oplus \frac{p}{6} \begin{bmatrix} \rho_{11}^{-1} \\ \rho_{21}^{-1} \\ \rho_{31}^{-1} \\ \rho_{12}^{-1} \\ \rho_{22}^{-1} \\ \rho_{32}^{-1} \end{bmatrix} \otimes \left(\begin{bmatrix} -7 & 8 & -1 & 0 & 0 & 0 \\ 0 & -7 & 8 & 0 & 0 & 0 \\ 0 & 0 & -7 & 0 & 0 & 0 \\ 0 & 0 & 0 & -7 & 8 & -1 \\ 0 & 0 & 0 & 0 & -7 & 8 \\ 0 & 0 & 0 & 0 & 0 & -7 \end{bmatrix} \begin{bmatrix} \sigma_{11} \\ \sigma_{21} \\ \sigma_{31} \\ \sigma_{12} \\ \sigma_{22} \\ \sigma_{32} \end{bmatrix}^{n} \right) \tag{3.4.8}$$

where σ denotes for simplicity the stress component σ_{xy}.

3.5 The source

Source design is one of the main concerns in finite differences. For two dimensional problems line sources perpendicular to the plane of propagation have been used (Alford et al, 1974). This type of source has two-dimensional spreading and it is illuminating in an axially symmetric three-dimensional medium. Since line sources can not be physically realized, we want to design a point source with three-dimensional spreading. For generation of the wavefield, the SH wave equation in a homogeneous three-dimensional medium with an isotropic point source is used. The analytical solution for the displacement can be evaluated from the Green's function in a free infinite space. For a point source located at $\mathbf{r} = \mathbf{r}_s$ the displacement in the y-direction is given by:(Tarantola, 1984)

$$v(\mathbf{r},t) = \frac{1}{4\pi} \frac{S\left(t - \frac{|\mathbf{r} - \mathbf{r}_s|}{c}\right)}{|\mathbf{r} - \mathbf{r}_s|} \qquad (3.5.1)$$

or in a two dimensional medium with three dimensional spreading:

$$v(x,y=0,z,t;\ x_s,y_s=0,z_s) = \frac{1}{4\pi} \frac{S\left(t - \frac{d}{c}\right)}{d} \qquad (3.5.2)$$

where c is the velocity and

$$d = \sqrt{(x-x_s)^2 + (z-z_s)^2}$$

(3.5.3).

The time variation of the source distribution, taken as a Gaussian function, is

$$S(t) = C\, e^{-\sigma(t-t_1)^2}$$

(3.5.4)

where σ and C are constants and t_1 is a positive time delay.

The particle velocity is given by

$$\dot{v} = \frac{\partial v}{\partial t} = \frac{1}{4\pi d}\frac{\partial S}{\partial t} = -\frac{C\sigma(t-t_1-\frac{d}{c})}{2\pi d}\; e^{-\sigma(t-t_1-\frac{d}{c})^2}$$

(3.5.5).

Also similar expressions can be determined for the stresses

$$\sigma_{xy} = \mu\frac{\partial v}{\partial x} = \mu\frac{(x-x_0)}{d^2}\frac{\partial v}{\partial d}$$

(3.5.6)

and

$$\sigma_{zy} = \mu\frac{\partial v}{\partial z} = \mu\frac{(z-z_0)}{d^2}\frac{\partial v}{\partial d}$$

(3.5.7)

where

$$\frac{\partial v}{\partial d} = C\left(-\frac{1}{d^2} - \frac{2\sigma\left(t - t_1 - \frac{d}{c}\right)}{d}\ \frac{1}{c}\right) e^{-\sigma\left(t - t_1 - \frac{d}{c}\right)^2}$$

(3.5.8).

An important factor in the design of the source is its frequency content. In order to evaluate the power spectrum the following change of variables is applied

$$t - t_1 - \frac{d}{c} \rightarrow t$$

(3.5.9).

Then the particle velocity is given by

$$\dot{v}(t) = A\, t\, e^{-\sigma t^2}$$

(3.5.10)

where $A = -C\sigma/(2\,\pi\, d)$ and its Fourier transform is

$$V(\omega) = \frac{i\,\omega\, C}{4\, d\sqrt{\pi\,\sigma}}\ e^{-\left(\frac{\omega^2}{4\sigma}\right)}$$

(3.5.11)

where i is the imaginary unit. The particle velocity (figure 3.1) is a bandlimited function with power spectrum shown in figure (3.2). By equating the first derivative of $V(\omega)$, to zero

$$V'(\omega) = \frac{V(\omega)}{\omega}\left(1 - \frac{\omega^2}{2\sigma}\right) = 0$$

(3.5.12)

the peak frequency depends on the source constant σ : $\omega_0 = \sqrt{2\sigma}$.

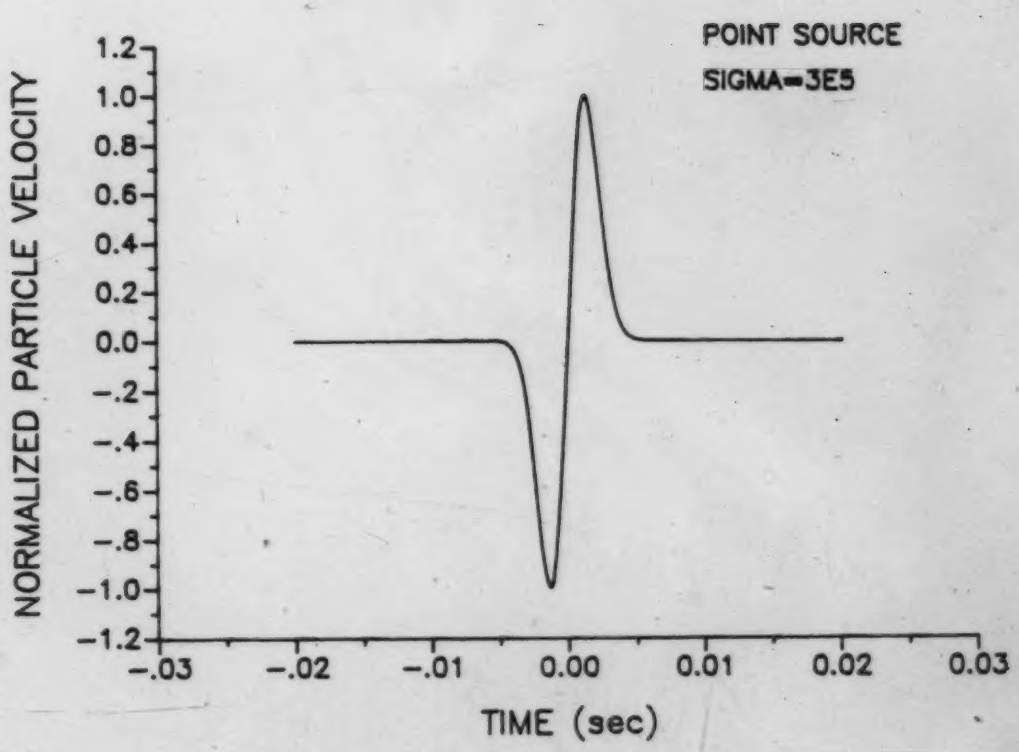

Figure 3.1 Normalized particle velocity for a point source with Gaussian excitation function (σ=3 10^5).

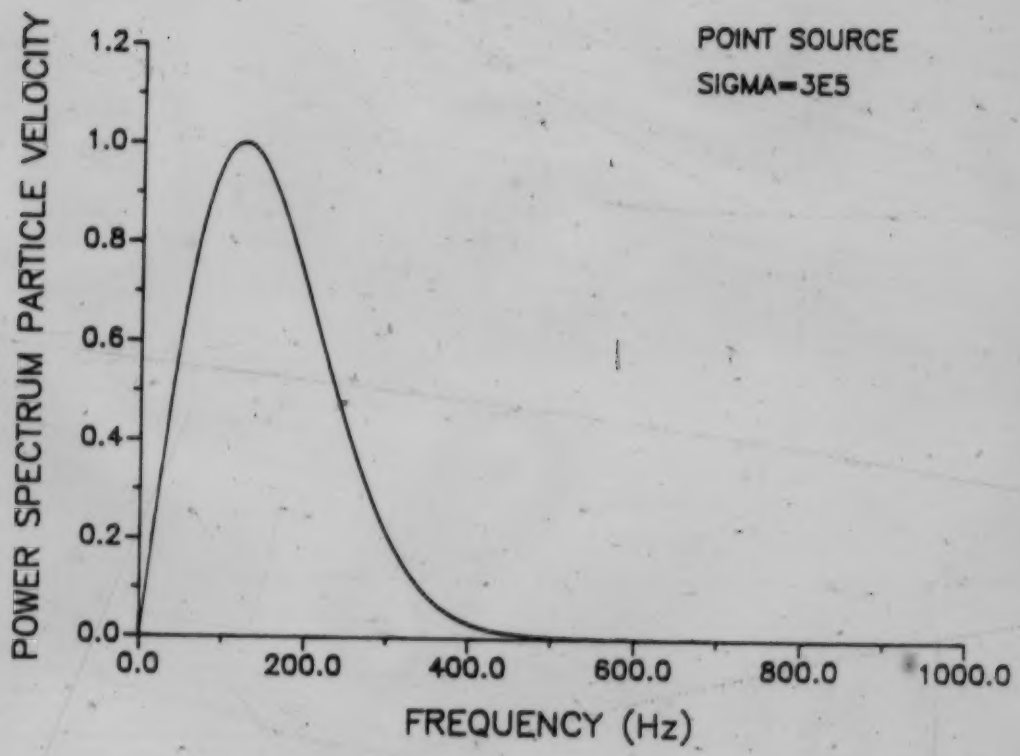

Figure 3.2 Normalized frequency response of the particle velocity shown in figure 3.1.

A measure of the frequency content is the upper half power frequency which is approximately equal to 2 times the peak frequency (Dablain, 1986). Also the peak to trough width of the pulse is $\sqrt{\frac{2}{\sigma}}$.

The displacement in an isotropic homogeneous medium due to a line source located at $(x_s, 0, z_s)$ is described by (Aki and Richards, 1980)

$$v\ (x,z,t) = \frac{H(t - d/c)}{2\pi\rho c^2} \int_{\frac{d}{c}}^{t} \frac{S(t-\tau)}{\sqrt{\tau^2 - \frac{d^2}{c^2}}}\, d\tau \qquad (3.5.13)$$

where H( ) is a Heaviside step function and S is given by (3.5.4). The integrals involved cannot be calculated analytically so they are evaluated numerically using either Romberg integration or Gauss integration (Gerald, 1980). The interval of integration in equation (3.5.13) increases proportionally with time. In Gauss integration the numerical error depends on the width of the integration interval when the number of segments is kept the same. For a Gaussian source excitation the integrand becomes negligible outside a small region. A truncation window can be applied without affecting the shape of the source. Since this window is not time dependent the error in the numerical integration does not depend on the integration interval.

The time window for equation (3.5.4) centered around $t = t_1$ is:

$$(t_1 - t_m,\ t_1 + t_m) \quad \text{where} \quad t_m = \sqrt{\frac{m}{\sigma} \ln 10}$$

where m is the power of 10 by which the amplitude decays outside the window. Assuming

$$t_m < t_1 \qquad \text{then} \qquad t - t_1 + t_m < t \ .$$

The limits of integration in equation (3.5.13) are then replaced by the ones resulting from the intersection of $(t - t_1 - t_m,\ t - t_1 + t_m)$ and $(d/c,\ t)$, that is

$$(d/c,\ t - t_1 + t_m) \quad \text{for} \quad t < t_1 + t_m + d/c$$

$$\text{and} \quad (t - t_1 - t_m,\ t - t_1 + t_m) \quad \text{for} \quad t > t_1 + t_m + d/c\ .$$

In Romberg integration the accuracy of the simple trapezoidal rule is improved by extrapolating a number of numerical integrals estimated by successive halving of the node interval. We used a maximum of four extrapolations starting with four nodal points.

The Gaussian quadrature method for numerical integration is based on the fact that the integral does not have to be evaluated at predetermined values. Having both the nodal points and the coefficients as variables, accuracy two times higher than the usual polynomial interpolation can be obtained. It is common practice to use a normalized symmetric interval around the source by changing the integration limits. In this way, the nodal points and the coefficients remain the same. A sixteen point Gauss integration has been used successfully. Figure (3.3) displays the components of the S-wave line source with a Gaussian source excitation.

In order to avoid the large values of the displacement vector Alterman and Karal (1968) inserted the effect of the source on the boundary of a rectangular (or square) region surrounding the source (Figure 3.4). They also proposed the following method where the rectangular boundary does not act as rigid reflector. They considered that the total field V_T consists of two components, the source component V_S and the residual field component V_R. The values of the source component V_S can be estimated analytically. The values of V_R represent the secondary field and they are calculated numerically inside the rectangular box (inner region). The total field V_T is calculated numerically outside the rectangular source region (outer region).

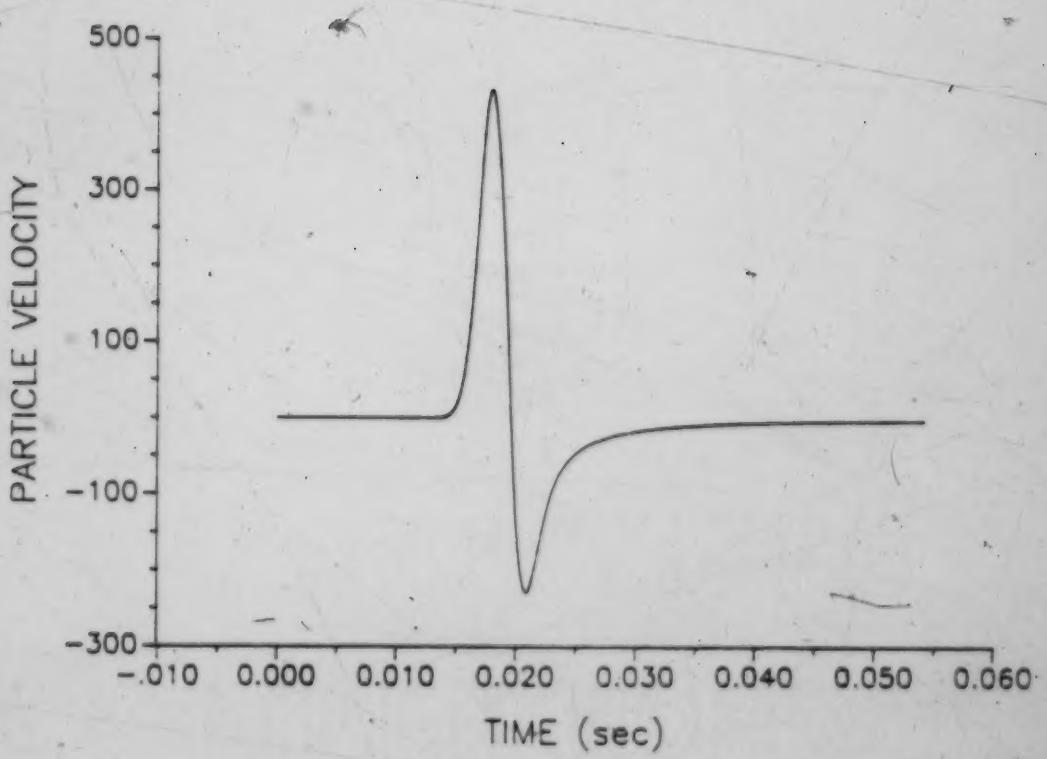

Figure 3.3 Particle velocity for a line source with Gaussian excitation function (σ=3 10^5) and time delay 0.02 sec.

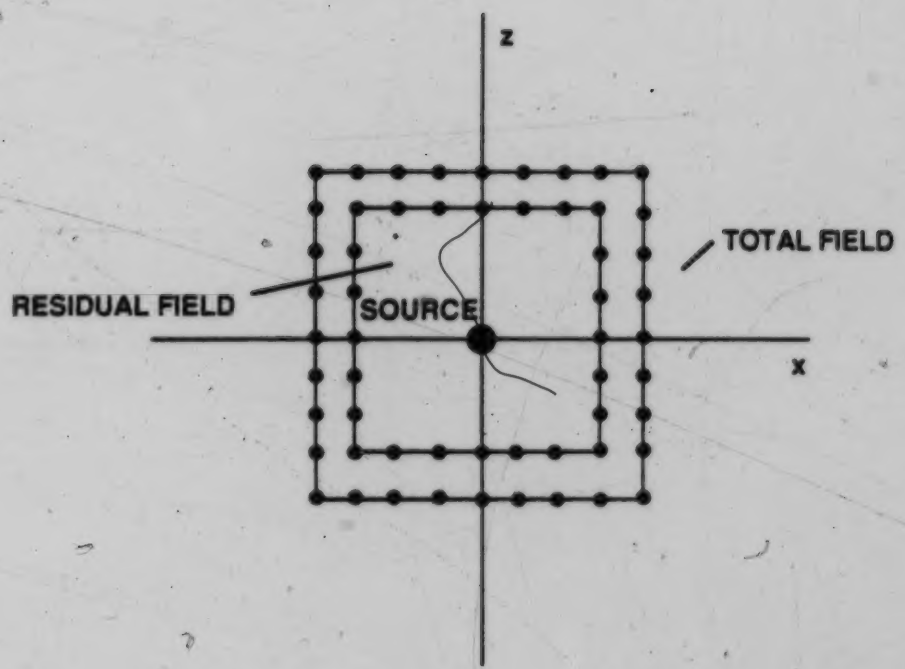

Figure 3.4 Alterman and Karal implementation of the source. In the inner region the residual field is calculated numerically while in the outer region the total field is calculated numerically.

In the early stages the total field is equal to the source field while the residual field is zero in the inner region. Later, when a ray due to a secondary source reaches the rectangular boundary, the residual field component V_R becomes different from zero and the ray propagates thoroughly through the rectangular inner region without being affected by the artificial boundary. This has been accomplished by solving the wave propagation problem twice: once with the source and once without the source. In this way the source region does not act as a rigid reflector.

3.6 The propagating enclosure method

Limitations on computer storage makes the problem of wave propagation in a medium unbounded in any direction non-realizable. Boundary conditions must be introduced on the edges to overcome this problem. Free surface (stress free) and rigid surface (zero velocity) boundary conditions are easy to implement but generate spurious reflections (Smith, 1974). Absorbing boundary conditions (Clayton and Engquist, 1977) remove the effect of these reflections in a more direct and efficient manner but not completely since it is almost impossible to design boundary conditions which will perfectly absorb all kinds of waves.

Another technique called the 'Propagating Enclosure Method' (Feng and Kanasewich, 1985) considers the boundaries of the computational model to be not fixed but propagating forward and backward along with the wavefront. All kinds of waves are transmitted at an artificial boundary in a simple and efficient way.

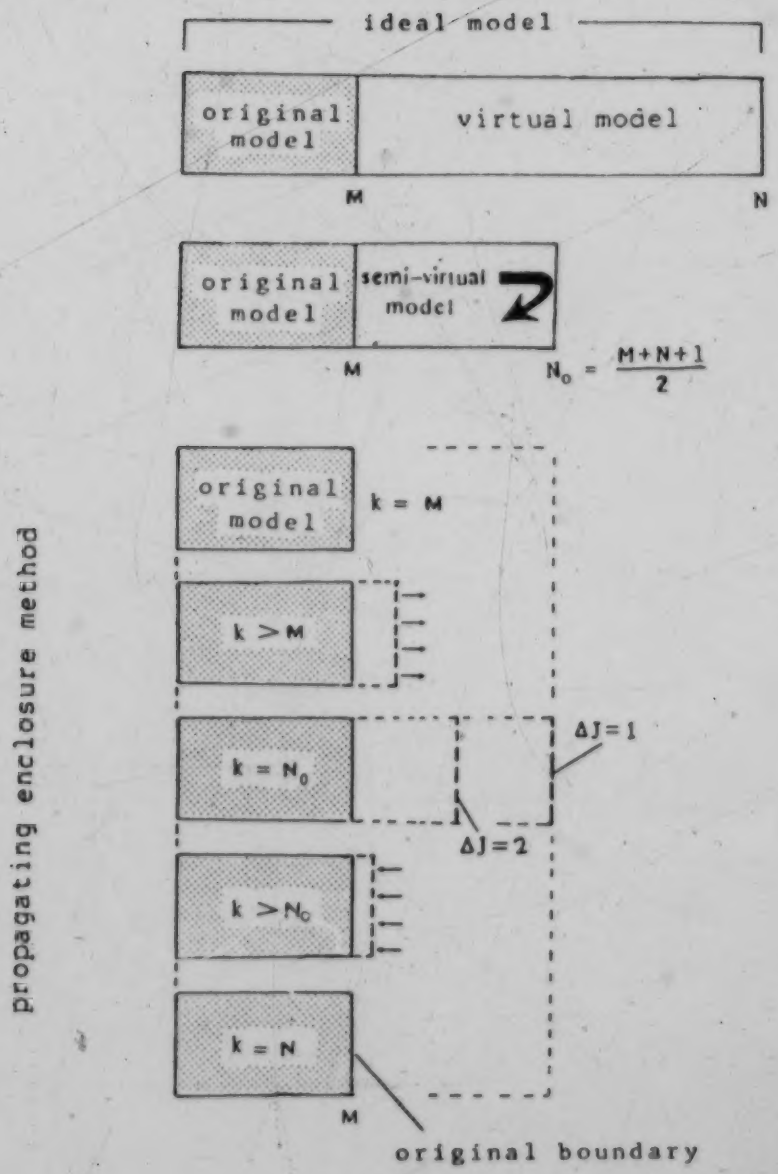

Figure 3.5 Propagating enclosure method.

The basic principle of the propagating enclosure method is illustrated employing only one artificial boundary. Finite differences is a time marching process where at every step the disturbance advances at neighboring grid points. Therefore, for a seismogram of time duration $T = N \kappa$, grid points N grid spacings away from the source are disturbed. The artificial boundary in this case should be placed at a distance of N grid spacings away from the source (figure 3.5) in order to avoid reflection artifacts caused by this boundary. Considering all four artificial boundaries this method requires a huge number of grid points.

If the original model has M+1 grid points in the direction perpendicular to the boundary (M<<N), the extra portion from (M+2)th grid point to Nth grid point is called the virtual model. The original model can still be free of artificial reflections, if the computations are done only in the first half of the virtual model namely, the semi-virtual model, which consists of N_0 grid points, where :

$$N_0 = \frac{N-(M+1)}{2} + M + 1 = \frac{N+M+1}{2} \qquad (3.6.1).$$

In this semi-virtual model the boundary can be either free or fixed. Artificial reflected waves are still generated from the boundary but they are not allowed to enter or propagate in the original model.

The first computation begins with the original model (M+1 grid points). The original model expands step by step by moving the boundary from the (M+1)th grid point to the Nth grid point. When the moving boundary reaches the edge of the semivirtual model, it starts propagating backwards. The physical parameters in the original model are extrapolated to the semivirtual model. The use of this semi-virtual model reduces the number of operations by one half.

The computational position of the disturbance front is far beyond the real propagating

waves. When the moving boundary propagates forward during the computation, errors at the propagating enclosure method move forward with the boundary without causing any serious harm behind the computational front. So, if the precision is reduced at the grid points belonging to the semivirtual model those at the original model still retains a high precision and the computational cost is further reduced.

In the propagating enclosure method for complicated structure models all four edges of the model are not fixed. The moving enclosure propagates just like the front of the travelling wave going forward so that the corresponding virtual model gradually increases. As soon as the number of iterations equals N_0 the boundary propagates back to the original model, step by step, together with the unwanted reflected wave from the boundary at N_0.

3.7 Numerical example

In this section both schemes are tested with a simple wave propagation problem of two half spaces separated by an interface (Aki and Richards, 1980, Abramovici et al, 1988). In generating synthetic seismograms the following procedure is taken (fig. 3.6).

First, a shear velocity and a density value are assigned to each grid point. Also the model parameters like grid spacing, source and receiver locations dimensions of the model etc must be given. It should be noted that any receiver and source geometry can be handled by the program. Second, from the stability condition and the maximum velocity the upper limit of the time step is evaluated. Third, the source is inserted in the computational grid through the particle velocity response specification and the stress (two components) response specification. Alterman's and Karal's technique specifies the source on the boundary of a rectangle to avoid errors due to large numbers close to the singularity and solves the wave equation twice to avoid a rigid reflector on that boundary. The computation

star, previously described, is applied at every grid point in order to advance in time the three components of the propagation vector. Finally, particle velocity synthetic seismograms are generated at all recording locations in the computational grid by extracting the particle velocity magnitude at those grid points for a sequence of time steps and then plotting these values as time series.

Figure 3.7 illustrates the source-receiver location with respect to the interface as well as the medium's velocities and densities. A Gaussian source excitation is employed (eq. 3.5.4) with σ = 3.E5, time delay t_1 = 10 ms, C = 1 and t_m = 7.8 ms. The peak frequecy is 123 Hz and the upper half power frequency is around 240 Hz while the shortest wavelength is λ = 2400/240 = 10 m. The numerical solutions shown in figures 3.8 and 3.9 are calculated for two different grid spacing (h = 0.5 m and 1.0 m) and the same time step κ = 0.034 ms by displaying every tenth point. The direct wave arrives at around 30 ms and the reflected wave whose amplitude is around one tenth of the direct arrives at around 40 ms. It is seen that for lower G = 10 (h = 1.0 m, fig 3.8a), the pulse is delayed and broadened and developes an oscillatory tail. These effects are called grid dispersion and are more pronounced for G = 10 than for G = 20 (fig 3.8b). The superiority of the fourth order scheme in terms of dispersion error is confirmed in figure 3.9.

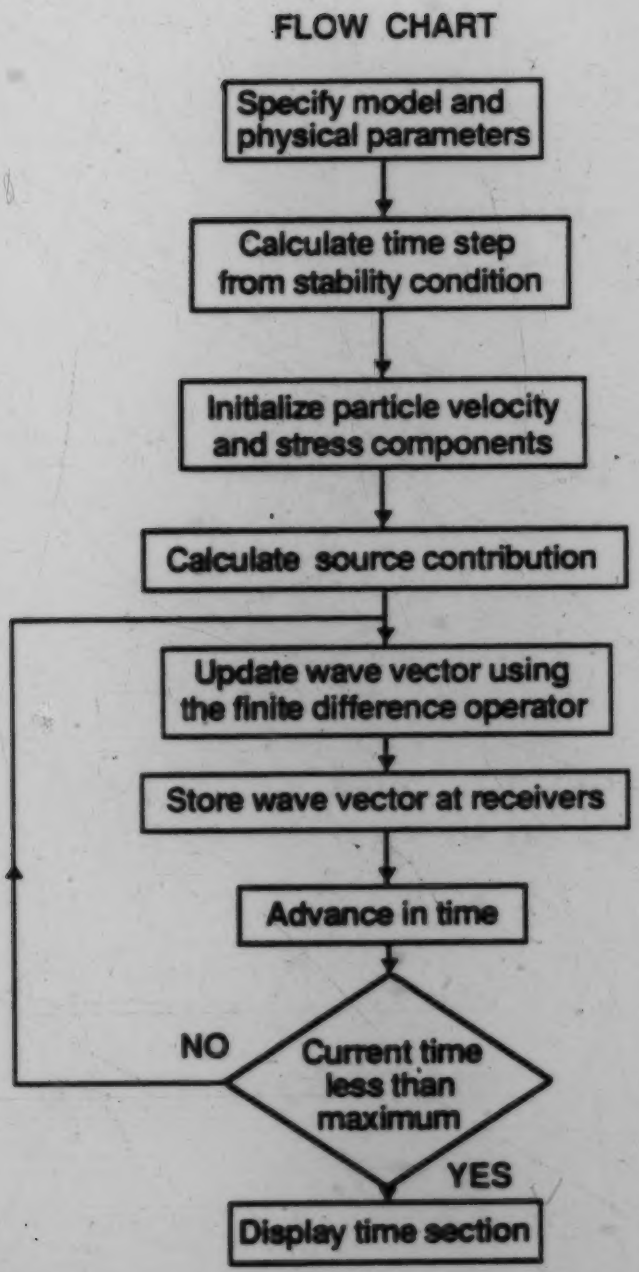
FLOW CHART
Specify model and physical parameters
Calculate time step from stability condition
Initialize particle velocity and stress components
Calculate source contribution
Update wave vector using the finite difference operator
Store wave vector at receivers
Advance in time
Current time less than maximum
NO
YES
Display time section

Figure 3.6 Flow chart for the SH finite difference algorithm.

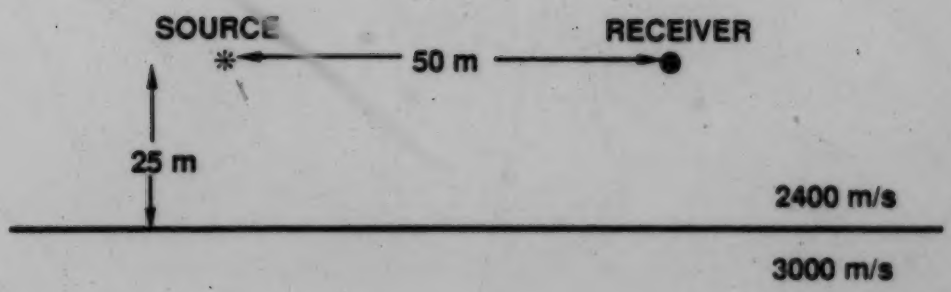

Figure 3.7 Source-receiver geometry in Lamb's problem.

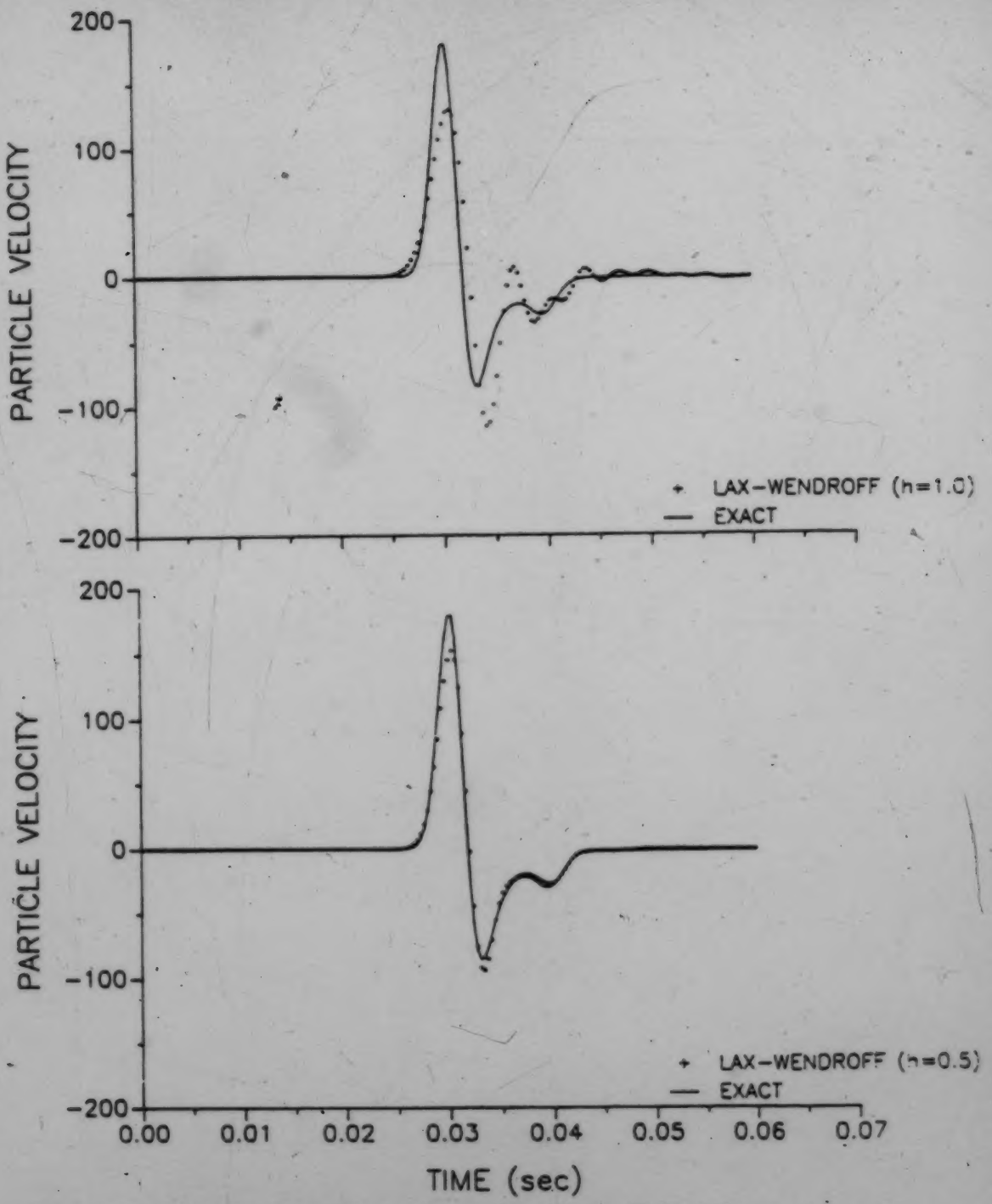

Figure 3.8 Analytical and numerical solutions (Lax-Wendroff) for different number of grid points per dominant wavelength, G.

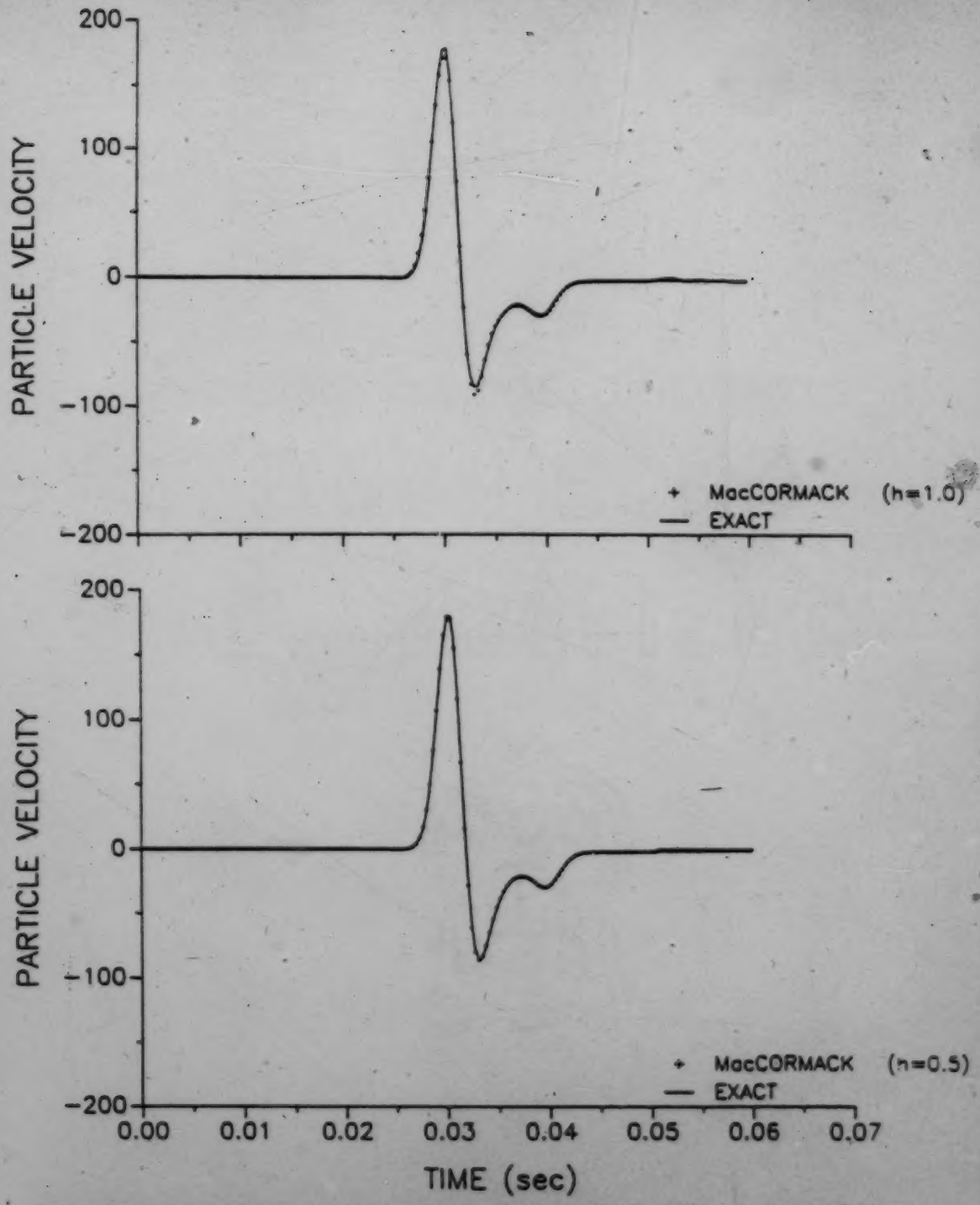

Figure 3.9 Analytical and numerical solutions (MacCormack) for different number of grid points per dominant wavelength, G.

CHAPTER 4

FINITE DIFFERENCES ON THE P-SV WAVE EQUATION

4.1 Introduction

Numerical solutions to the SH wave equation do not describe converted phases. A more realistic simulation can be performed thrbugh the heterogeneous elastic wave equation in two dimensions since coupling between P and SV waves is considered. Finite difference solutions to the elastic wave problem have been obtained by either the homogeneous formulation (Alterman and Lowenthal, 1972) or the heterogeneous formulation (Kelly et al, 1976, Stephen, 1983) both of which can be directly applied to the second order wave equations.

In this chapter the second and fourth order finite difference schemes are applied to the first order system (Virieux, 1986, Bayliss et al, 1986) instead of the second order elastic wave equation. The solution of the two dimensional elastic wave equation in a homogeneous infinitely extended medium with a line or point source is formulated and implemented in terms of the particle velocities and stress components for P or S wave sources. Finally a simple example is illustrated for comparison purposes.

4.2 Problem formulation

We consider the wave propagation problem where the earth's response can be resolved into components in the horizontal (x) and the vertical (z) directions while the (y) direction component is always zero. In order to calculate the elastic response of a model in

rectangular (x, z) coordinates two coupled second-order differential equations must be solved simultaneously. The basic equations for the two dimensional P-SV wave propagation in inhomogeneous media are

$$\rho(x,z)\frac{\partial^2 u(x,z,t)}{\partial t^2} = \frac{\partial}{\partial x}\left((\lambda(x,z)+2\mu(x,z))\frac{\partial u(x,z,t)}{\partial x}+\lambda(x,z)\frac{\partial w(x,z,t)}{\partial z}\right) + \frac{\partial}{\partial z}\left(\mu(x,z)\frac{\partial w(x,z,t)}{\partial x}+\mu(x,z)\frac{\partial u(x,z,t)}{\partial z}\right) \tag{4.2.1}$$

$$\rho(x,z)\frac{\partial^2 w(x,z,t)}{\partial t^2} = \frac{\partial}{\partial z}\left((\lambda(x,z)+2\mu(x,z))\frac{\partial w(x,z,t)}{\partial z}+\lambda(x,z)\frac{\partial u(x,z,t)}{\partial x}\right) + \frac{\partial}{\partial x}\left(\mu(x,z)\frac{\partial u(x,z,t)}{\partial z}+\mu(x,z)\frac{\partial w(x,z,t)}{\partial x}\right) \tag{4.2.2}$$

where u(x, z, t), w(x, z, t) are the displacements in the x and z directions respectively, μ(x, z) and λ(x, z) are the Lame parameters, ρ(x, z) is the density and ∂ denotes partial derivative. Body forces such as gravity have been neglected since they are negligible in these problems. The forces due to the source will be discussed in section 4.3.

Instead of solving this second order system, the equivalent first order system will be solved numerically. This system consists of the basic equations of motion in the x and z directions

$$\rho(x,z)\,\partial_t \dot{u}(x,z,t) = \partial_x \sigma_{xx}(x,z,t) + \partial_z \sigma_{xz}(x,z,t)$$

$$\rho(x,z)\,\partial_t \dot{w}(x,z,t) = \partial_x \sigma_{xz}(x,z,t) + \partial_z \sigma_{zz}(x,z,t) \tag{4.2.3}$$

and the stress-strain relations after taking the first time derivatives

$$\partial_t \sigma_{xx}(x,z,t) = (\lambda(x,z)+2\mu(x,z))\,\partial_x \dot{u}(x,z,t)+\lambda(x,z)\,\partial_z \dot{w}(x,z,t)$$

$$\partial_t \sigma_{xz}(x,z,t) = \mu(x,z)\, \partial_x \dot{w}(x,z,t) + \mu(x,z)\, \partial_z \dot{u}(x,z,t)$$

$$\partial_t \sigma_{zz}(x,z,t) = \lambda(x,z)\, \partial_x \dot{u}(x,z,t) + (\lambda(x,z)+2\mu(x,z))\, \partial_z \dot{w}(x,z,t)$$

(4.2.4)

where σ_{xx}, σ_{xz}, σ_{zz}, are the stress components and the dots denote time derivatives. In this formulation there are no space derivatives of the Lam« coefficients.

Equations (4.2.3) and (4.2.4) can be written in matrix form

$$\partial_t \begin{bmatrix} \dot{u} \\ \dot{w} \\ \sigma_{xx} \\ \sigma_{zz} \\ \sigma_{xz} \end{bmatrix} = \begin{bmatrix} 0 & 0 & \rho^{-1} & 0 & 0 \\ 0 & 0 & 0 & 0 & \rho^{-1} \\ \lambda+2\mu & 0 & 0 & 0 & 0 \\ \lambda & 0 & 0 & 0 & 0 \\ 0 & \mu & 0 & 0 & 0 \end{bmatrix} \partial_x \begin{bmatrix} \dot{u} \\ \dot{w} \\ \sigma_{xx} \\ \sigma_{zz} \\ \sigma_{xz} \end{bmatrix} + \begin{bmatrix} 0 & 0 & 0 & 0 & \rho^{-1} \\ 0 & 0 & 0 & \rho^{-1} & 0 \\ 0 & \lambda & 0 & 0 & 0 \\ 0 & \lambda+2\mu & 0 & 0 & 0 \\ \mu & 0 & 0 & 0 & 0 \end{bmatrix} \partial_z \begin{bmatrix} \dot{u} \\ \dot{w} \\ \sigma_{xx} \\ \sigma_{zz} \\ \sigma_{xz} \end{bmatrix}$$

or

$$\partial_t \mathbf{U} = \mathbf{A}\, \partial_x \mathbf{U} + \mathbf{B}\, \partial_z \mathbf{U}$$

(4.2.5).

This system can be written in divergence free form

$$\mathbf{E}_0\, \partial_t \mathbf{U} = \mathbf{A}_0\, \partial_x \mathbf{U} + \mathbf{B}_0\, \partial_z \mathbf{U}$$

(4.2.6)

where

$$A_0=\begin{bmatrix}0&0&1&0&0\\0&0&0&0&1\\1&0&0&0&0\\0&0&0&0&0\\0&1&0&0&0\end{bmatrix},\quad B_0=\begin{bmatrix}0&0&0&0&1\\0&0&0&1&0\\0&0&0&0&0\\0&1&0&0&0\\1&0&0&0&0\end{bmatrix}$$

$$E_0=\begin{bmatrix}\rho&0&0&0&0\\0&\rho&0&0&0\\0&0&\frac{\lambda+2\mu}{\lambda^*}&\frac{-\lambda}{\lambda^*}&0\\0&0&\frac{-\lambda}{\lambda^*}&\frac{\lambda+2\mu}{\lambda^*}&0\\0&0&0&0&\mu^{-1}\end{bmatrix}$$

with

$$\lambda^*=(\lambda+2\mu)^2-\lambda^2$$

are real symmetric matrices, so the system in (4.2.5) is hyperbolic. Various finite difference schemes for hyperbolic systems can be used to solve it. Applying the second order Lax-Wendroff explicit scheme in two dimensions, with A and B varying in space, to equation (4.2.5) gives rise to the following difference equations

$$\dot{u}^{n+1}_{j,m}=\left[1-\frac{p^2}{4}\rho^{-1}_{j,m}(\lambda_{j+1,m}+2\lambda_{j,m}+\lambda_{j-1,m}+2(\mu_{j+1,m}+2\mu_{j,m}+\mu_{j-1,m})+\mu_{j,m+1}+2\mu_{j,m}+\mu_{j,m-1})\right]\dot{u}^{n}_{j,m}$$

$$+\frac{p^2}{4}\rho^{-1}_{j,m}\left[\mu_{j,m+1}+\mu_{j,m-1}-2\mu_{j,m}+\lambda_{j+1,m}+\lambda_{j-1,m}-2\lambda_{j,m}\right]\dot{w}^{n}_{j,m}$$

$$+\frac{p^2}{4}\rho^{-1}_{j,m}\left[\lambda_{j+1,m}+\lambda_{j,m}+2(\mu_{j+1,m}+\mu_{j,m})\right]\dot{u}^{n}_{j+1,m}$$

$$+\frac{p^2}{4}\rho^{-1}_{j,m}\left[\lambda_{j-1,m}+\lambda_{j,m}+2(\mu_{j-1,m}+\mu_{j,m})\right]\dot{u}^{n}_{j-1,m}$$

$$+\frac{p^2}{4}\rho^{-1}_{j,m}(\mu_{j,m+1}+\mu_{j,m})\dot{u}^{n}_{j,m+1}+\frac{p^2}{4}\rho^{-1}_{j,m}(\mu_{j,m-1}+\mu_{j,m})\dot{u}^{n}_{j,m-1}$$

$$+\frac{p}{2}\rho^{-1}_{j,m}\left[(\sigma_{xx})^{n}_{j+1,m}-(\sigma_{xx})^{n}_{j-1,m}\right]+\frac{p}{2}\rho^{-1}_{j,m}\left[(\sigma_{xz})^{n}_{j,m+1}-(\sigma_{xz})^{n}_{j,m-1}\right]$$

$$+\frac{p^2}{4}\rho^{-1}_{j,m}(\mu_{j,m}-\mu_{j,m-1})\dot{w}^{n}_{j+1,m}-\frac{p^2}{4}\rho^{-1}_{j,m}(\mu_{j,m+1}-\mu_{j,m})\dot{w}^{n}_{j-1,m}$$

$$+\frac{p^2}{4}\rho^{-1}_{j,m}(\lambda_{j,m}-\lambda_{j-1,m})\dot{w}^{n}_{j,m+1}-\frac{p^2}{4}\rho^{-1}_{j,m}(\lambda_{j+1,m}-\lambda_{j,m})\dot{w}^{n}_{j,m-1}$$

$$+\frac{p^2}{8}\rho^{-1}_{j,m}(\lambda_{j,m}+\mu_{j,m})(\dot{w}^{n}_{j+1,m+1}-\dot{w}^{n}_{j-1,m+1}-\dot{w}^{n}_{j+1,m-1}+\dot{w}^{n}_{j-1,m-1})$$

(4.2.7)

$$\dot{w}^{n+1}_{j,m}=\left[1-\frac{p^2}{4}\rho^{-1}_{j,m}(\lambda_{j,m+1}+2\lambda_{j,m}+\lambda_{j,m-1}+2(\mu_{j,m+1}+2\mu_{j,m}+\mu_{j,m-1})+\mu_{j+1,m}+2\mu_{j,m}+\mu_{j-1,m})\right]\dot{w}^{n}_{j,m}$$

$$+\frac{p^2}{4}\rho^{-1}_{j,m}\left[\mu_{j+1,m}+\mu_{j-1,m}-2\mu_{j,m}+\tilde{\lambda}_{j,m+1}+\lambda_{j,m-1}-2\lambda_{j,m}\right]\dot{u}^{n}_{j,m}$$

$$+\frac{p^2}{4}\rho^{-1}_{j,m}\left[\lambda_{j,m+1}+\lambda_{j,m}+2(\mu_{j,m+1}+\mu_{j,m})\right]\dot{w}^{n}_{j,m+1}$$

$$+\frac{p^2}{4}\rho^{-1}_{j,m}\left[\lambda_{j,m-1}+\lambda_{j,m}+2(\mu_{j,m-1}+\mu_{j,m})\right]\dot{w}^{n}_{j,m-1}$$

$$+\frac{p^2}{4}\rho^{-1}_{j,m}(\mu_{j+1,m}+\mu_{j,m})\dot{w}^{n}_{j+1,m}+\frac{p^2}{4}\rho^{-1}_{j,m}(\mu_{j-1,m}+\mu_{j,m})\dot{w}^{n}_{j-1,m}$$

$$+\frac{p}{2}\rho^{-1}_{j,m}\left[(\sigma_{zz})^{n}_{j,m+1}-(\sigma_{zz})^{n}_{j,m-1}\right]+\frac{p}{2}\rho^{-1}_{j,m}\left[(\sigma_{xz})^{n}_{j+1,m}-(\sigma_{xz})^{n}_{j-1,m}\right]$$

$$+\frac{p^2}{4}\rho^{-1}_{j,m}(\lambda_{j,m}-\lambda_{j,m-1})\dot{u}^{n}_{j+1,m}-\frac{p^2}{4}\rho^{-1}_{j,m}(\lambda_{j,m+1}-\lambda_{j,m})\dot{u}^{n}_{j-1,m}$$

$$+\frac{p^2}{4}\rho^{-1}_{j,m}(\mu_{j,m}-\mu_{j-1,m})\dot{u}^{n}_{j,m+1}-\frac{p^2}{4}\rho^{-1}_{j,m}(\mu_{j+1,m}-\mu_{j,m})\dot{u}^{n}_{j,m-1}$$

$$+\frac{p^2}{8}\rho^{-1}_{j,m}(\lambda_{j,m}+\mu_{j,m})(\dot{u}^{n}_{j+1,m+1}-\dot{u}^{n}_{j-1,m+1}-\dot{u}^{n}_{j+1,m-1}+\dot{u}^{n}_{j-1,m-1})$$

(4.2.8)

$$(\sigma_{xx})^{n+1}_{j,m}=\left[1-\frac{p^2}{4}(\lambda_{j,m}+2\mu_{j,m})(\rho^{-1}_{j+1,m}+\rho^{-1}_{j-1,m}+2\rho^{-1}_{j,m})\right](\sigma_{xx})^{n}_{j,m}$$

$$-\frac{p^2}{4}\lambda_{j,m}(\rho^{-1}_{j,m+1}+2\rho^{-1}_{j,m}+\rho^{-1}_{j,m-1})(\sigma_{zz})^{n}_{j,m}$$

$$+\frac{p^2}{4}\left[(\lambda_{j,m}+2\mu_{j,m})(\rho^{-1}_{j+1,m}+\rho^{-1}_{j-1,m}-2\rho^{-1}_{j,m})+\lambda_{j,m}(\rho^{-1}_{j,m+1}+\rho^{-1}_{j,m-1}-2\rho^{-1}_{j,m})\right](\sigma_{xz})^{n}_{j,m}$$

$$+\frac{p^2}{4}(\lambda_{j,m}+2\mu_{j,m})(\rho^{-1}_{j+1,m}+\rho^{-1}_{j,m})(\sigma_{xx})^{n}_{j+1,m}+\frac{p^2}{4}(\lambda_{j,m}+2\mu_{j,m})(\rho^{-1}_{j-1,m}+\rho^{-1}_{j,m})(\sigma_{xx})^{n}_{j-1,m}$$

$$+\frac{p^2}{4}\lambda_{j,m}(\rho^{-1}_{j,m+1}+\rho^{-1}_{j,m})(\sigma_{zz})^{n}_{j,m+1}+\frac{p^2}{4}\lambda_{j,m}(\rho^{-1}_{j,m}+\rho^{-1}_{j,m-1})(\sigma_{zz})^{n}_{j,m-1}$$

$$+\frac{p^2}{4}(\lambda_{j,m}+2\mu_{j,m})(\rho^{-1}_{j,m}-\rho^{-1}_{j-1,m})(\sigma_{xz})^{n}_{j,m+1}\frac{p^2}{4}(\lambda_{j,m}+2\mu_{j,m})(\rho^{-1}_{j+1,m}-\rho^{-1}_{j,m})(\sigma_{xz})^{n}_{j,m-1}$$

$$+\frac{p^2}{4}\lambda_{j,m}(\rho^{-1}_{j,m}-\rho^{-1}_{j,m-1})(\sigma_{xz})^{n}_{j+1,m}-\frac{p^2}{4}\lambda_{j,m}(\rho^{-1}_{j,m+1}-\rho^{-1}_{j,m})(\sigma_{xz})^{n}_{j-1,m}$$

$$+\frac{p}{2}(\lambda_{j,m}+2\mu_{j,m})(\dot{u}^{n}_{j+1,m}-\dot{u}^{n}_{j-1,m})+\frac{p}{2}\lambda_{j,m}(\dot{w}^{n}_{j,m+1}-\dot{w}^{n}_{j,m-1})$$

$$+\frac{p^2}{4}\rho^{-1}_{j,m}(\lambda_{j,m}+\mu_{j,m})\left[(\sigma_{xz})^n_{j+1,m+1}-(\sigma_{xz})^n_{j-1,m+1}-(\sigma_{xz})^n_{j+1,m-1}+(\sigma_{xz})^n_{j-1,m-1}\right]$$

(4.2.9)

$$(\sigma_{zz})^{n+1}_{j,m}=\left[1-\frac{p^2}{4}(\lambda_{j,m}+2\mu_{j,m})(\rho^{-1}_{j,m+1}+\rho^{-1}_{j,m-1}+2\rho^{-1}_{j,m})\right](\sigma_{zz})^n_{j,m}$$

$$-\frac{p^2}{4}\lambda_{j,m}(\rho^{-1}_{j+1,m}+2\rho^{-1}_{j,m}+\rho^{-1}_{j-1,m})(\sigma_{xx})^n_{j,m}$$

$$+\frac{p^2}{4}\left[\lambda_{j,m}(\rho^{-1}_{j+1,m}+\rho^{-1}_{j-1,m}-2\rho^{-1}_{j,m})+(\lambda_{j,m}+2\mu_{j,m})(\rho^{-1}_{j,m+1}+\rho^{-1}_{j,m-1}-2\rho^{-1}_{j,m})\right](\sigma_{xz})^n_{j,m}$$

$$+\frac{p^2}{4}\lambda_{j,m}(\rho^{-1}_{j+1,m}+\rho^{-1}_{j,m})(\sigma_{xx})^n_{j+1,m}+\frac{p^2}{4}\lambda_{j,m}(\rho^{-1}_{j,m}+\rho^{-1}_{j-1,m})(\sigma_{xx})^n_{j-1,m}$$

$$+\frac{p^2}{4}(\lambda_{j,m}+2\mu_{j,m})(\rho^{-1}_{j,m+1}+\rho^{-1}_{j,m})(\sigma_{xx})^n_{j,m+1}+\frac{p^2}{4}(\lambda_{j,m}+2\mu_{j,m})(\rho^{-1}_{j,m-1}+\rho^{-1}_{j,m})(\sigma_{xx})^n_{j,m-1}$$

$$+\frac{p^2}{4}(\lambda_{j,m}+2\mu_{j,m})(\rho^{-1}_{j,m}-\rho^{-1}_{j,m-1})(\sigma_{xz})^n_{j+1,m}\frac{p^2}{4}(\lambda_{j,m}+2\mu_{j,m})(\rho^{-1}_{j,m+1}-\rho^{-1}_{j,m})(\sigma_{xz})^n_{j-1,m}$$

$$+\frac{p^2}{4}\lambda_{j,m}(\rho^{-1}_{j,m}-\rho^{-1}_{j-1,m})(\sigma_{xz})^n_{j,m+1}-\frac{p^2}{4}\lambda_{j,m}(\rho^{-1}_{j+1,m}-\rho^{-1}_{j,m})(\sigma_{xz})^n_{j,m-1}$$

$$+\frac{p}{2}(\lambda_{j,m}+2\mu_{j,m})(\dot{w}^n_{j,m+1}-\dot{w}^n_{j,m-1})+\frac{p}{2}\lambda_{j,m}(\dot{u}^n_{j+1,m}-\dot{u}^n_{j-1,m})$$

$$+\frac{p^2}{4}\rho^{-1}_{j,m}(\lambda_{j,m}+\mu_{j,m})\left[(\sigma_{xz})^n_{j+1,m+1}-(\sigma_{xz})^n_{j-1,m+1}-(\sigma_{xz})^n_{j+1,m-1}+(\sigma_{xz})^n_{j-1,m-1}\right]$$

(4.2.10)

$$(\sigma_{xz})^{n+1}_{j,m} = \left[1 - \frac{p^2}{4}\mu_{j,m}(\rho^{-1}_{j+1,m} + \rho^{-1}_{j-1,m} + \rho^{-1}_{j,m+1} + \rho^{-1}_{j,m-1} + 4\rho^{-1}_{j,m}) \right] (\sigma_{xz})^{n}_{j,m}$$

$$+ \frac{p^2}{4}\mu_{j,m}(\rho^{-1}_{j+1,m} - 2\rho^{-1}_{j,m} + \rho^{-1}_{j-1,m})(\sigma_{zz})^{n}_{j,m}$$

$$+ \frac{p^2}{4}\mu_{j,m}(\rho^{-1}_{j,m+1} - 2\rho^{-1}_{j,m} + \rho^{-1}_{j,m-1})(\sigma_{xx})^{n}_{j,m}$$

$$+ \frac{p^2}{4}\mu_{j,m}(\rho^{-1}_{j+1,m} + \rho^{-1}_{j,m})(\sigma_{xz})^{n}_{j+1,m} + \frac{p^2}{4}\mu_{j,m}(\rho^{-1}_{j,m} + \rho^{-1}_{j-1,m})(\sigma_{xz})^{n}_{j-1,m}$$

$$+ \frac{p^2}{4}\mu_{j,m}(\rho^{-1}_{j,m+1} + \rho^{-1}_{j,m})(\sigma_{xz})^{n}_{j,m+1} + \frac{p^2}{4}\mu_{j,m}(\rho^{-1}_{j,m} + \rho^{-1}_{j,m-1})(\sigma_{xz})^{n}_{j,m-1}$$

$$+ \frac{p^2}{4}\mu_{j,m}(\rho^{-1}_{j,m} - \rho^{-1}_{j,m-1})(\sigma_{xx})^{n}_{j+1,m} - \frac{p^2}{4}\mu_{j,m}(\rho^{-1}_{j,m+1} - \rho^{-1}_{j,m})(\sigma_{xx})^{n}_{j-1,m}$$

$$+ \frac{p^2}{4}\mu_{j,m}(\rho^{-1}_{j,m} - \rho^{-1}_{j-1,m})(\sigma_{zz})^{n}_{j,m+1} - \frac{p^2}{4}\mu_{j,m}(\rho^{-1}_{j+1,m} - \rho^{-1}_{j,m})(\sigma_{zz})^{n}_{j,m-1}$$

$$+ \frac{p}{2}\mu_{j,m}(\dot{w}^{n}_{j+1,m} - \dot{w}^{n}_{j-1,m}) + \frac{p}{2}\mu_{j,m}(\dot{u}^{n}_{j,m+1} - \dot{u}^{n}_{j,m-1})$$

$$+ \frac{p^2}{8}\mu_{j,m}\rho^{-1}_{j,m}\left[(\sigma_{xx})^{n}_{j+1,m+1} - (\sigma_{xx})^{n}_{j-1,m+1} - (\sigma_{xx})^{n}_{j+1,m-1} + (\sigma_{xx})^{n}_{j-1,m-1}\right]$$

$$+ \frac{p^2}{8}\mu_{j,m}\rho^{-1}_{j,m}\left[(\sigma_{zz})^{n}_{j+1,m+1} - (\sigma_{zz})^{n}_{j-1,m+1} - (\sigma_{zz})^{n}_{j+1,m-1} + (\sigma_{zz})^{n}_{j-1,m-1}\right]$$

(4.2.11).

Similar difference equations are given in Appendix C for MacCormack schemes.

4.3 Sources in the two-dimensional elastic (P-SV) problem

One of the main concerns in forward modelling is the implementation of the source. Expressions for both the point source and the line source of P waves are derived for infinitely extended homogeneous, isotropic, elastic media.

For the P-SV problem in three dimensions with a point source located at z=h, $x^2+y^2 = r^2 = 0$ the displacement vector is represented as (Aki and Richards, 1980)

$$\mathbf{u} = \nabla\phi + \nabla\times\nabla\times(0, 0, \psi) \tag{4.3.1}$$

where ϕ, ψ are the P- and SV- potentials. For a point source of P-waves $\psi = 0$ while ϕ satisfies

$$\ddot{\phi} = \frac{\Phi}{\rho} + \alpha^2 \nabla^2 \phi \tag{4.3.2}$$

where Φ is the potential for the body force **f** via

$$\mathbf{f} = \nabla\Phi \tag{4.3.3}$$

described by

$$\Phi = A\ 4\pi\rho\alpha^2\ \delta(x)\,\delta(y)\,\delta(z-h)\ S(t) \tag{4.3.4}$$

with body-wave velocities α, β and density ρ. Then the corresponding P-potential is

$$\phi(x,t) = A\,\frac{1}{d}\,S\left(t - \frac{d}{\alpha}\right) \quad \text{with } d = \sqrt{x^2+y^2+(z-h)^2} \tag{4.3.5}$$

The displacement components on the y = 0 plane are given by

$$\mathbf{u} = (u,\ 0,\ w) = \left(\frac{\partial \phi}{\partial x},\ 0,\ \frac{\partial \phi}{\partial z}\right)$$

(4.3.6)

while the stress components are given by

$$\sigma_{xx} = (\lambda+2\mu)\ \partial_x u + \lambda\ \partial_z w$$

$$\sigma_{zz} = (\lambda+2\mu)\ \partial_z w + \lambda\ \partial_x u$$

$$\sigma_{xz} = \mu\ (\partial_z u + \partial_x w)$$

(4.3.7)

and the particle velocity components by

$$\dot{u} = \frac{\partial u}{\partial t} \qquad \text{and} \qquad \dot{w} = \frac{\partial w}{\partial t}$$

(4.3.8).

For a Gaussian source excitation, given by equation (3.5.4) with $\sigma = 3.E5$ and $t_1 = 20$ ms, the horizontal and vertical particle velocity responses are shown in figure (4.1).

For the P-SV problem in two dimensions, motion is confined to the x-, z-directions only and the displacement is given by (Aki and Richards, 1980)

$$\mathbf{u} = \nabla\phi + \nabla \times (0,\ \psi,\ 0) = (u,\ 0,\ w)$$

(4.3.9)

For a P-wave line source the ψ-potential is always zero and the displacement is $\nabla\phi$. The ϕ-potential satisfies equation (4.3.2) and it is independent of the y-coordinate. The potential of the body force Φ is,

$$\Phi(x,z,t) = S(t)\ \delta(x)\ \delta(z-h)$$

(4.3.10)

and the corresponding potential ϕ is,

$$\phi(x,z,t) = \frac{H(t - d/\alpha)}{2\pi\rho\alpha^2} \int_{\frac{d}{\alpha}}^{t} \frac{S(t-\tau)}{\sqrt{\tau^2 - \frac{d^2}{\alpha^2}}}\, d\tau \qquad (4.3.11)$$

where H( ) is a Heaviside step function. A similar expression to (4.3.11) can be written for the ψ potential which can be used for a pure SV-wave line source.

Equations (4.3.6) to (4.3.8) calculate the particle velocity components and the stress components from the potential. The integrals are numerically evaluated using either Romberg integration or Gauss integration. Figure 4.2 displays the particle velocity components of the P-wave line source with a Gaussian source excitation.

4.4 Numerical examples

In calculating synthetic seismograms a compressional velocity is assigned to each grid point. A corresponding shear velocity is determined by Poisson's ratio. The source is then inserted into the computational grid using Alterman's and Karal's method. This involves both a vertical and horizontal response specification. From these initial grids, the horizontal and the vertical responses can be computed for the next finite-difference time step. Thus for the second order algorithm, five grids are involved at each time; vertical and horizontal responses and the three stress components at the current time step. The stability is given by

$p\alpha \leq \varepsilon$ where p is the mesh ratio, α is the local compressional wave velocity and ε is equal to $1/2\sqrt{2}$ for the Lax-Wendroff and 2/3 for the MacCormack formulation.

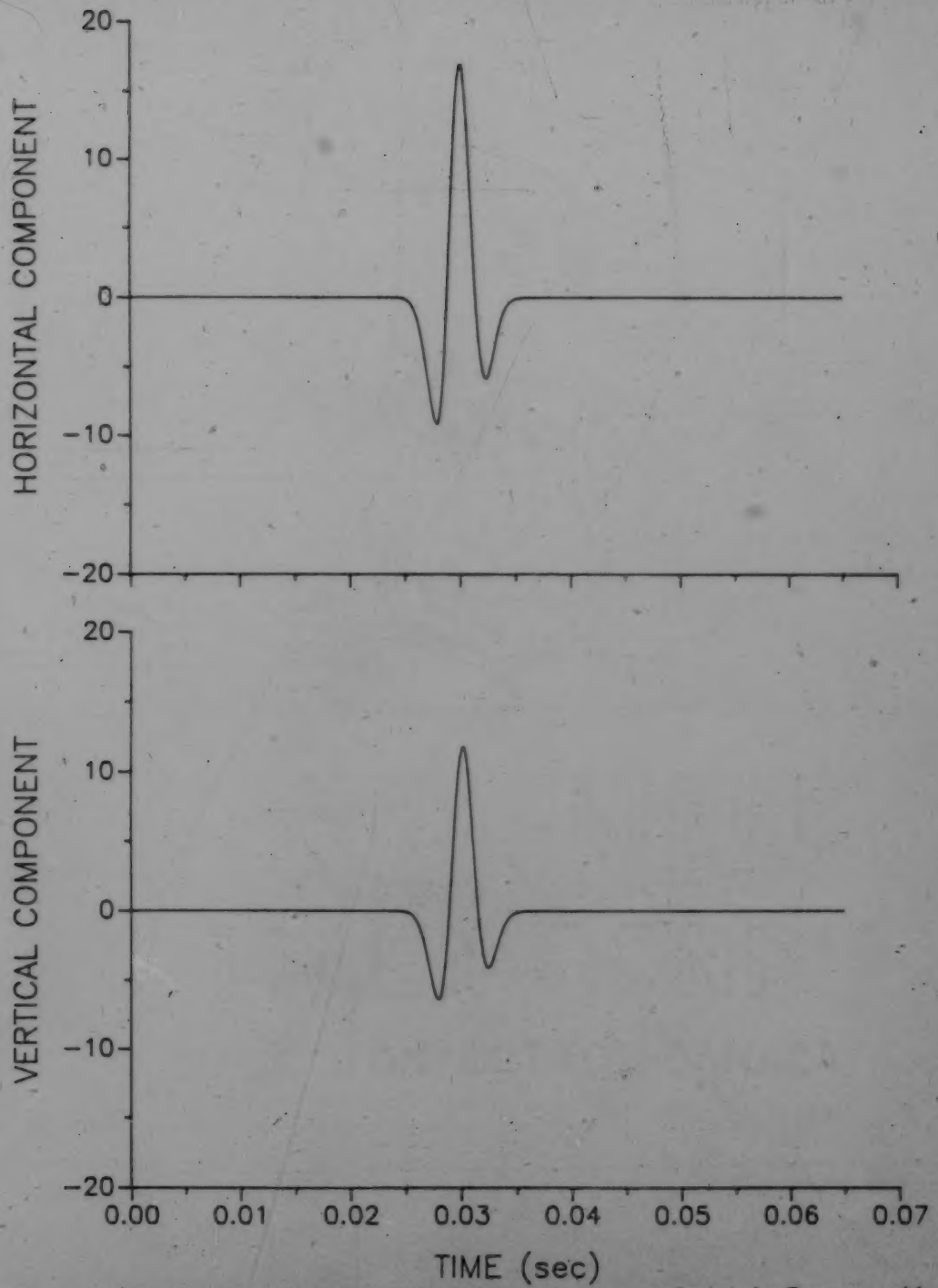

Figure 4.1 Horizontal and vertical particle velocity components for a point P-source with a gaussian excitation function.

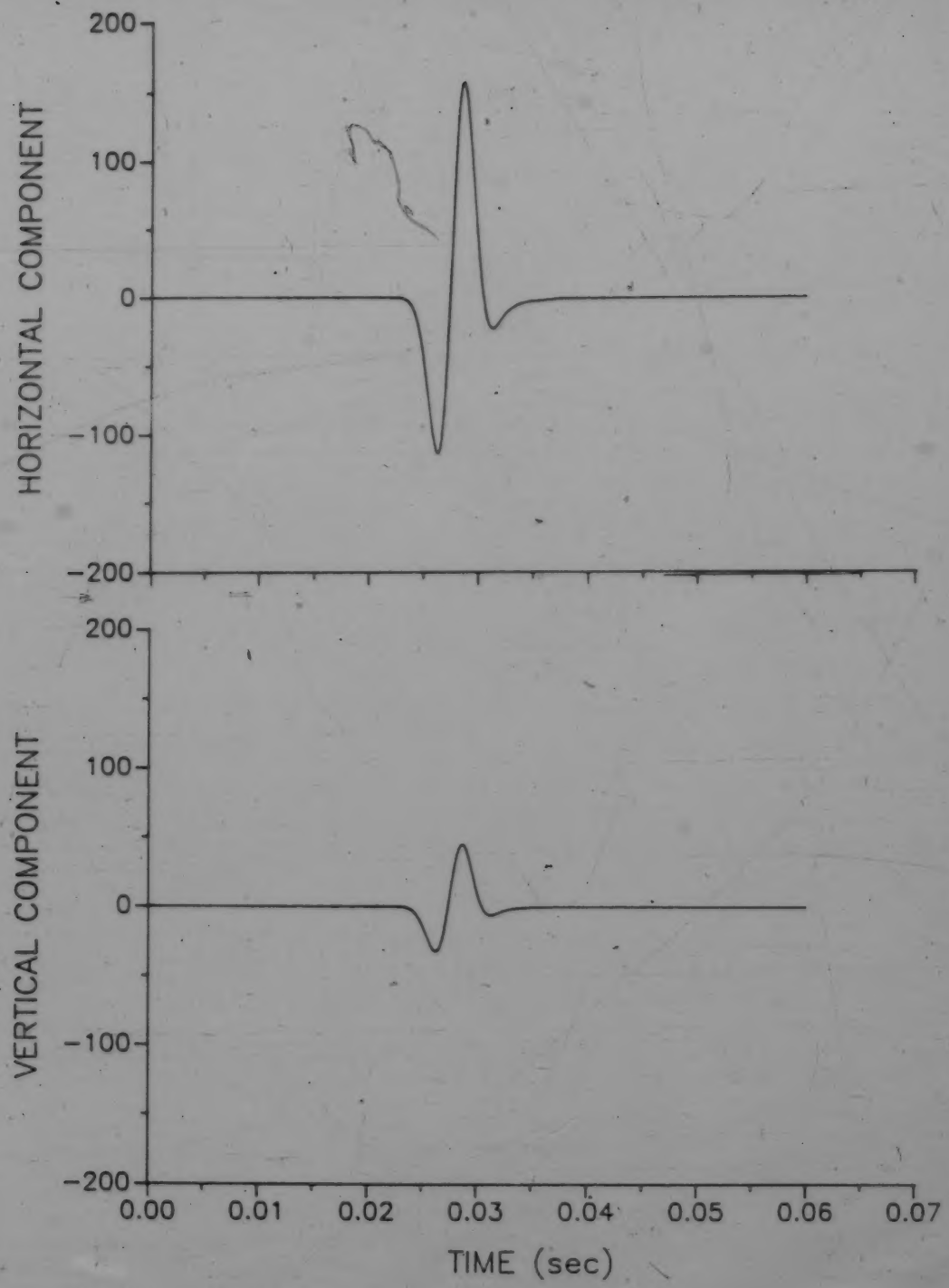

Figure 4.2 The same as in figure (4.1) for a line P-source.

Synthetic vertical and horizontal component seismograms can be produced for any desired recording point in the computational grid by extracting the vertical and horizontal amplitudes at that point for a sequence of time steps and then plotting these values as time series. The numerical solutions from both finite difference schemes are compared for the simple case of a P-wave propagation in a homogeneous space which is generated by a line P-source (figure 4.3). The numerical and the physical parameters for this example are given in table 4.1. It is clear that the fourth order scheme is superior in terms of numerical dispersion effects when compared to the second order for this particular model.

Table 4.1 Numerical parameters for a homogeneous model

Source :	$t_1 = 25$ ms	Velocity	2400 m/s
α	0.18 E5	(wavelength = 79.5 m)	
Density		2.1 gr / cc	
Grid spacing		3 m	
Time step		0.25 ms	
Receiver location		(198 m , 10 m)	
Poisson ratio		0.32	

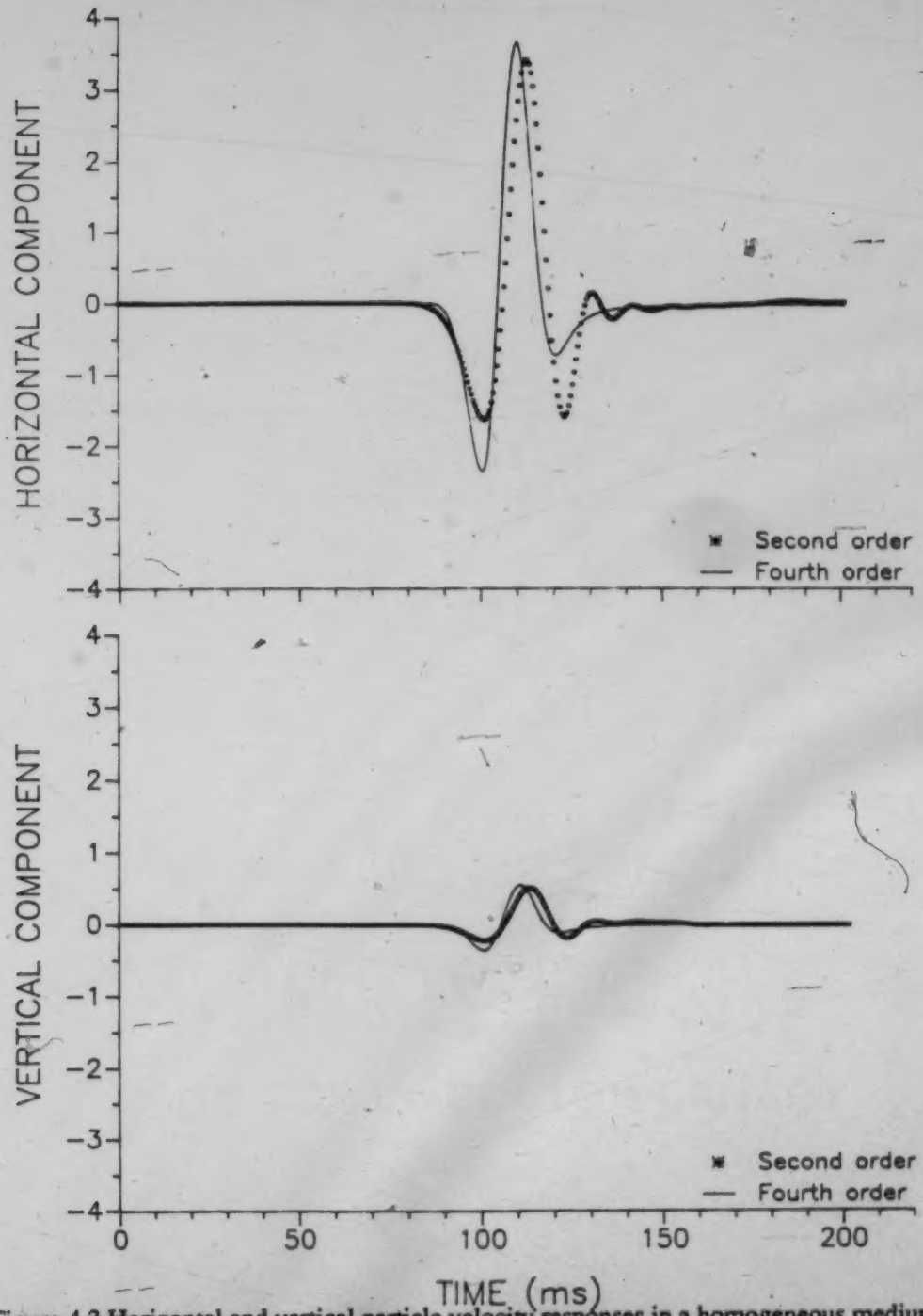

Figure 4.3 Horizontal and vertical particle velocity responses in a homogeneous medium at a receiver 200 m away from a line P-source for the Lax-Wendroff and MacCormack schemes.

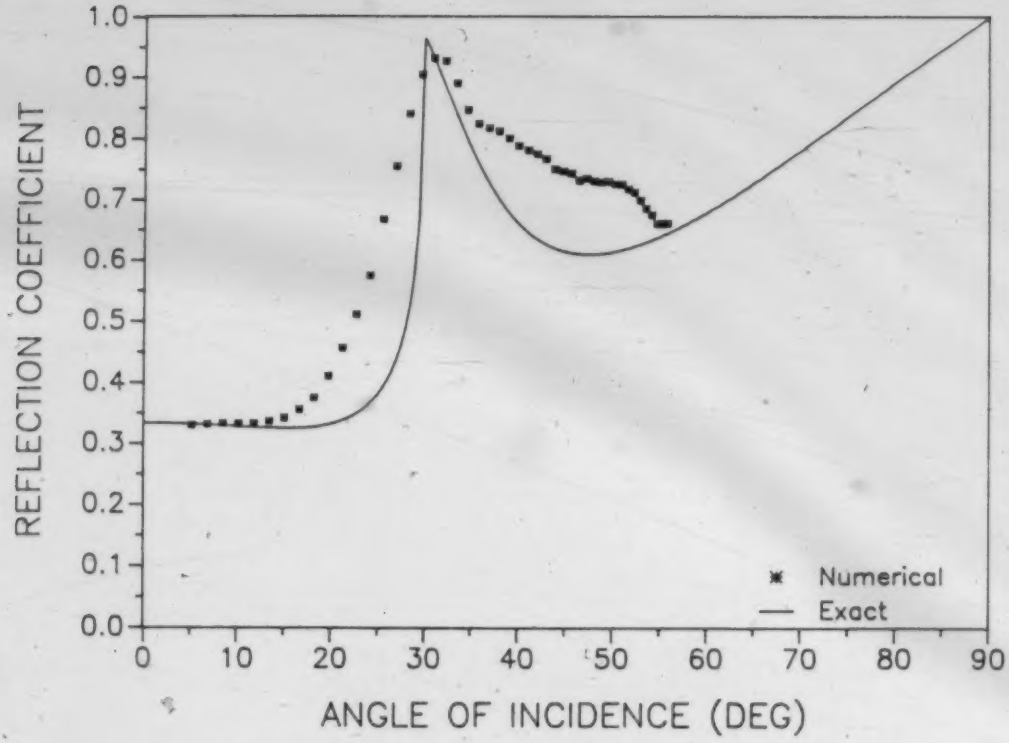

Figure 4.4 Exact and numerical P-wave reflection coefficients from a P-wave source.

The validity of the method is also examined by calculating the P-wave reflection coefficients in a two layer model (Table 4.2) for waves generated by a P-line source. The maximum amplitudes of the reflected P-wave as they are recorded at a finite number (48) of horizontal and vertical component receivers are added vectorially at each receiver location. A correction is then applied in order to remove the effect of cylindrical spreading. The amplitudes are then normalized so that the maximum amplitude is equal to the corresponding reflection coefficient which is calculated from the Zoeppritz equations (Grant and West, 1965). Finally, both the numerical and the exact reflection coefficients are displayed for different angles of incidence (figure 4.4). The numerical and the exact responses are in good agreement for angles smaller than the critical angle while the numerical reflection coefficients deviate from the exact ones at higher angles of incidence. Discrepancies can be explained on the basis that in finite differences we are dealing with cylindrical (two dimensional) wave propagation in the near field while the Zoeppritz equations are valid for one dimensional wave propagation and for plane waves (Zoeppritz, 1919).

Table 4.2 Numerical parameters for a two layer model

Source : t_1 = 50 ms	Velocities: 1500 m/s - 3000 m/s
α 0.10 E5	(wavelength = 66.6 m)
Density	2.1 gr / cc
Grid spacing	6 m
Time step	0.5 ms
Receiver location (1st)	(54 m , 0 m)
Poisson ratio	0.36
Receiver separation	18 m
Depth to the interface	150 m
Number of receivers	48

CHAPTER 5

MODELLING STEAM INJECTION PROBLEMS WITH FINITE DIFFERENCES

5.1 Introduction

The largest, and potentially the most valuable, of Alberta's subsurface mineral deposits is the crude oil in buried oil sands deposits. Since only 7% of these deposits are accessible to surface mining, a large amount of research and many pilot plant studies are being carried out to recover the oil through *in situ* methods. Most of these involve the application of heat to reduce the viscosity of bitumen so it may be pumped to the surface. It is always difficult to know the geometry of the heated zone. Drilling is very expensive and not always conclusive on the properties of the heated zone since the act of drilling disturbs the fluids and the strata. Crosshole seismic profiling is also expensive at the present time and one would also like to explore surface seismic methods for determining three-dimensional structure. Before the expensive field procedures are attempted it is useful to carry out computer simulation studies on various methods of carrying out the field procedures and also to develop methods for the interpretation of complex field data.

One of the main features of a heavy oil is its immobility under formation conditions. Since viscosity decreases drastically with temperature, thermal oil recovery techniques have been developed, the most widely used being the cyclic steam injection (Farouq Ali, 1982). This method has certain advantages since the same wells may be used for production and steam injection. The steam is injected into the well at very high pressures for several weeks followed by a short soak period (two weeks). During this time the rock's temperature

increases while the oil becomes mobilized. Then the production starts from the same well and the process is repeated many times. One of the very important factors in deciding whether the steam injection must be continued is to find the volume of the steam heated zone as well as details of its shape, including preferential propagation paths. The same problem is faced in all thermal recovery techniques (i.e. fire flooding, steam flooding). Seismic experiments have proven (Macrides, et al, 1987, Kanasewich and Vafidis, 1987) to be useful tools in imaging steam-heated rocks since they can provide high resolution remote sensing of the steam zone shape.

Several seismic experiments have been conducted by ESSO Resources Canada for monitoring steam injection projects in Cold Lake area and AMOCO has carried research in the Fort McMurray area. Here, two sets of data will be discussed, the first being from seismic crosshole experiments before and after steam injection and the second, from a seismic surface experiment over an area where the steam injection was performed. This chapter contains realistic computer simulation using finite differences applied both to the scalar and to the elastic wave equation in two dimensional heterogeneous media. The effects on the seismic response due to changes in the size and shape of the steam heated zone are examined. Synthetic data are finally compared with the real data and comments are included concerning the design of the seismic experiments for monitoring thermal fronts in oil recovery projects.

5.2 Hole to hole seismic experiments in Cold Lake area

The geometry of an initial crosshole experiment at Cold Lake conducted by ESSO Resources at the end of 1982, shown in figure 5.1, consists of one source well and one receiver well separated by 200 m. Ten vertical component seismometers were employed that recorded at a rate of 1000 samples /second and the shot was located at a depth of 440

m. An explosive source (100 grams of Primacord charge) that contained high frequency energy up to 500 hz was used, and the records had high signal to noise ratio. The heavy oil deposits at Cold Lake lie within the Lower Cretaceous Mannville Group which is subdivided into the McMurray, Clearwater and Grand Rapids Formations (Harrison et al, 1981). From sonic log information the 50 m thick Clearwater Formation has the same velocity as the Grand Rapids Formation (figure 5.2). Steam was injected from a well located half way between the receiver and source wells in the Clearwater. The perforations were at depths between 442 m and 450 m. The depths to the interfaces were derived from well log data (Kanasewich, 1983).

The experiment was conducted twice : the first time before steam injection and the second after injecting steam at a pressure of 10 Mpa for 48 days. The first 250 ms of the before and after steam injection experiments are shown in figure 5.3 where the seismic signals are rectified in such a way as to allow plotting the '*before*' records (blue color) entirely above the zero amplitude baseline and the '*after*' records (red color) entirely below it. The original positive parts of the signals are shaded with the appropriate color. This display is called BARS (Before / After Rectified Seismic) plots. The amplitudes of the arrivals from the two experiments show significant changes on receivers 2 to 5, and are lower in the after steam traces. Notice the very low amplitudes of the S-waves after injection. Also clear time delays of up to 2 ms in the P-arrivals and up to 10 ms in the S-arrivals are observed in the after steam experiment due to propagation through the low velocity steam zone. Reflections from layers below the Clearwater are difficult to identify in the records. Macrides et al (1987, Vafidis et al, 1987) extensively studied this data set and, based on evidence from theoretical and experimental studies (Tosaya et al, 1984, Nur et al, 1980), modelled it with rays and a P-velocity drop of 20% within the steam zone. Under this condition, delays of 2 ms are associated with a steam zone 29 m wide for P- velocity 2.4 km/s.

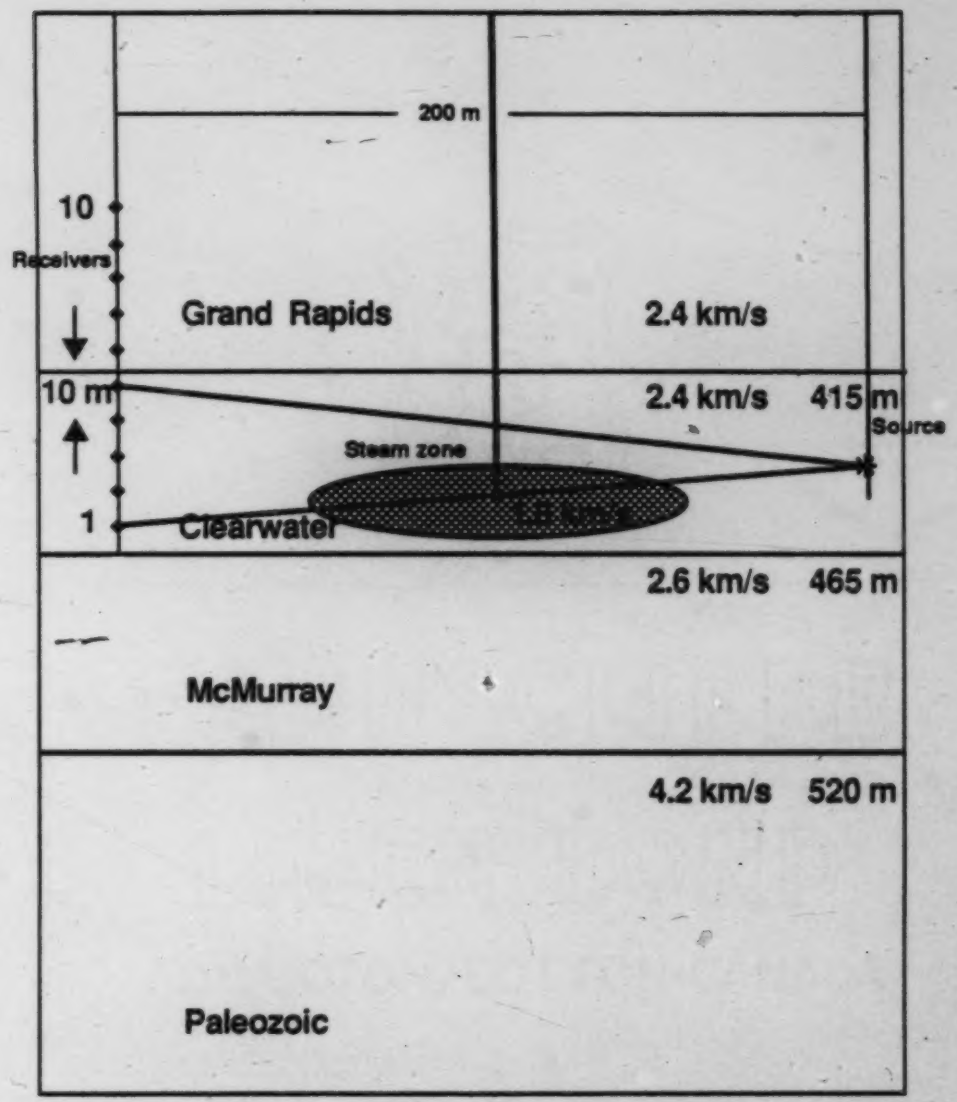

Figure 5.1 Model geometry of the 1982 seismic tomography experiment.

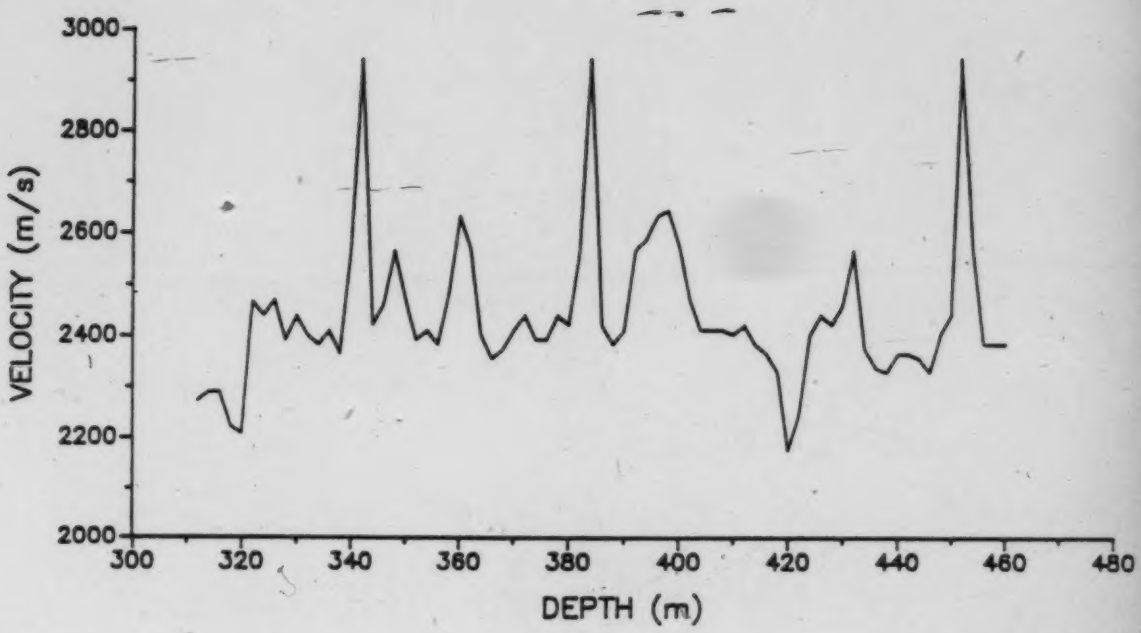

Figure 5.2 Sonic log at the receiver well after sampling at 2 m sampling interval.

THE QUALITY OF THIS MICROFICHE IS HEAVILY DEPENDENT UPON THE QUALITY OF THE THESIS SUBMITTED FOR MICROFILMING.

UNFORTUNATELY THE COLOURED ILLUSTRATIONS OF THIS THESIS CAN ONLY YIELD DIFFERENT TONES OF GREY.

LA QUALITE DE CETTE MICROFICHE DEPEND GRANDEMENT DE LA QUALITE DE LA THESE SOUMISE AU MICROFILMAGE.

MALHEUREUSEMENT, LES DIFFERENTES ILLUSTRATIONS EN COULEURS DE CETTE THESE NE PEUVENT DONNER QUE DES TEINTES DE GRIS.

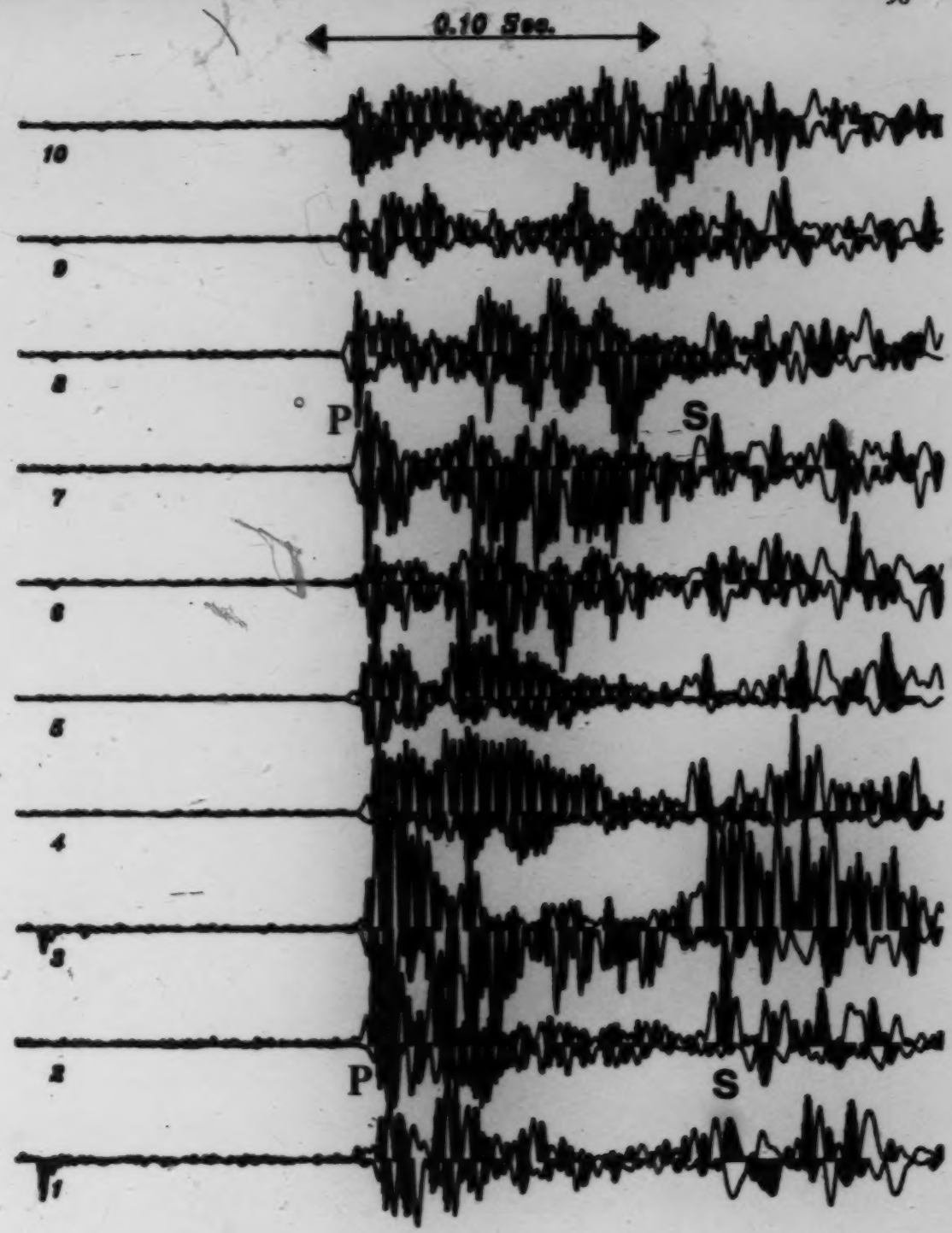

Figure 5.3 BARS plots for a steam injection experiment. The seismic signals are rectified in such a way as to allow plotting the 'before' records (blue color) entirely above the zero amplitude baseline and the 'after' records (red color) entirely below it. The original positive portions of the signals are shaded by the color. The original negative parts are unshaded.

Computer seismic wave simulations were carried out for the crosshole experiment employing a high frequency (120 Hz) line source whose excitation function is Gaussian shaped. The numerical parameters are shown in table 5.1. The SH wave equation, using compressional velocities, implementation was employed as a first attempt to generate synthetic data. Figure 5.4 shows the first 240 ms of the seismic rectified records in an SH simulation before and after steam injection for the model shown in figure 5.1 while figure 5.5 illustrates selected rays for the same geometry. The traces before steam injection show the direct arrivals as well as reflections from the McMurray and Paleozoic. The reflections from the McMurray interface are very weak due to small velocity contrast. The reflections from the Paleozoic can provide additional information about the low velocity region. After steam injection, strong events that arrive at 100 ms are present in addition to the events seen in the before steam injection experiment. Also, delays of 2-3 ms in the direct arrivals are measured in the after steam injection experiment for rays passing through the low velocity steam-zone.

Table 5.1 Numerical parameters - Crosshole experiment

Source :	t_1 = 18 ms;	Minimum velocity :	1800 m/s
α	0.71 E4	(wavelength = 15 m)	
Receiver separation :		10 m	
Grid spacing :		2 m	
Time step :		0.1 ms	
Semiaxis of the ellipse :			
Major :		24 m	
Minor :		5 m	

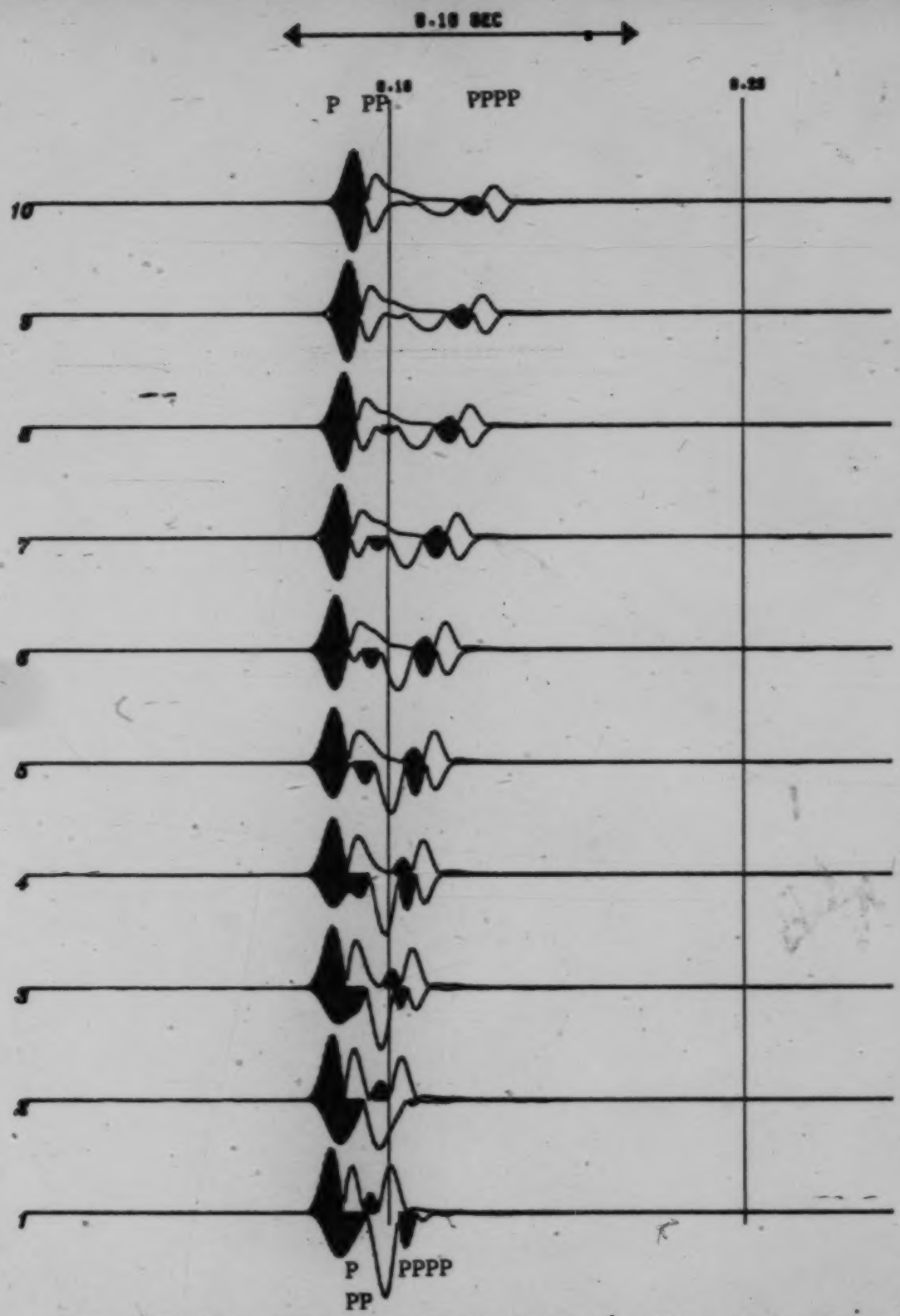

Figure 5.4 BARS plots for an SH computer simulation of the 1982 crosshole experiment.

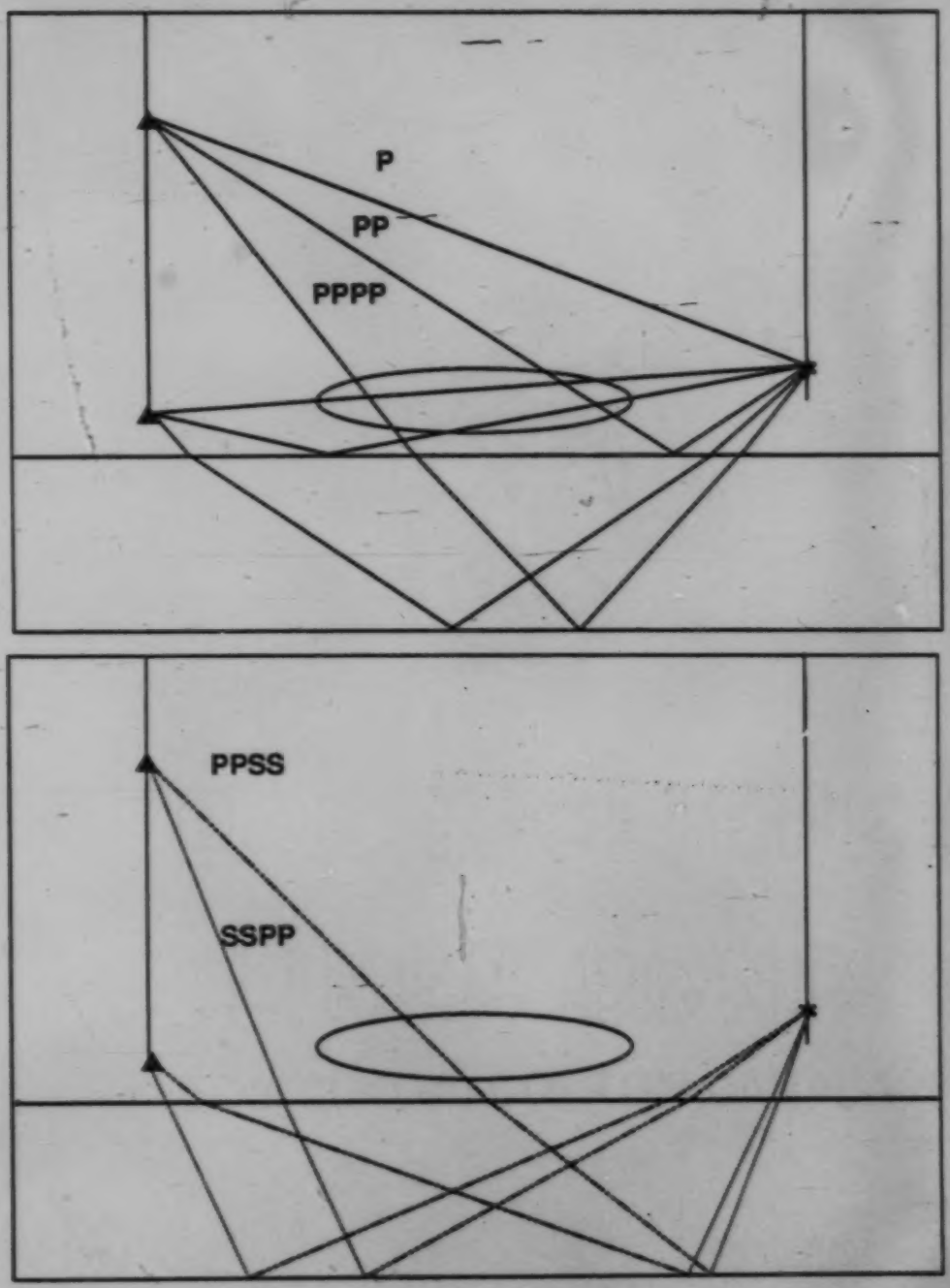

Figure 5.5 Ray diagrams for the 1982 crosshole experiment (a) P arrivals before steam injection and (b) converted arrivals before steam injection.

The results from the SH computer simulation of the 1982 experiment, shown in figure 5.4, give a simplistic but very useful view of the effects of the steam zone. As a next step a more detailed model based on sonic log information is employed in the simulation. The velocities, after redigitization at 2 m sampling interval, are displayed in figure 5.2. The results from this simulation (figure 5.6) look quite similar to the previous ones. So the small variations in the sonic velocity to the formation do not affect the propagation as drastically as the presence of the steam zone.

Next a P-SV computer simulation was carried out in order to include converted phases. The particle velocity components in the vertical (x) (figure 5.7) and horizontal (z) (figure 5.8) directions are displayed for the before and after steam injection experiments. A high frequency P-wave line source, described in section 4.3, is employed to excite the system. Clear direct P arrivals are present whose energy is mostly recorded on the horizontal component receiver. Delays of up to 2 ms are measured in the direct P arrivals after steam injection for the first five receivers in agreement with the real experiment. For the reflected upgoing P-waves most of the energy is recorded on the vertical component. Apart from the reflections from the interfaces below the Clearwater, that may be clearly observed in the before traces, reflections from the top and the bottom of the steam zone are also observed in the after traces. The reflected and direct P events described above look similar to the ones simulated from the SH program using P-wave velocities. Apart from those events, SV converted phases (PPSS) reflected from the top of the Paleozoic formation are present at around 180 ms and show no delays after steam injection. Those phases can be useful for resolving the extent of the steam heated zone in the region between the injector and the receiver wells.

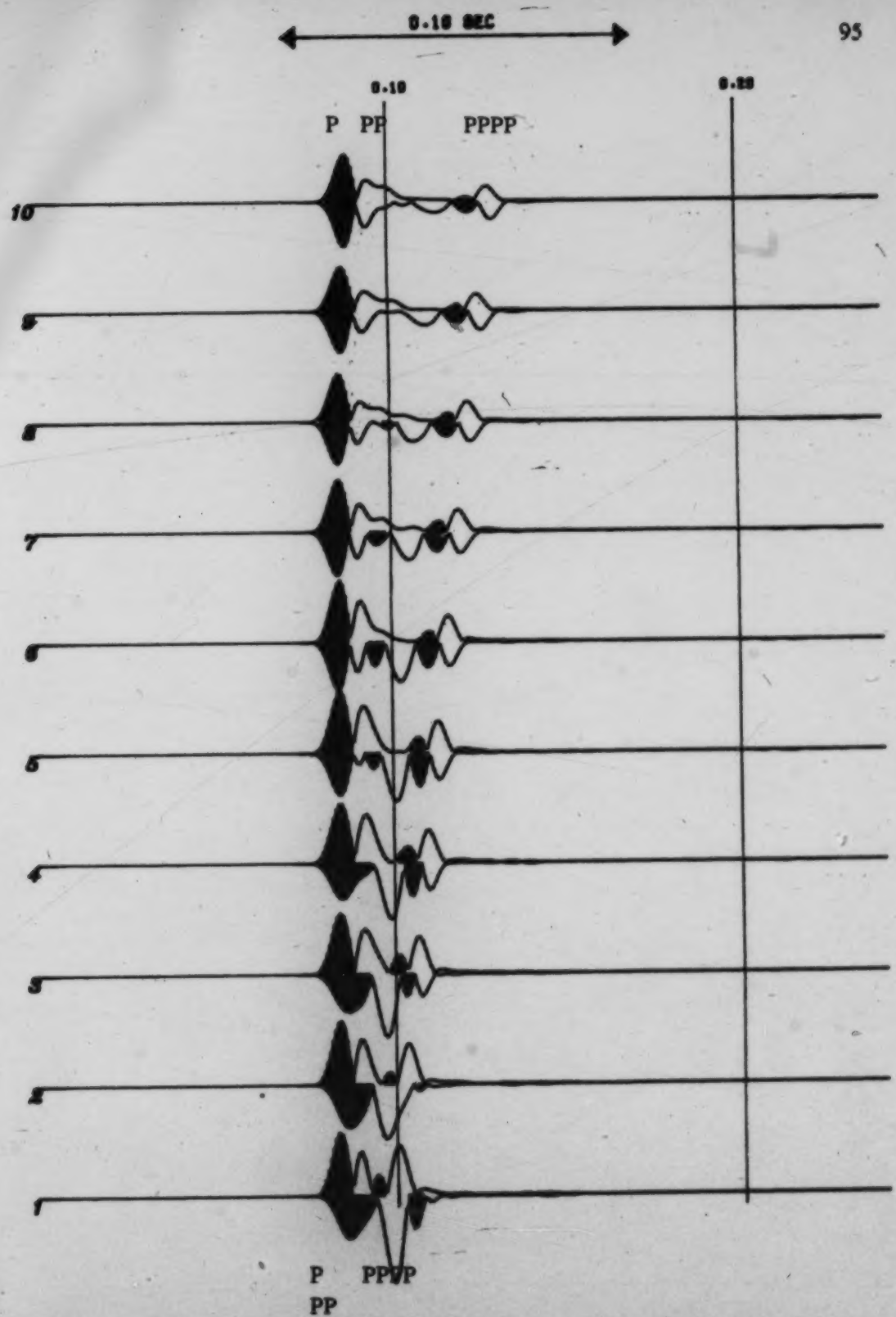

Figure 5.6 BARS plots for an SH computer simulation of the 1982 crosshole experiment. Velocity varies vertically according to the sonic log.

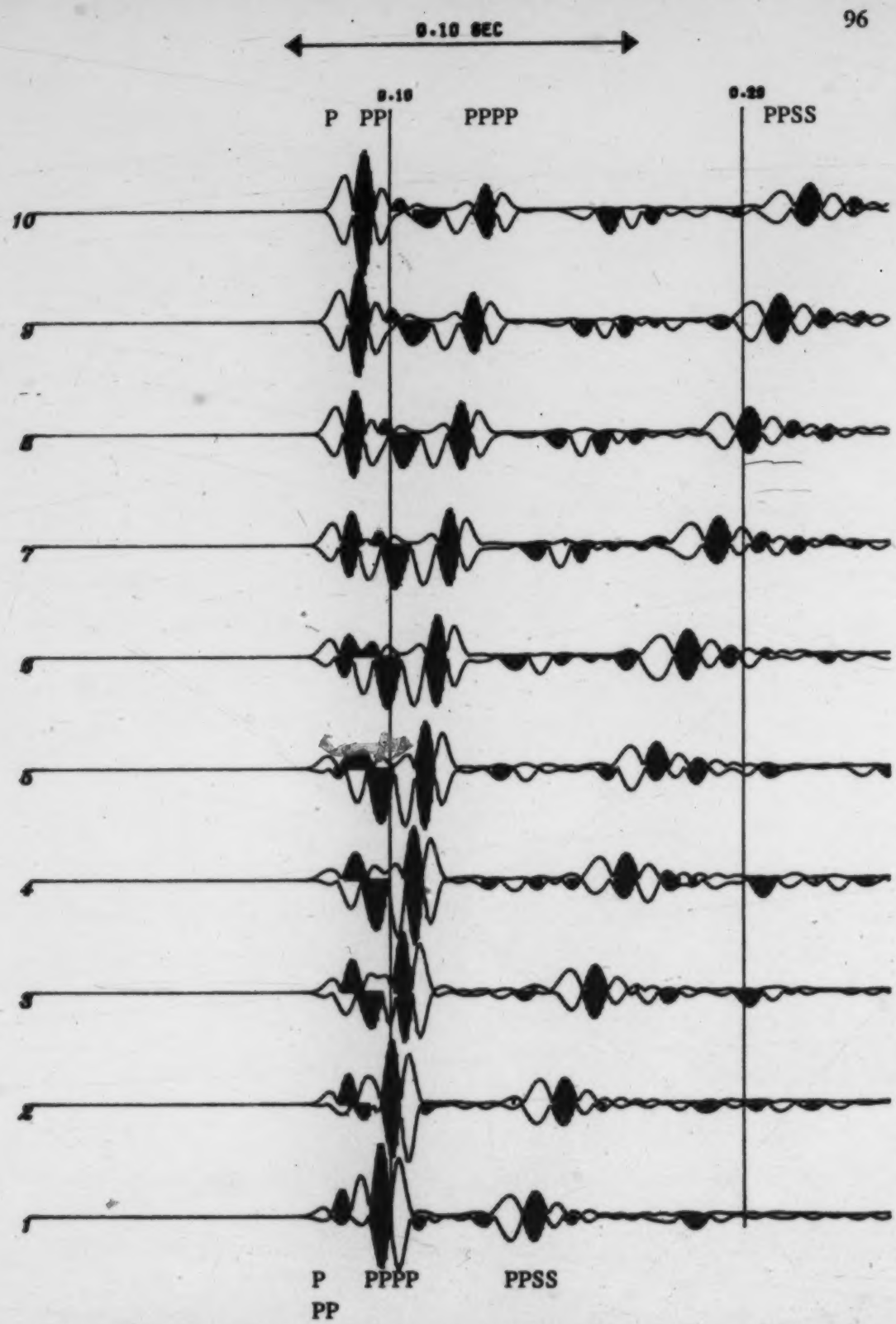

Figure 5.7 BARS plots for a P-SV computer simulation of the 1982 crosshole experiment using a P-wave line source: Vertical component of particle velocity.

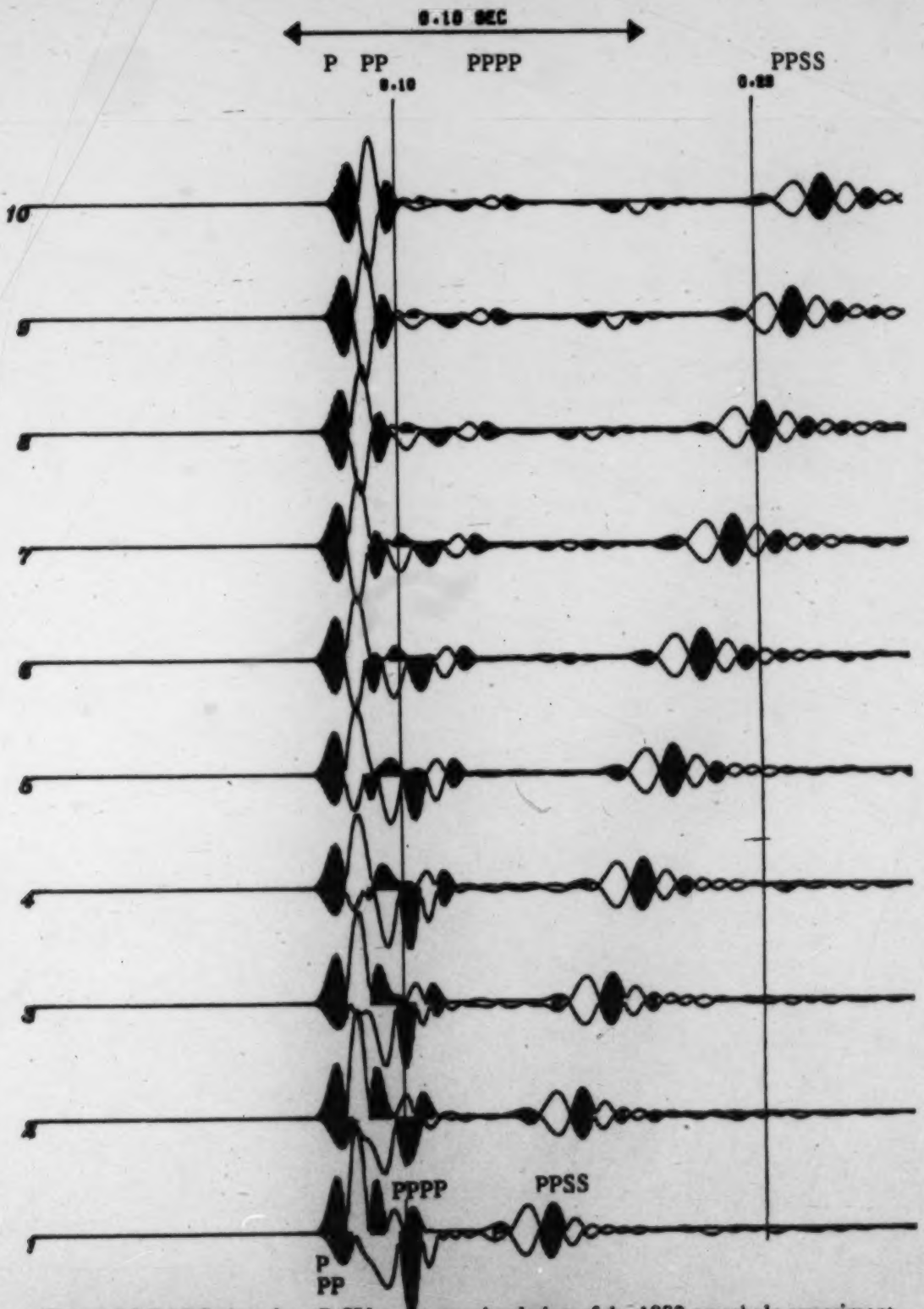

Figure 5.8 BARS plots for a P-SV computer simulation of the 1982 crosshole experiment using a P-wave line source: Horizontal component of particle velocity.

Since the explosive source in the hole to hole experiment generates both P-and S-waves, we consider in the P-SV computer simulation a SV-line source whose frequency content is up to 60 Hz in accordance to the real experiment. Direct S waves are recorded in the hole to hole simulations (figure 5.9 and 5.10) which are delayed in the after steam injection experiment by 5-10 ms for receivers 1 to 3. Those delays are similar to the ones observed in the real experiment and can give useful information concerning the shape and the size of the heated zone. In the synthetic sections the direct S wave can be completely resolved and this helps to identify it in the real sections. The delays on the direct S arrivals can be explained by the increase of the Poisson ratio from 0.36 outside the steam heated zone to 0.4 inside. Notice the reflections (SSSS) from the Paleozoic at around 200 ms for receivers 1 to 6. Finally, the converted phases (SSPP) from the same interfaces present at earlier times (120 ms) remain undisturbed after steam injection.

Finally, the responses from the P and SV source simulations are combined and the total field (fig 5.11 and 5.12) is compared with the real data. The real data in figure 5.3 shows similar delays on both the P and S phases for ray paths that pass through the anomalous steam zone. The S wave pattern shows similar phase and amplitude changes apart, from the difference in source frequencies. The total response from the simulation is comparable to the outcome from the real data. In the computer seismic wave simulation above, the size of the steam zone is larger (48m wide) than that proposed by Macrides et al (1987) which produces the same delays in the P and S direct arrivals after steam injection. Macrides et al (1987) based their calculations on simple straight ray theory. Simple ray theory is adequate for most purposes in applied seismology but it does not give a complete physical description of seismic phenomena. In this experiment the rays diverge from the low velocity steam zone (Singh and Nyland, 1988) and straight ray theory fails to predict this effect. In wave theory this effect is taken into account, so observed delays correspond to larger low velocity zones. Also a complete picture of the experiment is given in figures

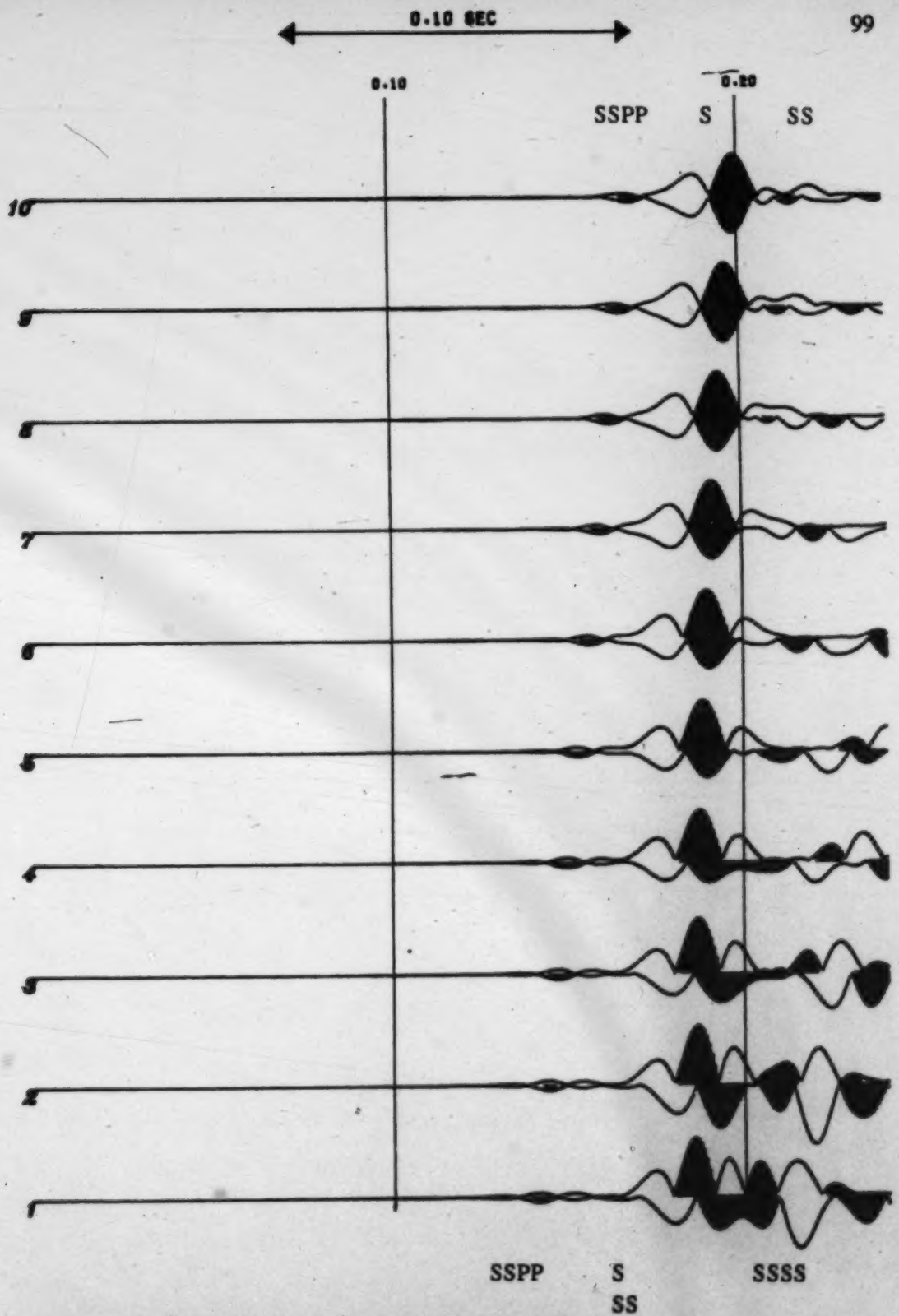

Figure 5.9 BARS plots for a P-SV computer simulation of the 1982 crosshole experiment using a SV-wave line source: Vertical component of particle velocity.

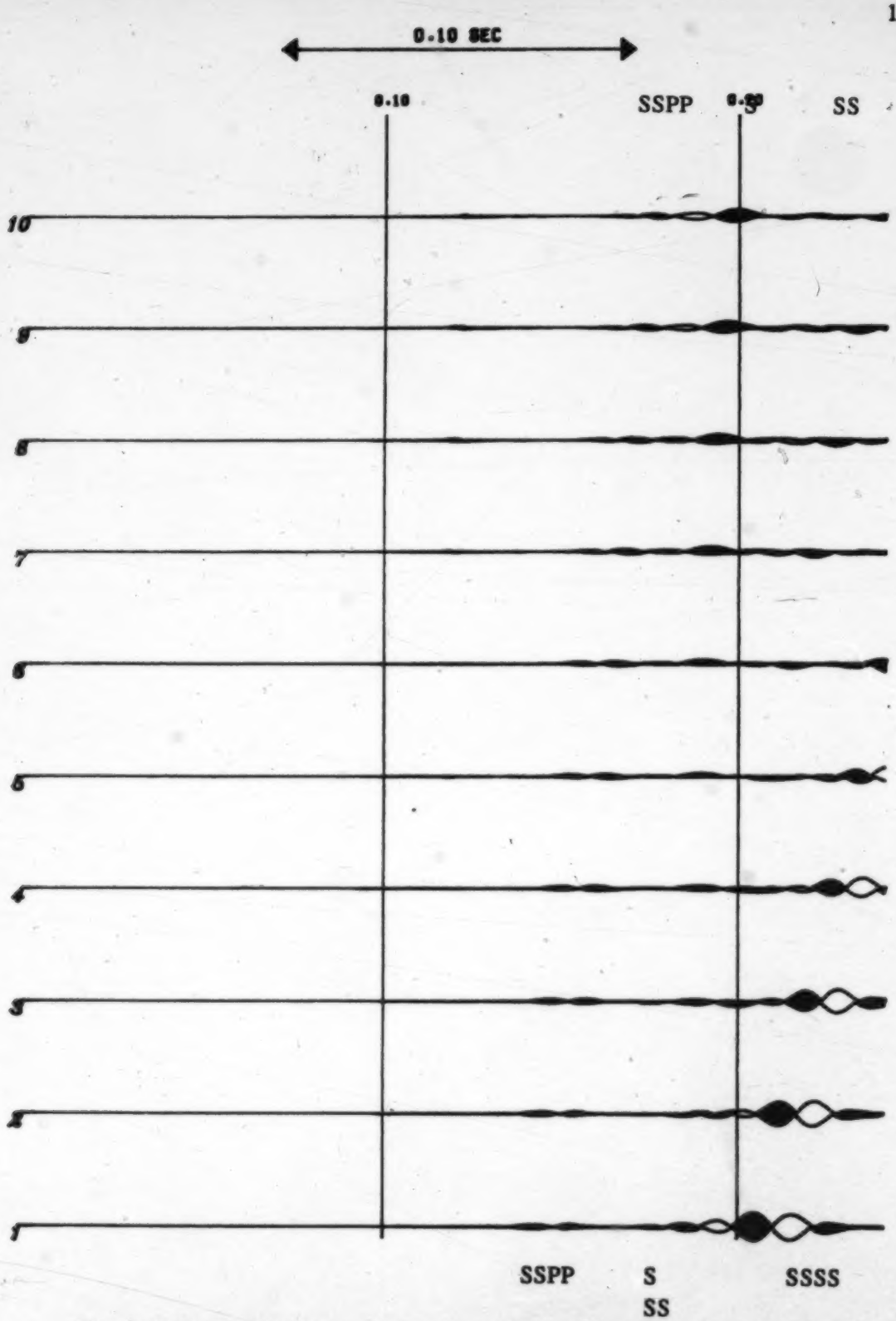

Figure 5.10 BARS plots for a P-SV computer simulation of the 1982 crosshole experiment using a SV-wave line source: Horizontal component of particle velocity.

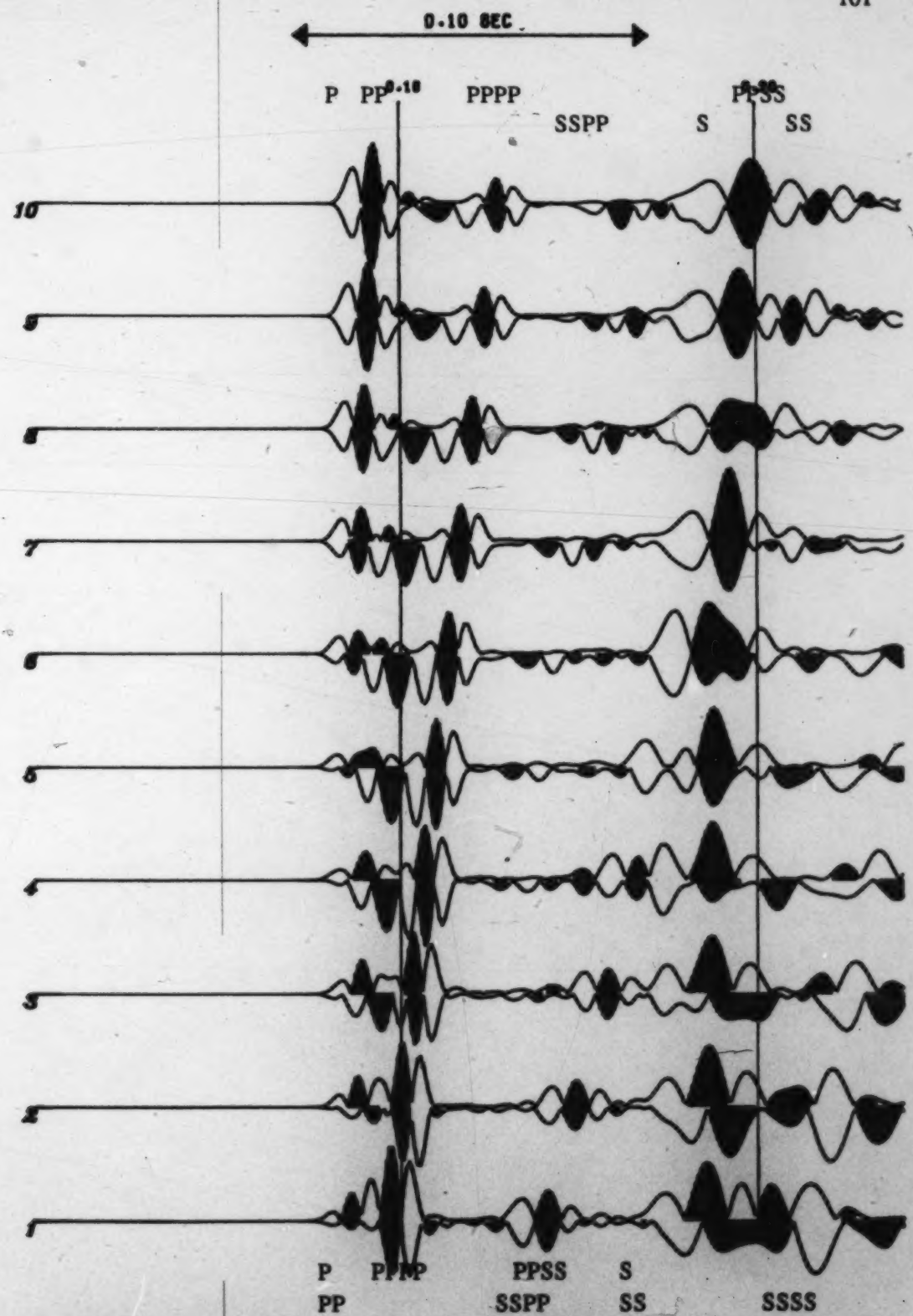

Figure 5.11 BARS plots for a P-SV computer simulation of the 1982 crosshole experiment the outcome after summing the P- and the SV-wave line source results: Vertical component of particle velocity.

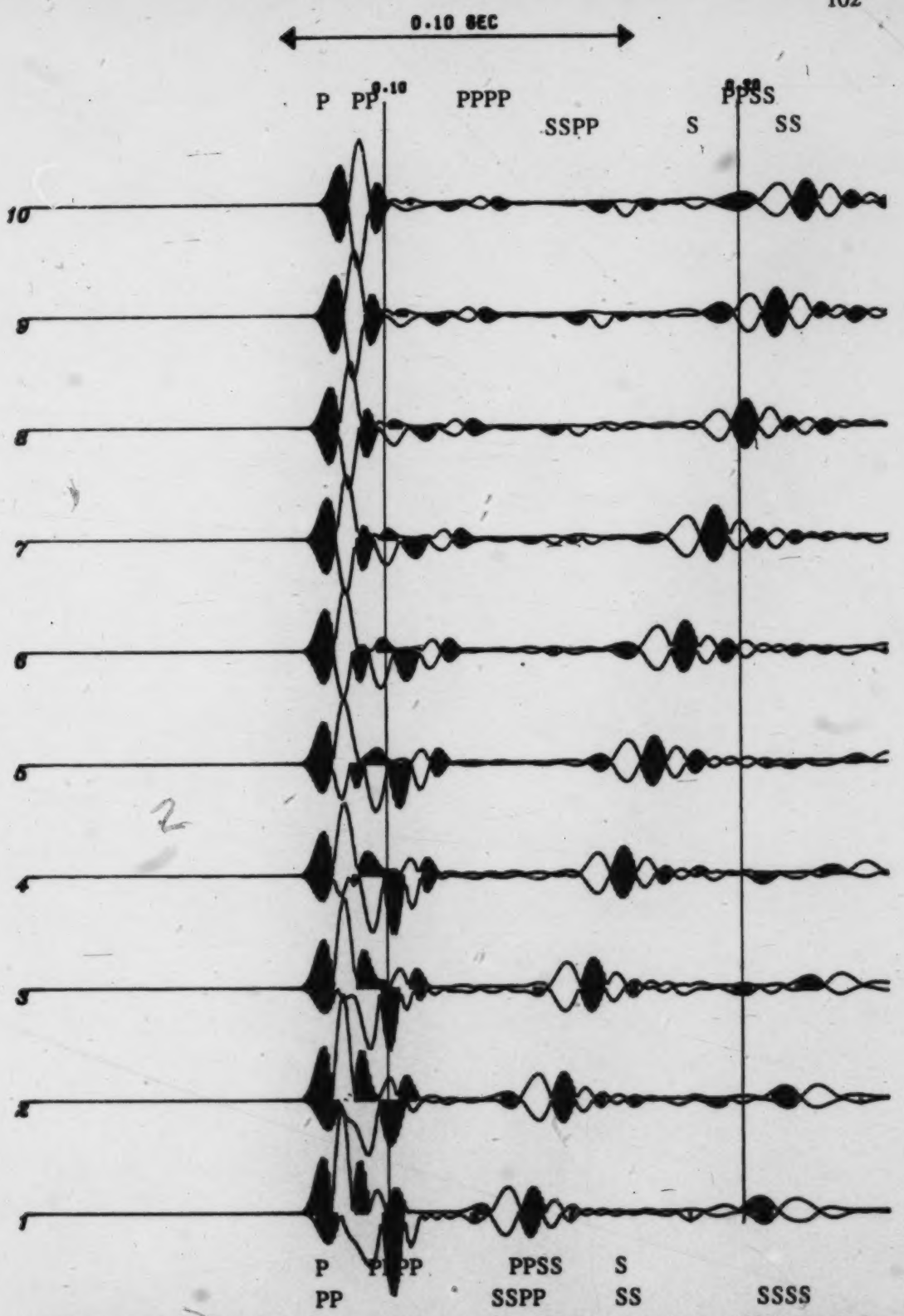

Figure 5.12 BARS plots for a P-SV computer simulation of the 1982 crosshole experiment the outcome after summing the P- and the SV-wave line source results: Horizontal component of particle velocity.

(5.10) and (5.11) where, apart from the delays, information about the amplitudes is preserved.

We have obtained a better model using forward modelling of the real experiment. This should provide a better understanding of the complex processes by identifying direct, reflected or converted events. The simplistic shape of the steam zone (ellipse) seems to be a good first approximation which introduces most of the events that are present in the real experiment. A band of events not present in the simulations recorded between 150 - 180 ms may be due to high velocity discontinuous stringers which are present in the Clearwater formation but their exact disposition cannot be determined from the limited number of sonic logs. Another possibility is that those thin (2m) carbonate stringers are continuous but they prograde so that they appear at different depths on different wells. Future modelling will focus on this difficult problem. The forward iteration procedure will require a large number of computer runs. The shape of the steam zone is also more complex than the simple elliptical shape we have specified. It is worth noting that those simulations, apart from reconstructing the full wave field, gave us insight on which rays are converted and so aided in the interpretation of the real data. Finally this study strongly suggests the necessity for two component acquisition as well as the importance of S-waves.

5.3 Surface experiment

Hole to hole seismic measurements are expensive and a more cost effective procedure is to monitor with near surface sources and receivers. In this experiment the sources and the receivers were located at the surface with a source to first receiver distance of 36 m. The geologic formations of the area as well as sonic log velocities are illustrated in figure 5.13. Figure 5.14 displays 24 traces from a common shot gather consisting of 48 vertical component receivers separated by 18 m and recorded every 2 ms in split spread geometry

with the source exactly above the center of the steam zone. It can be seen that the reflections from interfaces below the Clearwater are delayed, probably due to the presence of the steam zone. In the simulation we used 24 receivers, taking into consideration that the model is symmetric. The reflections from the weathered layer are weak in the real data due to destructive interference patterns on the glacially eroded surface layer. In the simulation, the near-surface multiples are eliminated by not including the surface interface in the model.

In the SH computer simulation for the surface experiment the frequency content of the Gaussian line source was lowered to 60 Hz (see table 5.2 for the rest of the parameters) since the real data do not contain higher frequency components. A sequence of four synthetic sections shows the seismic response during the steam injection i.e. while steam is injected into the formation (figures 5.15 to 5.18). The final section corresponds to the model shown in figure 5.13 where a more complicated heated zone consists of an inside steam zone surrounded by a condensation zone. In the steam zone both temperature and pressure are expected to be constant. Since the seismic velocity depends highly on these two parameters it seems justifiable to consider a constant velocity within the steam zone. In the condensation zone, temperature and pressure gradually decrease until undisturbed reservoir conditions are encountered. For simplicity a constant average velocity is assumed within this zone. In both the before and after steam injection sections an exponential gain function was applied in order to reduce the high amplitudes of the direct arrivals. In order to emphasize phase changes, the positive and negative amplitudes are colored differently for absolute values above a certain threshold. Clear reflected arrivals are also observed from the various interfaces along with multiples. A change in amplitude in the reflections from the first two interfaces is due to the fact that the SH reflection coefficient decreases with the angle of incidence until it reaches the critical angle (Daley and Hron, 1979). The presence of the steam zone causes delays to the arrivals below Clearwater while additional arrivals are observed due to reflections on the top and the bottom interfaces of the steam

zone. Those additional arrivals have a 90^0 phase shift and indicate the extent of the steam heated zone.

Similar responses are recorded in the P-SV simulation using a P-line source (fig. 5.19 to 5.22). Most of the reflected energy is recorded on the vertical component while the direct wave as well as converted phases are observed on the horizontal component.

5.4 Conclusions

Seismic methods can play a major role in helping to solve production and recovery problems by determining the spatial distribution of reservoir properties and their changes with time. Since large velocity changes occur in rocks with heavy hydrocarbons in their pores upon heating, the seismic measurements may be used as reservoir thermometers to track temporal and spatial changes in temperature associated with the thermal recovery techniques. Computer simulations can tell us how to extract information about the direction of propagation and details of the shape, rate of movement and spatial heterogeneity of the steam front. The richness of the seismic effects discussed above and the sensitivity of density and velocity to reservoir parameters clearly indicate the future direction of reservoir seismology. It appears possible to describe reservoirs in more detail and to monitor their modification, particularly if high frequency sources can be used together with high resolution seismic recording techniques. These could include use of repetitive small explosives, buried geophones that record at 1/2 or 1/4 ms sampling intervals.

Table 5.2. Numerical parameters for the surface experiment

Source :	t_1 = 50 ms;	Minimum velocity :	1785 m/s
α	1.77 E4	(wavelength = 29.75 m)	
Receiver separation:		18 m	
Grid spacing:	6 m;	Time step:	0.5 ms

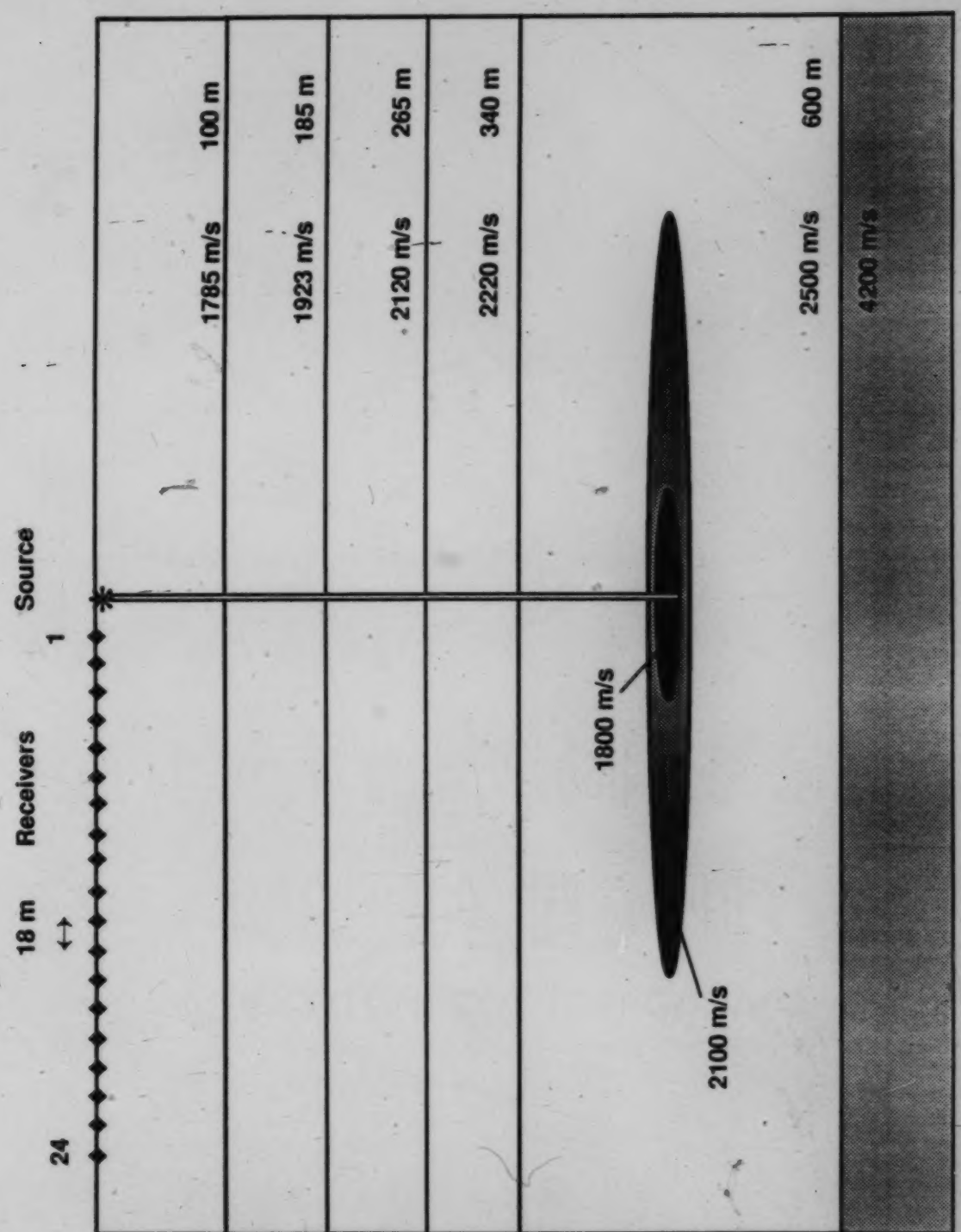

Figure 5.13 Model geometry of the surface experiment.

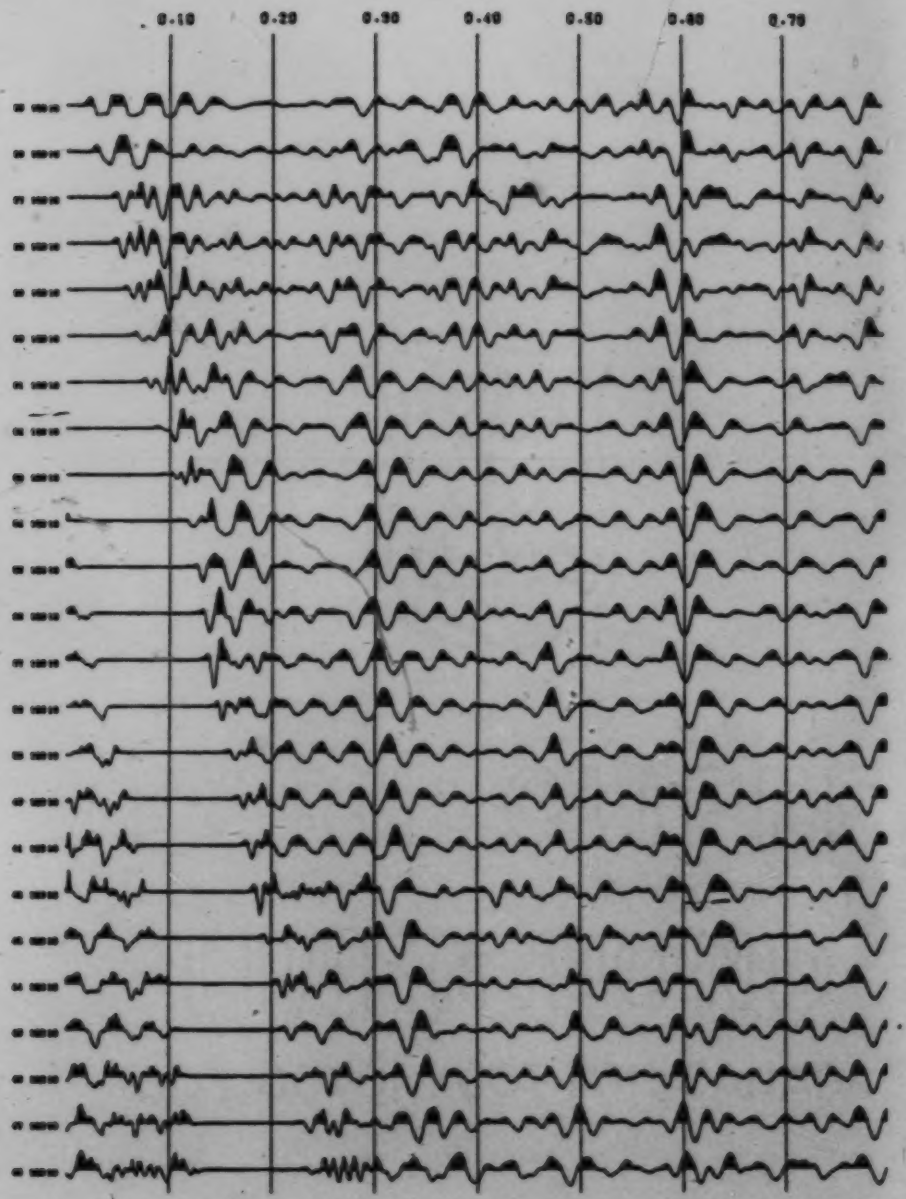

Figure 5.14 Common shot gather surface data over a steam injected area.

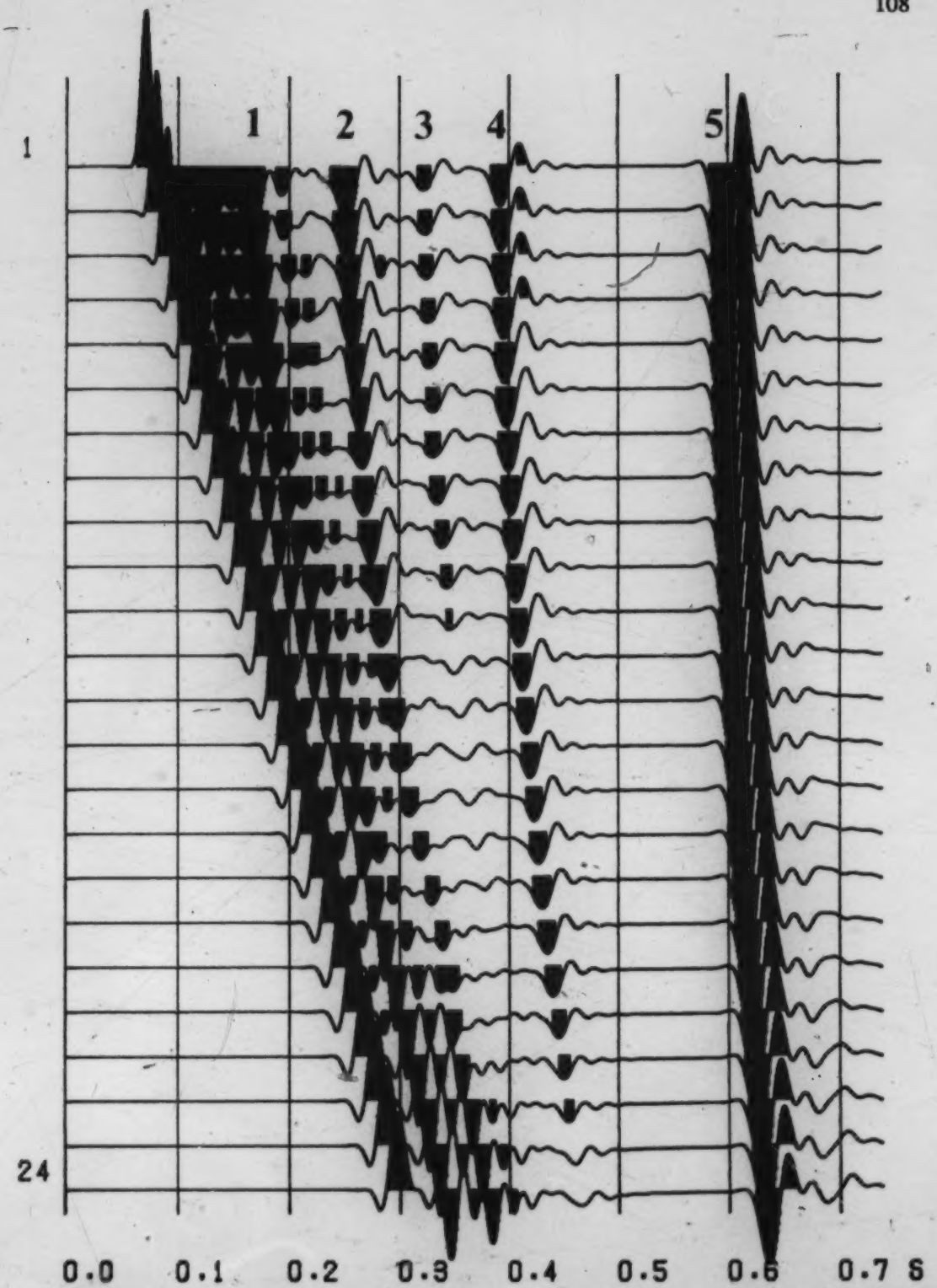

Figure 5.15 SH computer simulation of the surface experiment: Section before steam injection.

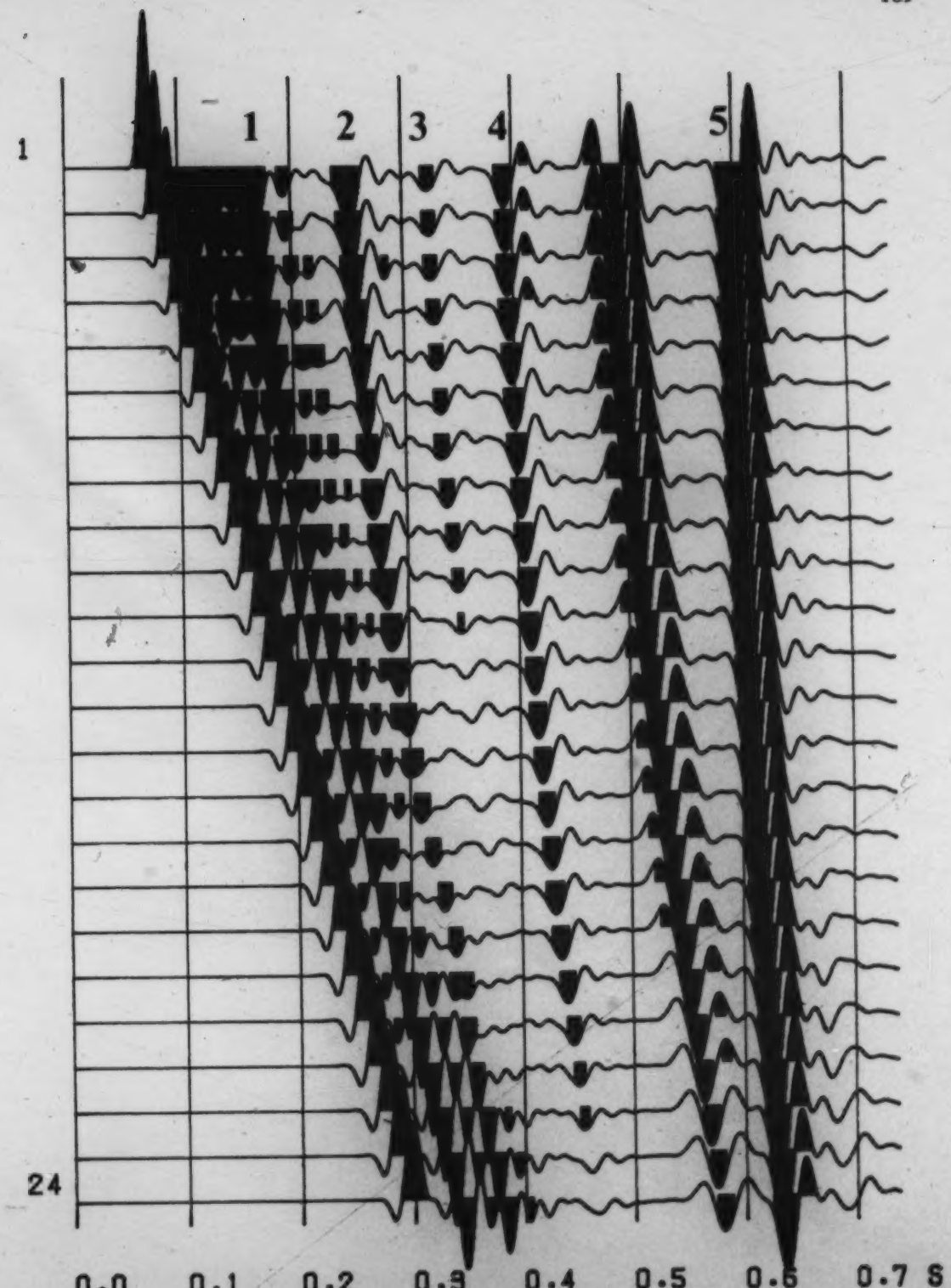

Figure 5.16 SH computer simulation of the surface experiment: Section with a steam zone of elliptical shape whose major semiaxis is 36 m.

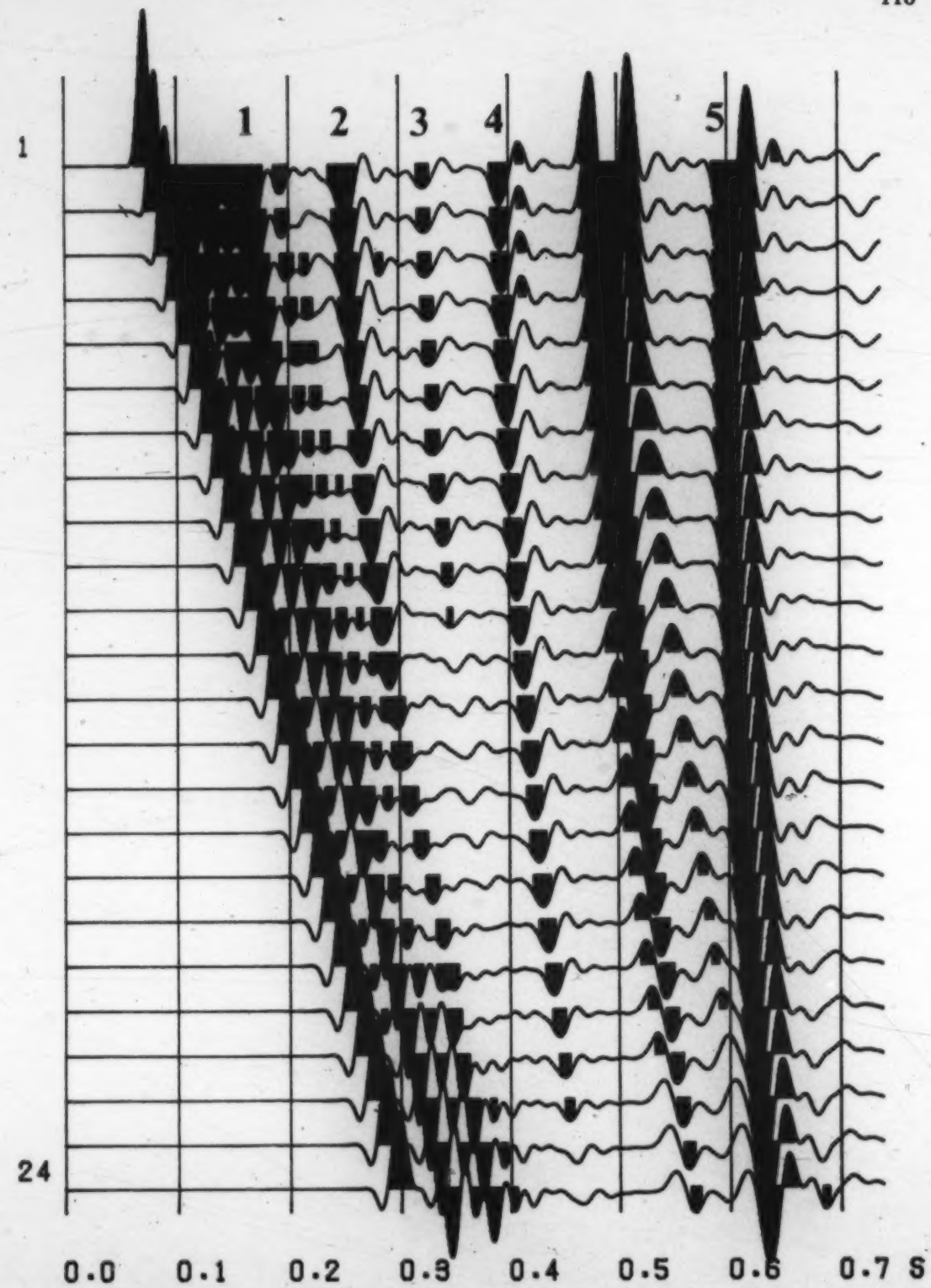

Figure 5.17 The same as in figure 5.16 with major semiaxis is 78 m.

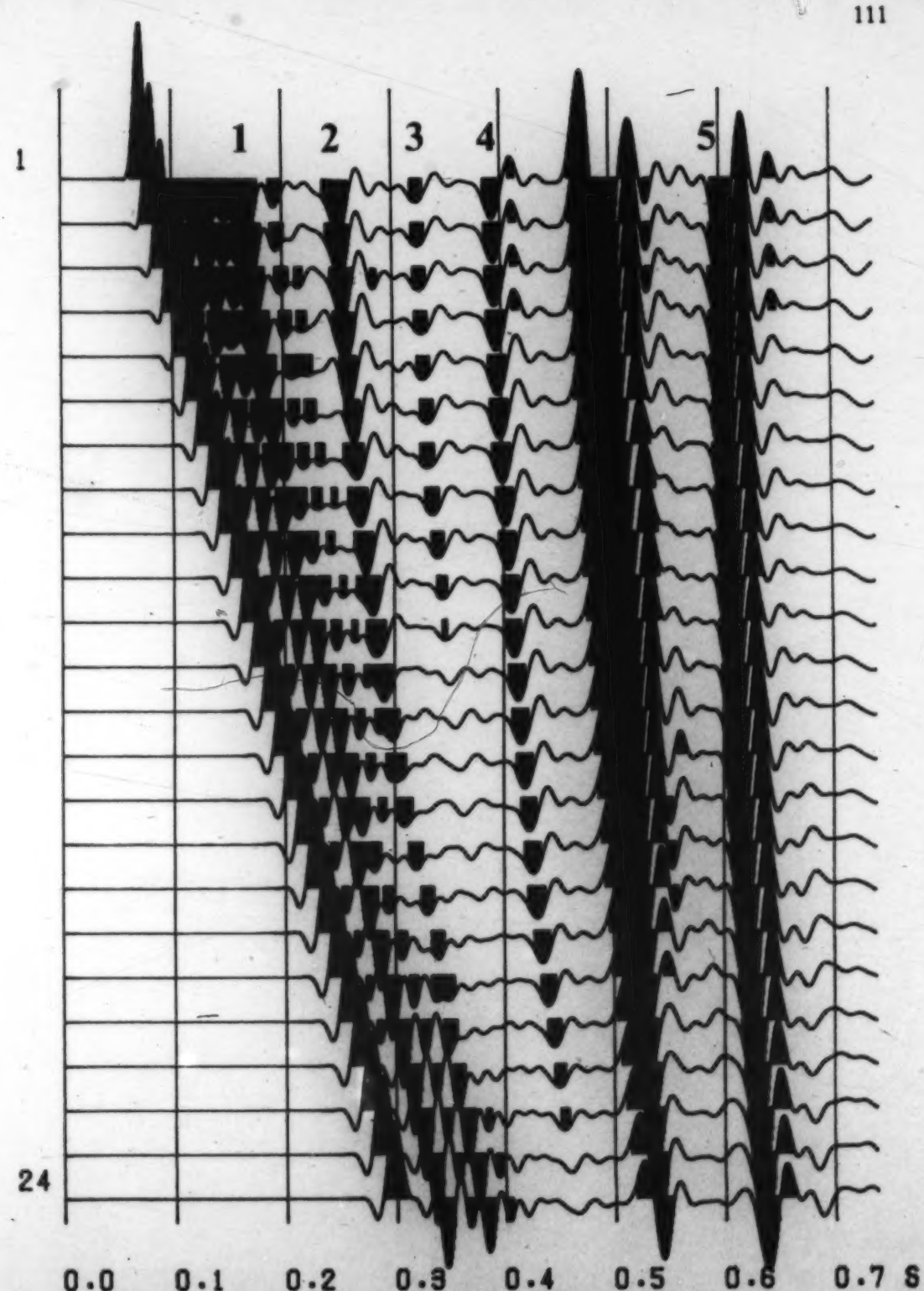

Figure 5.18 SH computer simulation of the surface experiment: Section with a steam zone inside and a condensation zone outside both of elliptical shape.

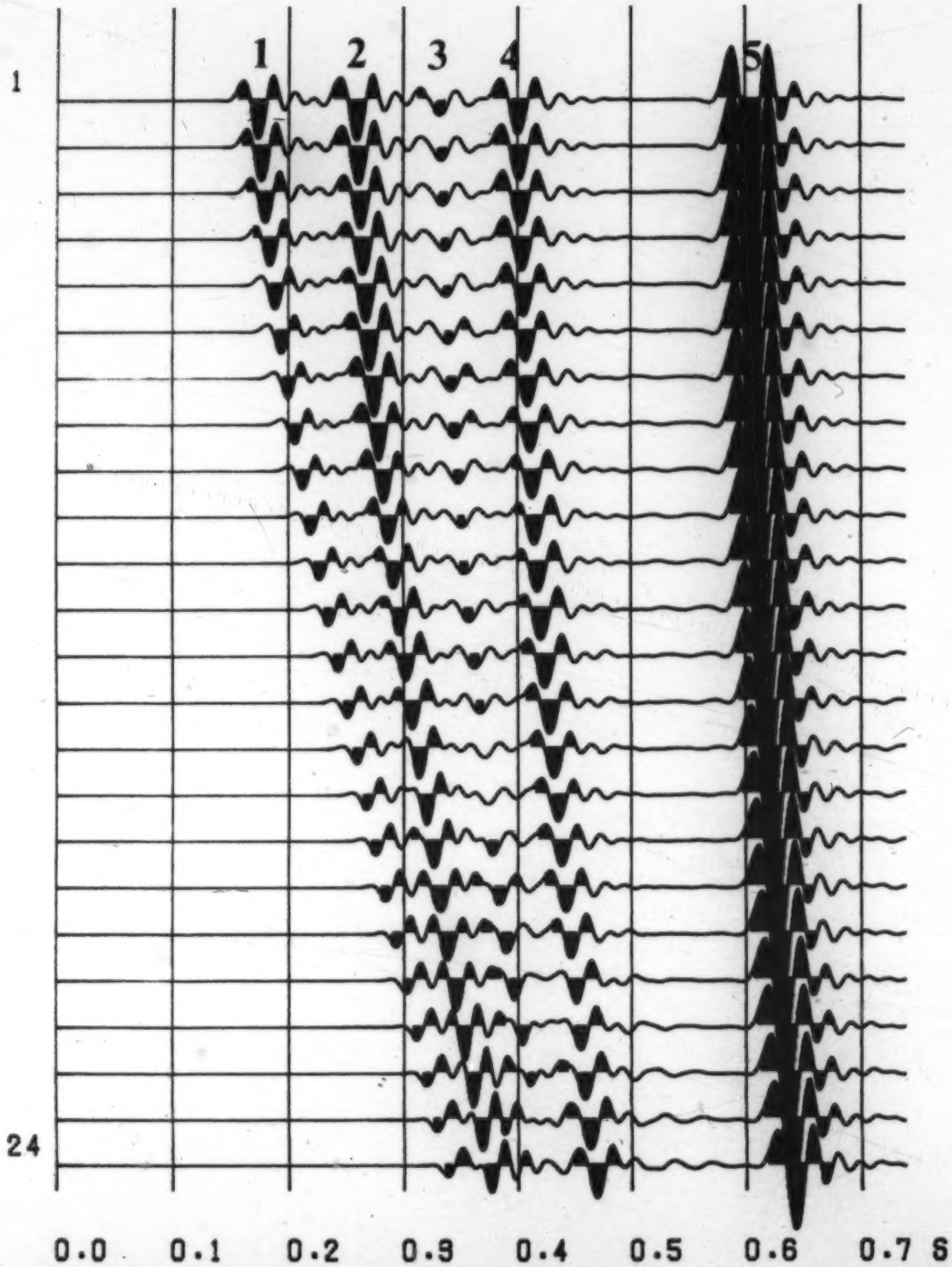

Figure 5.19 P-SV computer simulation of the surface experiment: Section before steam injection for the vertical component of the particle velocity.

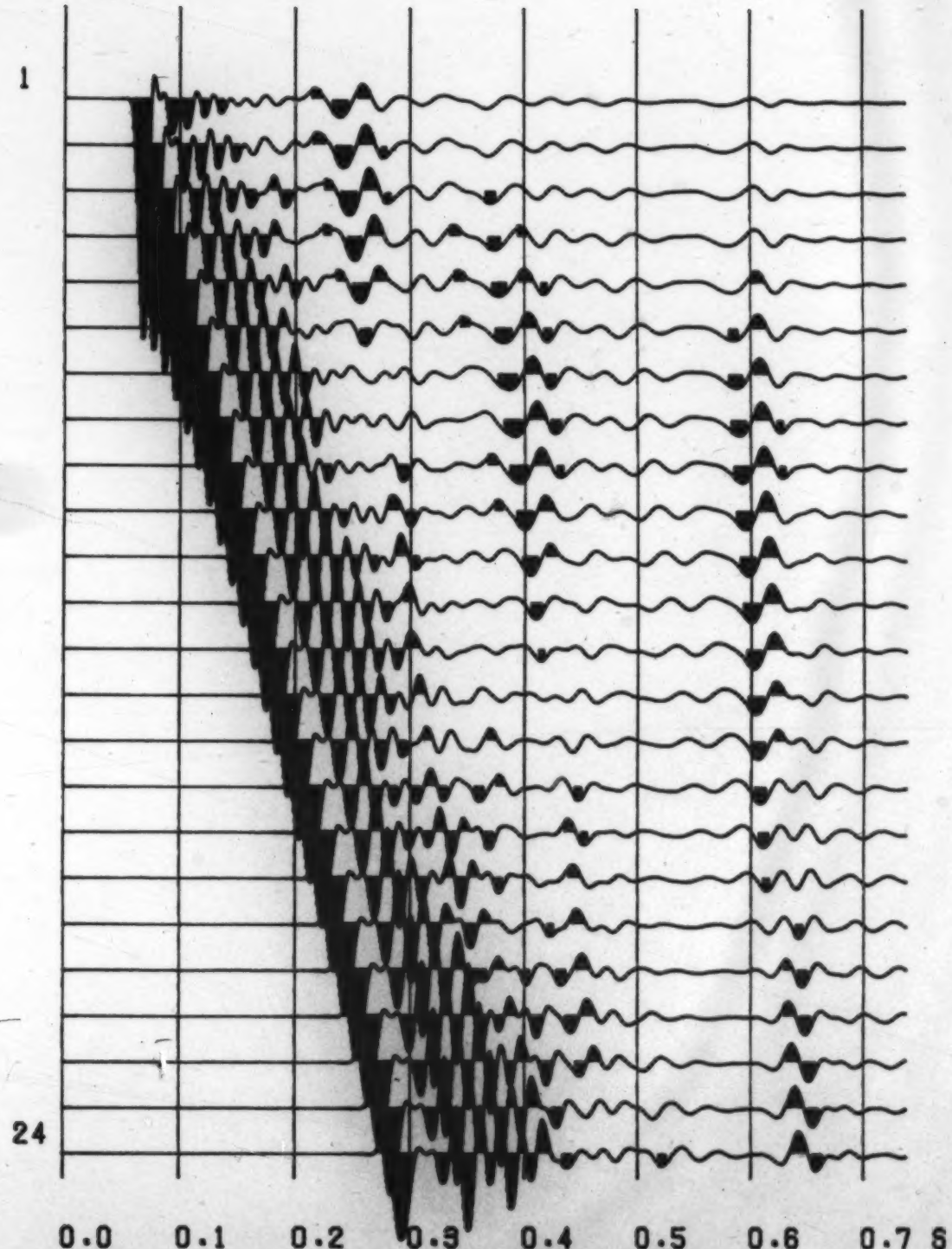

Figure 5.20 The same as in figure 5.19 for the horizontal component.

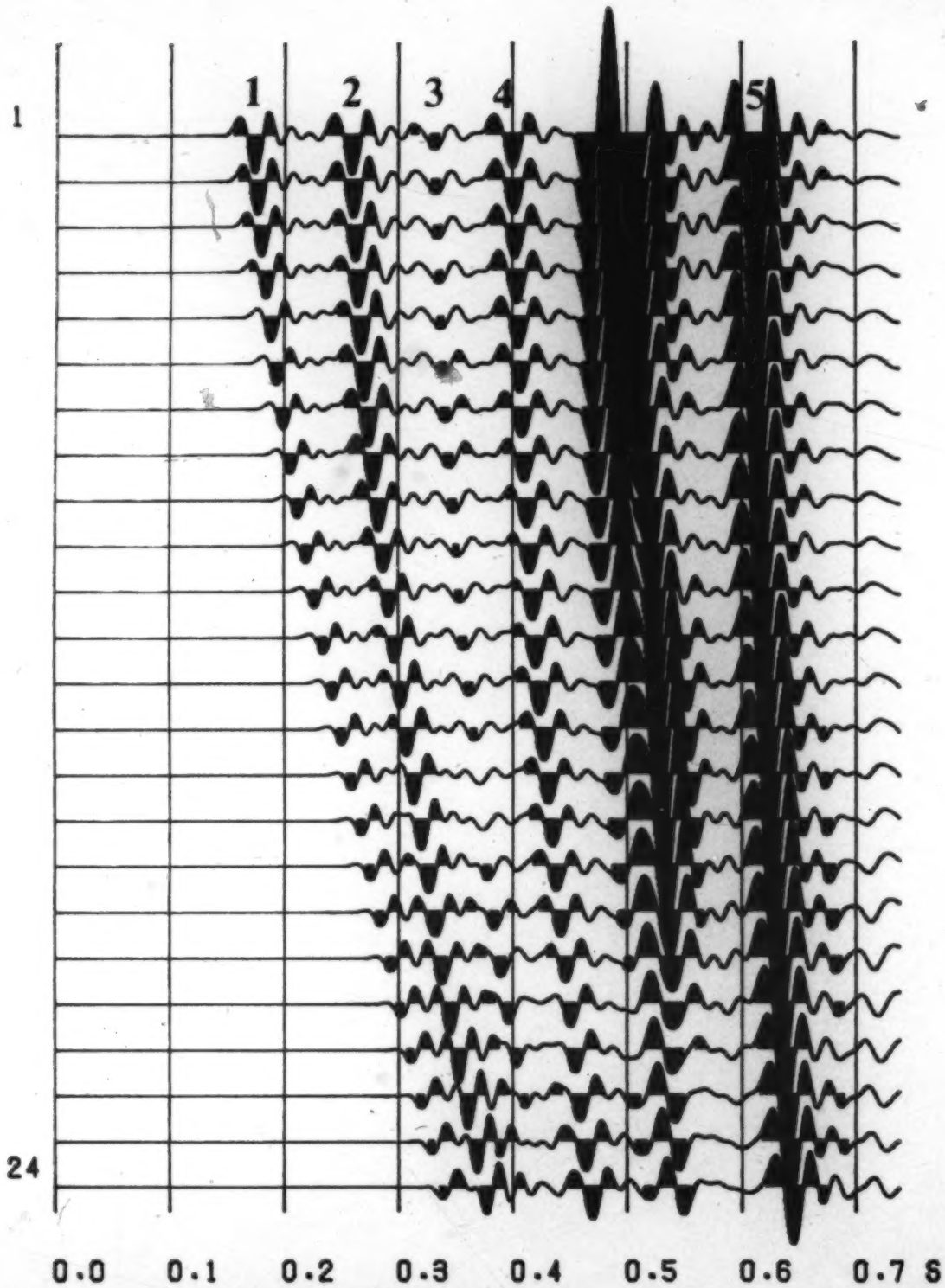

Figure 5.21 P-SV computer simulation of the surface experiment: Section after steam injection for the vertical component of the particle velocity.

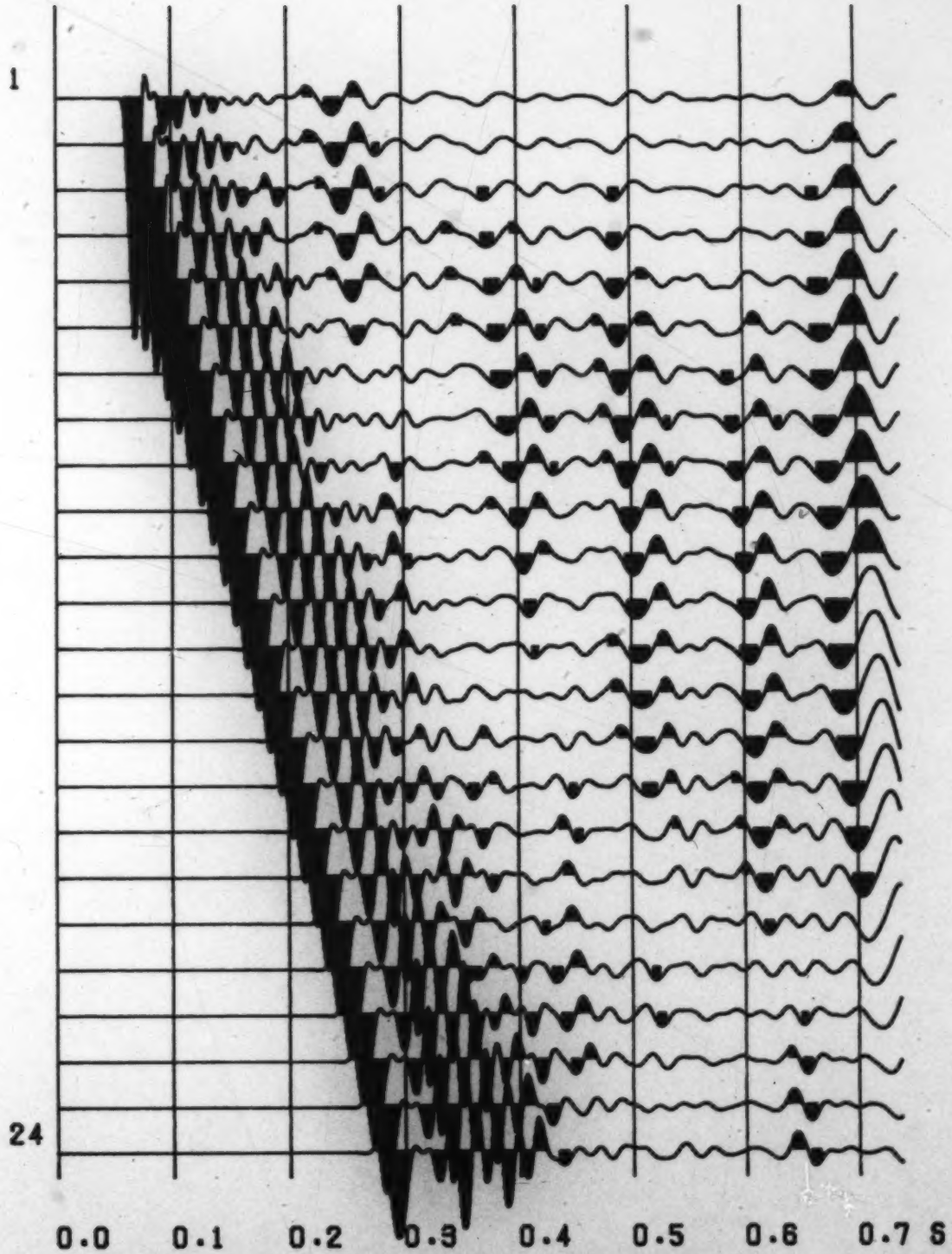

Figure 5.22 The same as in figure 5.21 for the horizontal component.

CHAPTER 6

ATTENUATION IN TIME DOMAIN

6.1 Introduction

Considerable progress has been made during the past two decades on aspects of seismic attenuation. By seismic wave attenuation one describes any irreversible energy losses other than spherical divergence, transmission loses and mode conversions which a seismic wave experiences as it propagates through a medium. This definition is a broader concept than is the mechanism of dissipation which describes energy lost due to friction between moving rocks or fluid motion within rock pores. For seismic waves in the shallow crust, attenuation proportional to frequency is the rule rather than the exception. In principle, velocity must depend upon frequency in an attenuating medium, and much of the disagreement concerns the search for a mathematical description which is consistent with the experimental attenuation and velocity data that satisfies the physical boundary conditions.

Evidence from different experiments supports the fact that several physical mechanisms must contribute to seismic attenuation in rocks. The dramatic increase in attenuation due to the addition of trace amounts of water to a dry, porous rock has focused attention on details of flow within fine cracks (Nur et al., 1980). At seismic prospecting frequencies viscous flow does not provide the dominant loss mechanism in porous and permeable rocks that are fully saturated with water. Some mechanisms for energy loss must be acting within the solid matrix. Coulomb friction between grains yields attenuation which depends upon the amplitude of vibration, whereas measurements indicate attenuation to be independent of

amplitude. The demonstration that the motion of lattice dislocations within the solid gives the right dependence on frequency and the correct magnitude of attenuation in granite makes this an attractive choice for the loss mechanism (Mason, 1969).

Even before loss mechanisms and mathematical models are established, it is possible to view attenuation as a diagnostic lithologic parameter and to put it to use. In some articles anomalously high attenuation has been attributed to heterogeneous gas saturation in the section above an oil field. Based on empirical observation, attenuation has been proposed as an indicator of the sand-shale ratio. Some measure of attenuation can be obtained from acoustic logs in a routine fashion. With the sophisticated seismic modeling programs now in use to correct for spherical spreading, transmission coefficients, etc, that portion of the amplitude loss due to attenuation can be determined with some certainty. Although we may not be able to avoid the effects of attenuation, we may at least be able to use it as a source of valuable subsurface information.

In this chapter, sections 2 and 3 contain definitions of the loss factor Q and a short review of attenuation models. In section 4 a new method for implementing attenuation in the time domain is described and in section 5 the assumptions are enumerated. Section 6 describes the design of a recursive filter for the logarithmic law and its vectorization. Plane waveforms with attenuation are generated and are compared with the ones resulting from the convolution of the wavelet with a dissipation operator.

6.2 Definitions of Q

Attenuation measurements are important because attenuation losses affect seismic wave amplitudes and also because attenuation values are a function of the lithology, fluid saturation, overpressuring and the general physical state of subsurface rocks. A measure of the amplitude loss is the specific attenuation factor Q, defined as

$$\frac{2\pi}{Q} = -\frac{\Delta E}{E} \qquad (6.2.1)$$

In this definition ΔE is the amount of energy dissipated per cycle of a harmonic excitation in a certain volume and E is the peak elastic energy in the system in the same volume.Another measure of attenuation is obtained from the logarithmic decrement of a harmonic wave. The logarithmic decrement is equal to the quantity π/Q. The spatial attenuation factor for a wave function observed throughout space at a fixed time will be of the form $exp(-\alpha x)$, where $\alpha = \omega/2cQ$ and c is the phase velocity. For comparison, the observation of this wave function as a function of time at a fixed point in space yields the damping factor $exp(-\gamma t)$, where $\gamma = \omega/2Q$. In heterogeneous media some difficulty is encountered in relating the several definitions.

6.3 Attenuation models

In perfect elasticity, strain is linearly proportional to stress and independent of the duration of the stress. When the stress is removed the original form is recovered at once. In viscoelasticity, the strain under constant stress increases at a decreasing rate. When the stress is removed there is an immediate recovery by the amount of the initial strain and the strain decreases further, ultimately tending to zero (Jeffreys, 1976).

Several attempts have been made to find modifications of Hooke's law that would account for the effects of anelasticity. The attempts to account for the observed variation of Q with frequency can be divided into two groups: those invoking linear models and those invoking non linear models (Knopoff, 1964). Non-linearity seems to have been largely ignored, because of the mathematical difficulties associated with non linear systems. In this section a number of linear models, mainly for Q independent of frequency, will be

reviewed.

In Boltzmann's early theory (1876) to explain the nature of acoustic loss, the strain due to an applied stress is delayed by some sort of '*memory*' behavior in the material. For a stress excitation, which is a complicated function of time this can be expressed as a convolution with an elementary creep function which expresses the delay. Thus

$$M_u\, \varepsilon(t) = \sigma(t) + \int_{-\infty}^{t} \sigma(\tau)\, \dot{\phi}(t-\tau)\, d\tau \qquad (6.3.1)$$

where $\varepsilon(t)$, $\sigma(t)$ are strain and stress respectively, M_u an elastic modulus and $\phi(t)$ a creep function.

For plane waves propagating in one direction at a fixed frequency ω, the dispersion relation can be evaluated (Aki and Richards, 1980) from

$$\frac{\omega}{c(\omega)} + i\,\alpha(\omega) = \frac{\omega}{c_\infty}\left[\, 1 + \int_0^\infty \dot{\phi}(t)\, \exp(i\omega t)\, dt \,\right]^{\frac{1}{2}} \qquad (6.3.2)$$

and the Q factor

$$\frac{1}{Q(\omega)} = \frac{2c(\omega)\alpha(\omega)}{\omega} = \frac{\mathrm{Im}\left\{ \int_0^\infty \dot{\phi}(t)\exp(i\omega t)dt \right\}}{1 + \mathrm{Re}\left\{ \int_0^\infty \dot{\phi}(t)\exp(i\omega t)dt \right\}} \qquad (6.3.3)$$

where

$$c_\infty = \sqrt{\frac{M_U}{\rho}} \qquad (6.3.4)$$

and ρ is the density. Employing these relations, various creep laws can be translated into laws of attenuation and dispersion.

Lomnitz (1957), (see also Nyland, 1986) has indicated that a logarithmic creep law gives a linear behavior of attenuation over a large frequency range. He cites evidence for a logarithmic creep function from laboratory experiments in rocks at strains in the range 10^{-5} to 10^{-4} (Lomnitz, 1956). A difficulty encountered with the Lomnitz model is that the function *ln t* is singular at time *t=0*. To remove this singularity a characteristic time t_0 must be introduced so that the creep function $\phi(t)$ will be *ln* $(t+t_0)$. An estimate of t_0 can be obtained from causality conditions.

Lomnitz proposed that the strain under constant stress can be given by

$$M_u\, \varepsilon(t) = \sigma\,(1 + \phi(t)) \tag{6.3.5}$$

with

$$\phi(t) = \begin{cases} 0 & t \le 0 \\ q \ln(1+at) & t \ge 0 \end{cases} \tag{6.3.6}$$

where the constant *a* appears to be related to the frequency of a vacancy in a crystal lattice (between 10^6 to 10^{10} Hz) and the constant *q* may be viewed as a proportionality factor between the creep rule and time. Over a wide range of periods, the dissipation per period is close to $1/2\ \pi^2 q$ of the total energy. $1/Q$ and q are dimensionless quantities of the same magnitude

$$q = \frac{2}{\pi Q}\,\frac{c_\infty}{c(\omega)} \approx \frac{2}{\pi Q} \tag{6.3.7}$$

They are both measures of dissipation, the first applying to the dynamic case while the second is significant in the static or creep case. Figure 6.1 shows various strain responses

in units of $1/M_u$ under constant (unity) stress for different values of Q. The essential part is that this logarithmic law is linear in that stress and it can be applied to small strains. For variable stress the deformation can be built up by superposition according to Boltzmann's formula (eq. 6.3.1). By replacing $\phi(t)$ from equation (6.3.6) into equation (6.3.2) and integrating the dispersion relation for plane wave propagation and $\omega << a$ becomes (Aki and Richards, 1980),

$$\frac{1}{c(\omega)} = \frac{1}{c_\infty} \left\{ 1 - \frac{1}{\pi Q} \left[\gamma + \ln\left(\frac{\omega}{a}\right) \right] \right\} \qquad (6.3.8)$$

and it is in agreement with the relation for Azimi's attenuation law. Attenuation can be controlled from the parameter q which can be taken space dependent for heterogeneous media.

Savage and O'Neil (1975) have shown that Lomnitz and Futterman's theories to be similar. The basic difference is that Futterman's theory contains a low frequency cutoff while Lomnitz theory does not require the low frequency cutoff because the coefficient governing the proportionality between attenuation and frequency varies slowly with frequency. They suggest that Lomnitz theory is more preferable since it is based on experimental grounds in contrast to Futterman's theory which is ad hoc.

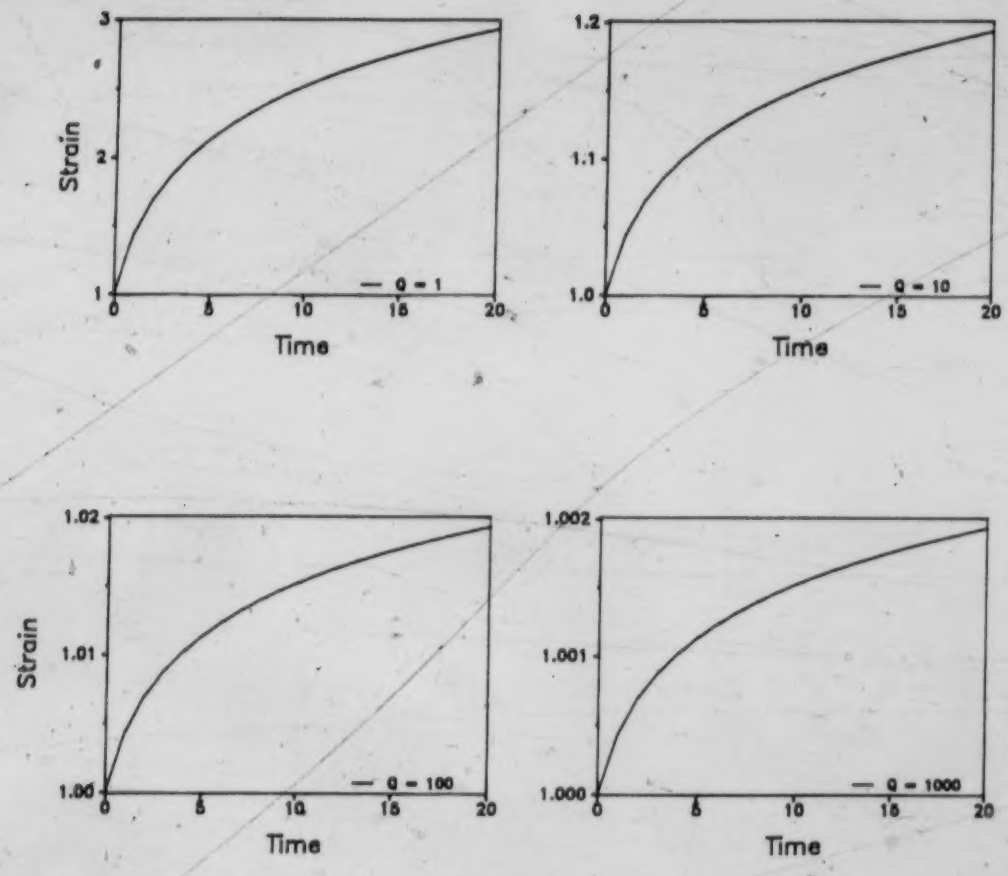

Figure 6.1 The constant Q creep function as given by (6.3.5) in units of $1/M_u$ plotted versus time in units of $1/a$.

6.4 Attenuation in the time domain

The problem of introducing attenuation in the time domain for the heterogeneous two dimensional SH problem will be discussed in this section. For a homogeneous layer the effects of absorption can be simulated by passing the loss free theoretical seismogram through a time varying filter. When absorption varies with depth, a simple time varying filter is not sufficient to provide a proper simulation. Trorey (1962) proposed the application of time varying filters for every layer in order to account for absorption without including the dispersive nature of dissipative materials. For a propagating plane wave in a homogeneous medium, the effect of attenuation can be introduced by convolving the wavelet with a dissipation operator (Muller, 1983). Other authors have worked in the time domain by using an asymptotic ray theory (Krebes and Hron, 1980a, b) or an extended Haskell-Thomson matrix method (Silva, 1976). Recently Emmerich and Korn (1987) proposed a method which incorporates attenuation in the time domain based on the rheological model of the generalized Maxwell body.

The most popular method (Kennett, 1979, Aki and Richards, 1980, Kelamis et al, 1983, Bourbie and Gonzalez-Serrano, 1983) which simulates absorption is the one of obtaining a solution in the frequency domain. For a propagating plane wave in a homogeneous medium described by $exp\ i\omega[x/c - t]$, the effect of attenuation can be introduced by multiplying it with a damping function $exp(-\alpha x)$ while the phase velocity is given by the corresponding dispersion relation. By synthesizing several attenuating plane wave components we get the response for homogeneous anelastic media. For a multilayer earth this method becomes too complicated since each homogeneous layer must be treated separately.

The equations of motion for the inhomogeneous anelastic SH problem in two dimensions are

$$\rho(x,z)\ \frac{\partial^2 v(x,z,t)}{\partial t^2} = \frac{\partial\, \sigma_{xy}(x,z,t)}{\partial x} + \frac{\partial\, \sigma_{zy}(x,z,t)}{\partial z} \tag{6.4.1}$$

while the stress-strain relations according to Boltzmann's model are

$$\mu(x,z)\ \varepsilon_{xy}(x,z,t) = \mu(x,z)\partial_x\, v(x,z,t) = \sigma_{xy}(x,z,t) + \int_{-\infty}^{t} \sigma_{xy}(x,z;\tau)\, \dot{\phi}(x,z;t-\tau)\, d\tau \tag{6.4.2}$$

$$\mu(x,z)\ \varepsilon_{zy}(x,z,t) = \mu(x,z)\partial_z\, v(x,z,t) = \sigma_{zy}(x,z,t) + \int_{-\infty}^{t} \sigma_{zy}(x,z;\tau)\, \dot{\phi}(x,z;t-\tau)\, d\tau \tag{6.4.3}$$

where $\rho(x,z)$ is the density, $\mu(x,z)$ is the rigidity, $v(x,z,t)$ is the displacement component and $\phi(t)$ is the creep function.

The first time derivative of the convolutional integrals in (6.4.2) and (6.4.3) is

$$\int_{-\infty}^{t} \sigma(\tau)\, \ddot{\phi}\,(t-\tau)\, d\tau + \sigma(t)\ \dot{\phi}(0) \tag{6.4.4}.$$

Then the stress-strain relations, after taking partial time derivatives of both sides and considering that $\dot{\phi}(0) = 0$, become

$$\mu \frac{\partial^2 v}{\partial t \partial x} = \frac{\partial \sigma_{xy}}{\partial t} + \int_{-\infty}^{t} \sigma_{xy}(\tau) \ddot{\phi}(t-\tau)\, d\tau$$

$$\mu \frac{\partial^2 v}{\partial t \partial z} = \frac{\partial \sigma_{zy}}{\partial t} + \int_{-\infty}^{t} \sigma_{zy}(\tau) \ddot{\phi}(t-\tau)\, d\tau$$

(6.4.5).

Setting

$$\dot{v} = \frac{\partial v}{\partial t}$$

(6.4.6)

in the equations of motion and the stress-strain relation, they can be written in matrix form

$$\partial_t \begin{bmatrix} \dot{v} \\ \sigma_{xy} \\ \sigma_{zy} \end{bmatrix} = \begin{bmatrix} 0 & \rho^{-1} & 0 \\ \mu & 0 & 0 \\ 0 & 0 & 0 \end{bmatrix} \partial_x \begin{bmatrix} \dot{v} \\ \sigma_{xy} \\ \sigma_{zy} \end{bmatrix} + \begin{bmatrix} 0 & 0 & \rho^{-1} \\ 0 & 0 & 0 \\ \mu & 0 & 0 \end{bmatrix} \partial_z \begin{bmatrix} \dot{v} \\ \sigma_{xy} \\ \sigma_{zy} \end{bmatrix} + \begin{bmatrix} 0 \\ \zeta_{xy} \\ \zeta_{zy} \end{bmatrix}$$

or

$$\partial_t \mathbf{U} = \mathbf{A}\, \partial_x \mathbf{U} + \mathbf{B}\, \partial_z \mathbf{U} + \mathbf{Z}$$

(6.4.7)

where

$$\zeta = -\int_{-\infty}^{t} \sigma(\tau) \ddot{\phi}(t-\tau)\, d\tau = -\int_{0}^{\infty} \sigma(t-\tau) \ddot{\phi}(\tau)\, d\tau$$

(6.4.8).

Assuming that ζ does not depend on the current stress ($\ddot{\phi}(0) = 0$), the convolution integral can be considered as an averaging function of the stress history. Since the homogeneous part in equation (6.4.7) (omitting the extra term **Z**) is identical to equation (3.2.4), the system is hyperbolic. Applying dimensional splitting in a similar manner as in section 2.2, a fourth order one dimensional scheme for inhomogeneous hyperbolic systems proposed by Gottlieb and Turkel (1976) (see chapter 2), when applied in the x-direction, results in

$$\dot{v}^{(1)}_{j,m} = \dot{v}^{n}_{j,m} - \frac{p}{6}\,\rho^{-1}_{j,m}\,(7\,(\sigma_{xy})^{n}_{j,m} - 8\,(\sigma_{xy})^{n}_{j+1,m} + (\sigma_{xy})^{n}_{j+2,m})$$

$$\dot{v}^{n+1}_{j,m} = \frac{1}{2}(\dot{v}^{(1)}_{j,m} + \dot{v}^{n}_{j,m}) + \frac{p}{12}\,\rho^{-1}_{j,m}\,(7\,(\sigma_{xy})^{(1)}_{j,m} - 8\,(\sigma_{xy})^{(1)}_{j-1,m} + (\sigma_{xy})^{(1)}_{j-2,m}) \qquad (6.4.9)$$

$$(\sigma_{xy})^{(1)}_{j,m} = (\sigma_{xy})^{n}_{j,m} - \frac{p}{6}\,\mu_{j,m}\,(7\,\dot{v}^{n}_{j,m} - 8\,\dot{v}^{n}_{j+1,m} + \dot{v}^{n}_{j+2,m}) + \kappa\,(\zeta_{xy})_{j,m}$$

$$(\sigma_{xy})^{n+1}_{j,m} = \frac{1}{2}\,((\sigma_{xy})^{(1)}_{j,m} + (\sigma_{xy})^{n}_{j,m}) + \frac{p}{12}\,\mu_{j,m}\,(7\,\dot{v}^{(1)}_{j,m} - 8\,\dot{v}^{(1)}_{j-1,m} + \dot{v}^{(1)}_{j-2,m}) + \frac{\kappa}{2}\,(\zeta_{xy})_{j,m} \qquad (6.4.10)$$

where κ is the time step and

$$\zeta_t = -\sum_{k=1}^{m} \sigma_{t-k}\,\ddot{\phi}_k\,\kappa \qquad (6.4.11).$$

Similar expressions (see Appendix C) exist for the propagation in the z-direction.

6.5 Assumptions

A number of assumptions have been imposed throughout this development:

First the basic formulas that relate phase velocity and Q factor with the creep function apply for plane waves in homogeneous media. The numerical solution of the wave equation from finite differences is more accurate in the near field region. So this assumption is only valid a few wavelengths away from the source.

Second, since the general formulas apply for homogeneous media, the heterogeneity must be relaxed in areas of low Q. So as a first attempt one can introduce attenuation in heterogeneous media by using the results from the theory in homogeneous media. In this way the effect of attenuation is taken only locally.

Finally, we assume in this approach that the convolutional integral which describes the effect of attenuation is independent of the current vector of displacement and stress components.

6.6 Recursive filter design for Lomnitz logarithmic law

This section describes a recursive filter implementation for Lomnitz law. The stress-strain relation given by Boltzmann's equation (1876) accounts for attenuation effects. For a stress excitation, which is a complicated function of time, this can be expressed by a convolution integral. The second time derivative of the creep function involved in (6.4.11) for the Lomnitz logarithmic law is described in discrete form by

$$\ddot{\phi}_k = -\frac{q a^2}{(1 + a k \kappa)^2} \quad , \; k = 0, 1, \ldots \tag{6.6.1}$$

Then, by setting $\zeta_t' = \kappa\,\zeta_t$ and

$$\xi_t = -\sigma_t \ddot{\phi}_0 \kappa^2 + \zeta_t' = -\sum_{k=0}^{\min(K,t)} \sigma_{t-k} \ddot{\phi}_k \kappa^2 = \sum_{k=0}^{\min(K,t)} \sigma_{t-k} \frac{q\,a^2\kappa^2}{(1+a\,k\,\kappa)^2}$$

(6.6.2),

a recursive filter will be designed for $f_k = -\ddot{\phi}_k \kappa^2$. For K very large the standard convolution becomes quite expensive. In order to reduce the computational cost we can make use of a recursive filter (Shanks, 1967, Treitel et al, 1967, Kanasewich, 1981). The decaying function f_k can be approximated by an AR filter. If F(z) is its z-transform

$$F(z) = \sum_{k=0}^{K} \frac{q\,a^2\kappa^2}{(1+a\,k\,\kappa)^2}\, z^{-k}$$

(6.6.3)

we want to find two polynomials A(z), B(z), so that

$$F(z) \approx \frac{A(z)}{B(z)} = \frac{\sum_{n=0}^{N} a_n\, z^{-n}}{1 + \sum_{m=1}^{M} b_m\, z^{-m}}$$

(6.6.4)

where N, M are arbitrary numbers which fix the number of A and B coefficients. Then, the z-transform of equation (6.6.2) can be expressed as

$$\Xi(z) \approx S(z)\,\frac{A(z)}{B(z)}$$

(6.6.5)

$$\text{or} \quad \Xi(z) = -\Xi(z) \sum_{m=1}^{M} b_m z^{-m} + S(z) \sum_{n=0}^{N} a_n z^{-n}$$

(6.6.6).

So the recursive filter in time domain is

$$\xi_t = -\sum_{m=1}^{M} b_m \xi_{t-m} + \sum_{n=0}^{N} a_n \sigma_{t-n}$$

(6.6.7).

A recursive filter which closely approximates the decaying function is computed as follows:

(1) the decaying function is calculated at 400 consecutive finite time steps and serves as the desired output;

(2) the denominator coefficients b_m, m=1, ..., M are determined by solving a linear system whose coefficients are given functions of the desired output;

(3) a standard Wiener problem must be solved for the numerator a_n, n= 0,1, ..., N with input the impulse response of $B^{-1}(z)$ and desired output the one at the first step.

For a (4,4) recursive filter, the coefficients of the impulse response of equation (6.6.7) illustrated in figure (6.2) agree well with the ones calculated exactly. For N=M=3, the recursive filter requires seven multiplications and six additions per output value while the standard convolution filter, over 400 multiplications and additions. Therefore, the recursive filter in this case is approximately sixty times faster than the convolution filter.

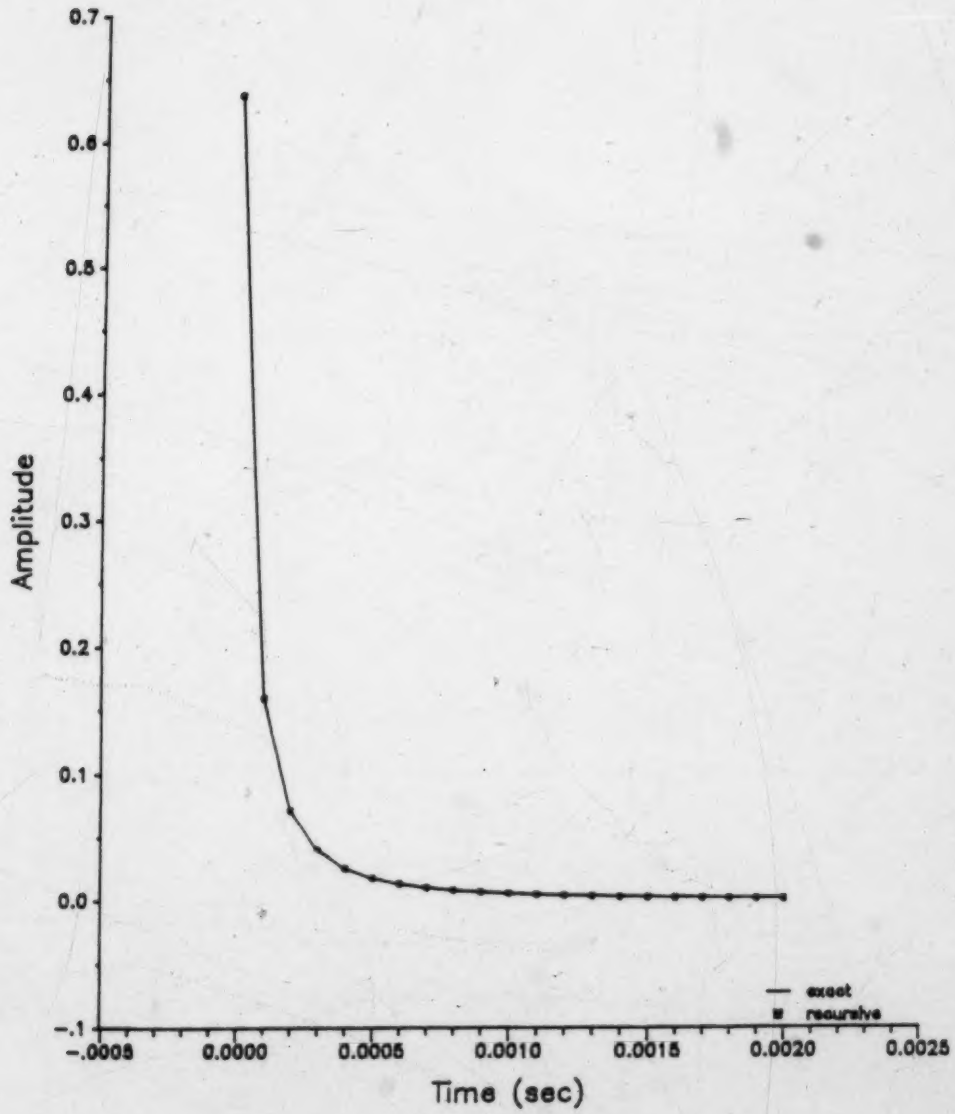

Figure 6.2 Comparison of the exact impulse response of $\ddot{\phi}_t$ and the one given by the recursive relation (the value at zero is missing).

In vector notation σ can be expressed as,

$$\Psi = (\Psi_m^T) \quad m = 1, \ldots , M \tag{6.6.8}$$

with

$$\Psi_m = (\sigma_{jm}) \qquad j = 1, \ldots J$$

the columns of the matrix

$$((\sigma_{jm}) \qquad j = 1, \ldots J \;), m = 1, \ldots M$$

where M,J denote the number of columns and rows respectively and T denotes transpose. Then by rearranging equation (6.6.2), it can be expressed in vector form as

$$Z_t' = X_t \oplus \Psi_t \kappa^2 \dot{\Phi}_0 \tag{6.6.9}$$

while the recursion relation (equation 6.6.7) in matrix form becomes :

$$X_t = - \sum_{m=1}^{M} B_m \otimes X_{t-m} \oplus \sum_{n=0}^{N} A_n \otimes \Psi_{t-n} \tag{6.6.10}.$$

Vectors Φ, **X**, **A**, **B** describe respectively the creep function, the function ξ and the recursion coefficients at all grid points. The lateral and vertical variations of Q are inserted through **A** and **B**.

This realization calculates the effect of attenuation in terms of vector operations. It is economic since the number of vector multiplications is equal to the number of coefficients involved in the recursion. Extra memory is required for the output at previous time steps. Finally, the number of computations per time step can be further reduced by only applying this attenuation correction in regions of low Q. In conclusion the Lomnitz logarithmic law can be implemented in the time domain through a convolutional model. A good

approximation to the standard convolution is given by a recursive representation which is economic since a small number of coefficients is required.

6.7 Dissipation operators in time domain

One way to incorporate attenuation in synthetic seismogram calculation is to convolve them with a dissipation operator (Muller, 1983). Dissipation operators are the wave responses of a plane wave when the input is a delta function

$$\dot{v}(x,t) = \frac{1}{2\pi}\int_{-\infty}^{\infty} \exp\{ -\alpha(\omega)\, x + i\,\omega\,(t - \frac{x}{c(\omega)})\}\, d\omega = \frac{1}{2\pi}\int_{-\infty}^{\infty} D(\omega) \exp\{ i\,\omega\,(t - \frac{x}{c(\omega_r)})\}\, d\omega$$

or

$$\dot{v}(x,t) = d(t) * \delta(t - \frac{x}{c(\omega_r)})$$

(6.7.1)

where ω_r is the reference frequency and δ is the delta function. The Fourier transform of d(t) can be expressed in terms of the *Q* factor and the phase velocity *c(ω)* (Muller, 1983)

$$D(\omega) = \exp\{ i\omega t^* Q(\omega_r)[1 - c(\omega_r)(\frac{1}{c(\omega)} - i\frac{\alpha(\omega)}{\omega})]\}$$

(6.7.2)

where $t^* = x / c(\omega_r)\, Q(\omega_r)$ is the relaxation time. The velocity $c(\omega)$ as well as the attenuation factor $\alpha(\omega)$ depend on the attenuation law. Dissipation operators in the time domain are computed by an inverse Fourier transforming equation (6.7.2).

In Boltzmann's model the dispersion relation for plane wave propagation is given by equation (6.3.2)

$$\frac{\omega}{c(\omega)} + i\,\alpha(\omega) = \frac{\omega}{c_\infty}\left[\,1 + \int_0^\infty \dot{\phi}(t)\,\exp(i\omega t)\,dt\,\right]^{\frac{1}{2}}$$

(6.3.2).

For the Lomnitz logarithmic creep function, equation (6.3.2) becomes (Aki and Richards, 1980)

$$\frac{\omega}{c(\omega)} + i\,\alpha(\omega) \approx \frac{\omega}{c_\infty}\left\{\,1 - \frac{q}{2}\left[\,\gamma + \ln\left(\frac{\omega}{a}\right)\right] + i\,\frac{\pi q}{4}\,\right\}$$

(6.7.3)

for q<<1, and the dissipation operator D(ω) is given by

$$D(\omega) = \exp\left[-\frac{\omega t^*}{2}\right]\ \exp\left[\,i\,\frac{\omega t^*}{\pi}\left(\gamma + \ln\frac{\omega}{a}\right)\right]$$

(6.7.4).

The dissipation operator d(t) is computed numerically using the fast Fourier transform. The function d(t) is kept real by setting the real part of D(ω) symmetric around the Nyquist and the imaginary part antisymmetric. Figure 6.3 displays the impulse response of d(t) at different distances with a =1E4 and Q=30.

In order to verify the validity of the finite difference technique, we consider a plane wave propagating in the x-direction. The elastic response is given by

$$\dot{v}(x,t) = \left(t - \frac{x}{c} - T\right)\exp\left[-b\left(t - \frac{x}{c} - T\right)^2\right]$$

$$\sigma_{xy}(x,t) = -\frac{1}{c}\left(t - \frac{x}{c} - T\right)\exp\left[-b\left(t - \frac{x}{c} - T\right)^2\right]$$

$$\sigma_{zy}(x,y) = 0.0$$

(6.7.4).

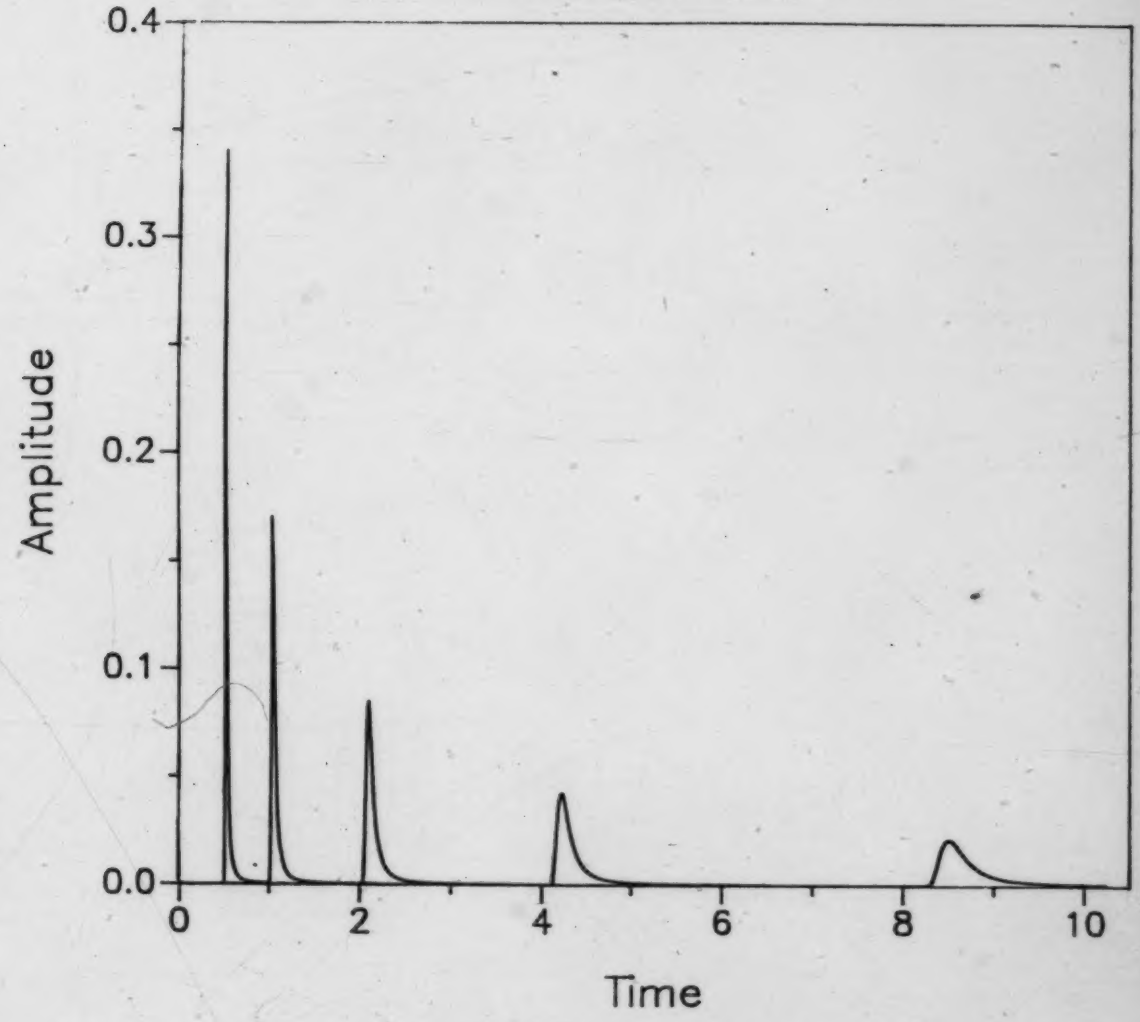

Figure 6.3 Impulse response of the dissipation operator d_t resulting from sources at distances of .5, 1, 2, 4 and 8 times c_0, Q=30.

The anelastic response can be calculated by convolving the dissipation operator d(t) with the particle velocity $\dot{v}$. For the propagation in a homogeneous anelastic medium with a phase velocity of 2400 m/s at the reference frequency and Q factor of 30 or 1000, the responses are shown in figure (6.4a). This is compared to the response (figure 6.4b) calculated from the finite difference technique described in section 6.4. The results from finite differences are calculated with spatial discretization interval of 20 m and time step of 1 ms. The finite difference technique effectively attenuates the amplitudes but does not disperse the wavelet properly.

For plane wave propagation the effect of attenuation can also be introduced by dividing the grid into constant Q regions and by performing subsequent convolution operations with a dissipation operator (given by 6.7.2) whose spatial variable is equal to the width X of the constant Q region. For media with Q factor varying spatially, we can apply the same procedure by considering the Q factor is constant within the base region. Taking X small so that the curvature of the wavefront is negligible the method above can be also applied for non-plane wave propagation. This method is implemented in the finite difference algorithm for the wave propagation as follows: The elastic response from the finite differences is corrected for the local effect of attenuation by convolving it with a dissipation operator and the outcome serves as the anelastic response of the system. By subdividing the grid into constant Q regions, the convolution operators are applied at a distinct number of locations in order to avoid excessive memory requirements but X is kept small enough so that the plane wave assumption is valid. A comparison of the results from the plane wave propagation described above with the ones calculated directly from equation (6.7.2) (figure 6.5) gives excellent agreement between the exact and numerical solutions. This technique is still quite computationally expensive since the convolution operations are time consuming and require excessive memory.

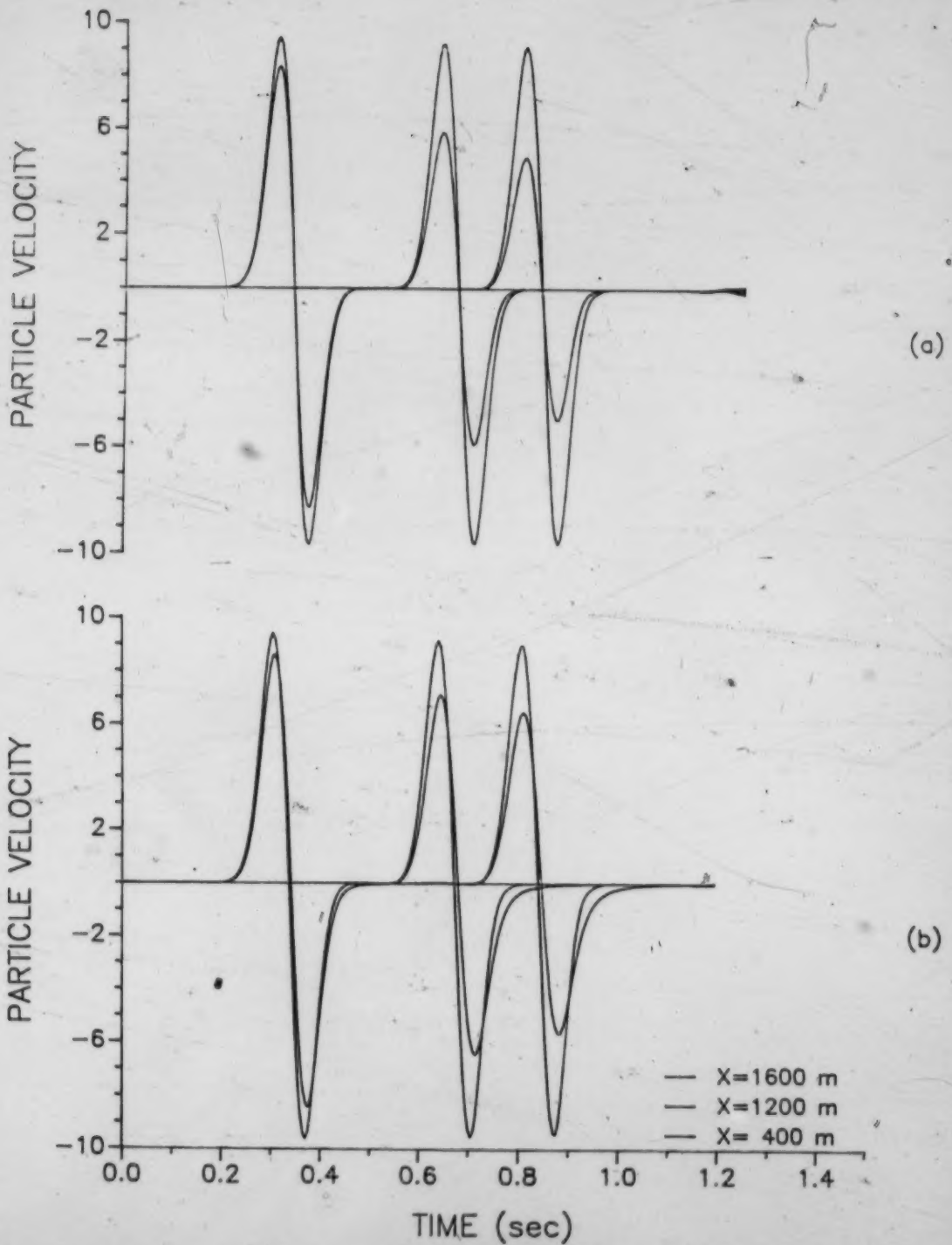

Figure 6.4 Comparison of the plane waveforms with attenuation (Q=30 or 1000) from finite differences (a) and from the convolution of the wavelet with dissipation operators (b).

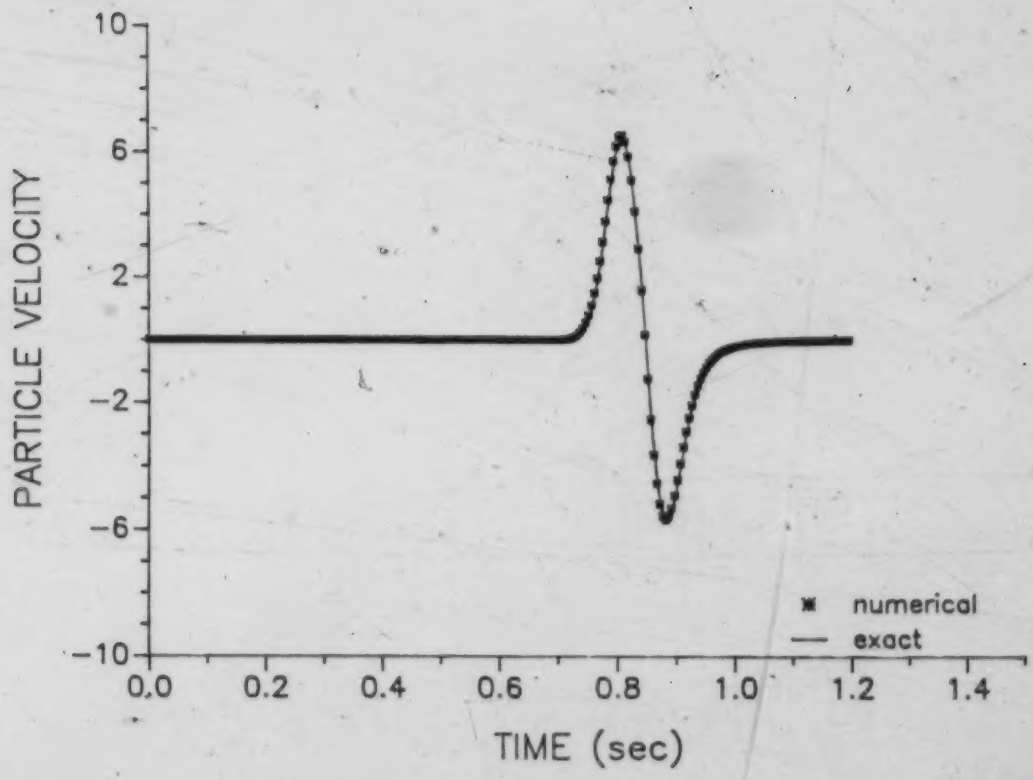

Figure 6.5 Comparison of the plane waveforms with attenuation (Q=30) from finite differences after the elastic response is convolved with dissipation operators at distinct locations (numerical) and from the convolution of the wavelet with a dissipation operator (exact).

CHAPTER 7
CONCLUSION

Seismic wave propagation in laterally varying media or in generally non-homogeneous media can be accurately simulated with high order finite difference techniques. Stability as well as numerical dispersion impose certain limits on the domain of applicability of finite differences. The stability condition, on the one hand, states that the time step must be less than a value which depends on the maximum velocity and the grid spacing. The dispersion criterion, on the other hand, requires a minimum number of grid points per minimum wavelength which depends on the maximum frequency and the minimum velocity. So high resolution simulations require small grid spacings and smaller grid spacing means more grid points for a certain model. Small time steps also make finite differences computationally very expensive on conventional computers.

The new generation of vector and parallel computers can perform faster and have larger memories and word length. In order to take advantage of a vector computer new vectorized algorithms have been developed for a new modified Lax-Wendroff second order scheme and a splitting method based on an one dimensional fourth order scheme of MacCormack type. The vectorization technique employed proved to be efficient and is based on the matrix times vector multiplication by diagonals method. The program vectorization is facilitated by defining an innovative set of *SuperC* operations (Abramovici et al, 1987) for vectors and matrices. Computation times are reduced by several decades. This enabled us to apply finite differences to high resolution experiments. Still, memory limitations (i.e. 2 megawords and 64 K words page size) existing, on supercomputers, does not allow us to

apply the method for very large models.

A new modified Lax-Wendroff scheme has been designed for first order hyperbolic systems in two dimensions whose coefficients are space dependent. This scheme has been compared with a fourth order MacCormack type one dimensional scheme in terms of accuracy, stability, convergence, numerical dispersion and dissipation. The proposed Lax Wendroff scheme performs faster than the MacCormack but the latter provides results with smaller relative error.

Algorithms for SH and elastic wave propagation have been developed for the Lax-Wendroff and MacCormack techniques. They are set up to handle SH and P-SV cases for sources of both compressional and shear energy and for receivers in any geometric configuration. Their numerical solutions have been tested against the exact solutions for simple problems. By numerically solving the equivalent first order systems instead of the second order wave equations the derivatives of the medium's parameters are avoided. Line sources of P, SH and SV waves have been implemented by means of Alterman's and Karal's technique.

A new technique for including attenuation in the time domain based on a superposition model with a logarithmic creep function expressed in terms of a recursive filter is applied at intermediate steps during the finite difference process to account for attenuation. The method effectively preserves the amplitudes but does not introduce dispersion. Dissipation operators based on plane wave attenuation are also incorporated in the finite difference algorithms. At the present time the technique has only been applied to a one dimensional problem.

The supercomputer finite difference algorithms presented in this thesis can be modified to accommodate anisotropy. The splitting technique can be easily extended in three dimensions. In this case the memory limitations will be more pronounced and extra effort must be focussed towards improving memory management. Another alternative is to use

variable grid methods which have not been discussed in this thesis. The memory requirements can be reduced by applying the heterogeneous approach only within an area including the anomalous zone while the homogeneous approach is applied elsewhere.

Two sets of data from seismic experiments conducted by ESSO Resources, Canada for monitoring steam injection projects in the Cold Lake area have been compared with realistic computer simulations using finite differences. Those simulations, apart from reconstructing the full wave field, gave insight into complicated interactions and helped to interprete the real data. The results of the simulations strongly suggest the necessity for two component acquisition as well as the importance of S-waves. These model simulations indicate that seismic experiments, when carefully designed, can play a major role in helping to solve production and recovery problems by determining the spatial distribution of reservoir properties and their changes with time.

BIBLIOGRAPHY

Abramovici, F., Vafidis, A. and E.R. Kanasewich, 1987, Supercomputer programs for solving elastic wave propagation problems in two-dimensions, Proceedings of the Supercomputing Symposium '87, June 15-16, Calgary, Alberta, Canada.

Abramovici, F., Le, L. H. T. and Kanasewich, E. R., 1988, Propagation of an SH-pulse in two homogeneous half spaces in welded-contact, in preparation.

Aki, K., and Richards, P., 1980, Chapter 5, Quantitative seismology theory and methods: v. I., San Fransisco, W. H. Freeman and Co.

Alford, R.M., Kelly, K.R., and Boore, D.M., 1974, Accuracy of finite difference modelling of the acoustic wave equation: Geophysics, **39**, 834-842.

Alterman, Z. and Karal, F.C., 1968, Propagation of elastic waves in layered media by Finite Difference methods: B.S.S.A., **58**, 367-398.

Alterman , Z. and Loewenthal, D., 1972, Computer generated seismograms, Methods in Computational Physics, v.12, Bolt B.A. (ed.); Academic Press, N. Y., p. 35-164.

Azimi, S.A., Kalinin, A.V., Kalinin, V.V., and Pivorarov, B.L., 1968, Impulse and transient characteristics of media with linear and quadratic absorption laws, Izvestia (Earth Physics), p. 42-54.

Bayliss, A., Jordan, K.E., LeMesurier, B.J. and Turkel, E., 1986, A fourth order accurate finite difference scheme for the computation of elastic waves, Bull. Seism. Soc. Am., v.76, p.1115-1132.

Boore, D.M., 1972, Finite-difference methods for seismic wave propagation in heterogeneous materials, Methods in Computational Physics, v.11, Bolt B.A. (ed.); Academic Press, N. Y., p. 1-37.

Bourbie, T., and Gonzalez-Serrano, A., 1983, Synthetic seismograms in attenuating media: Geophysics, v.48, n. 12, p. 1575- 1587.

Clayton, R., and Enquist, B., 1977, Absorbing boundary conditions for acoustic and elastic wave equations, Bull. Seism. Soc. Am., v. 67, pp. 1529-1540.

Clifton, R.J., 1967, A difference method for plane wave problems in elasticity, Quart. Appl. Math., v.25, p. 97-116.

Courant, R., and Hilbert, D., 1962, Methods in Mathematical Physics, Interscience, New York.

Dablain, M. A., 1986, The application of high order differencing to the scalar wave equation: Geophysics, v.51, n. 1, p. 54-66.

Daley, P.F. and Hron, F., 1979, SH waves in layered transversely isotropic media- An asymptotic expansion approach, Bull. Seism. Soc. Am., v. 69, pp. 689-711.

Emmerich, H., and Korn, M., 1987, Incorporation of attenuation into time domain computations of seismic wave fields, Geophysics, v.52, p. 1252- 1264.

Farouq Ali, S.M., 1982, Elements of Heavy Oil Recovery, University of Alberta Press.

Feng, R. and Kanasewich, E.R., 1985, Propagating enclosure method in Finite Element analysis, Acta Geoph. Sinica, v.28, pp. 27-63.

Futterman, W. I., 1962, Dispersive body waves: J. Geophys. Res., v. 67, p. 5279-5291.

Fuchs, K. and Muller, G., 1971, Computation of synthetic seismograms with the reflectivity method and comparison with observations, Geophys. J. R. Astr. Soc., v. 23, p. 417-435.

Gerald, C.F., 1980, Applied numerical analysis, Addison-Wesley Publishing Company Inc.

Gottlieb, D. and Turkel, E., 1976, Dissipative two-four methods for time dependent problems: Math. Comp., 30, 703-723.

Grant, F. S. and West, G. F., 1965, Interpretation theory of Applied Geophysics, McGraw-Hill , New York.

Jeffreys, H., 1976; The Earth, Cambridge Press, 6th edition.

Harrison, D.B., Glaister, R.P., and Nelson, H.W., 1981, Reservoir description of the Clearwater oil sand, Cold Lake, Alberta, Canada. In: The future of Heavy Crude and Tar Sands, McGraw-Hill, p. 264-279.

Kanasewich, E.R., 1981, Time sequence analysis in geophysics: The University of Alberta Press, (third edition).

Kansewich, E.R. Cold Lake Seismicity Project : Report No 3, April 1983.

Kansewich, E.R., and Vafidis A., 1987, Simulation of seismic wave propagation in oil sands projects on the supercomputer,Super-C Newsletter, v. 3, n. 4, p. 7-10.

Kelly, K.R., Ward, R.W., Treitel, S., and Alford, R.M., 1976, Synthetic seismograms: A finite difference approach: Geophysics, **41**, 2-27.

Kelamis, P.G., Kanasewich, E.R., and Abramovici, F., 1983, Attenuation of seismograms obtained by Cagniard-Pekeris method: Geophysics, v.48, p. 1204-1211.

Kennett, B. L. N., 1974, Reflections, Rays and Reverberations, Bull. Seism. Soc. Am., v. 64, pp. 1685-1696.

Kennett, B. L. N., 1979, Theoretical reflection seismogram for elastic media: Geoph. Prosp., v. 27, p. 301- 321.

Kittel, C., 1976, Solid State Physics, John Wiley & Sons, Inc., 5th Edition.

Knopoff, L., 1964, Q: Rev. Geophys., v. 2, p. 625- 660.

Krebes, E. S., and Hron, F., 1980a, Ray-synthetic seismograms for SH waves in anelastic media, Bull. Seism. Soc. Am., v. 70, p. 29-46.

Krebes, E. S., and Hron, F., 1980b, Synthetic seismograms for SH waves in a layer anelastic medium by asymptotic ray theory, Bull. Seism. Soc. Am., v. 70, p. 2005-2020.

Lax, P., and B. Wendroff, 1964, Difference schemes for hyperbolic equations with high order accuracy, Comm. in Pure and Applied Math., v. 17, p. 381-398.

Lomnitz, C., 1956, Creep measurements in igneous rocks: J. Geol., v. 64, p. 473-479.

Lomnitz, C., 1957, Linear dissipation in solids: J. Appl. Phys., v. 28, p. 201-205.

Liu, H. P., Anderson, D. L., and Kanamori, H., 1976, Velocity dispersion due to anelasticity; implications for seismology and mantle composition: Geophys. J. R. Astr. Soc., v. 47, p. 41-58.

MacCormack, Z. W., 1971, Numerical solution of the interaction of a shock wave with a laminar boundary layer, Proceedings of the second international Conference on Numerical Methods in Fluid Dynamics, (ed. M. Holt) Lecture notes in Physics, v. 8, Springer-Verlag.

Macrides, C., 1987, Seismic tomography in oil sands for monitoring thermal recovery: Ph. D. Dissertation, University of Alberta.

Macrides, C., Kanasewich, E.R., and Baratha, S., 1987, Cross-borehole seismic imaging in steam injection projects, in preparation.

Madsen, N.K., Rodrigue, G.H., and Karush, J.I., 1976, Matrix multiplication by diagonals on a vector/parallel processor, Inform. Proc. Lett., 5, 41-45.

Mason, W.R., 1969, Internal friction mechanism that produces an attenuation in the Earth's crust proportional to frequency: J. Geophys. Res., v. 74, p. 4963-4966.

Mitchell, A.R., 1969, Computational methods in Partial Differential equations, Wiley, N.Y.

Mitchell, A.R., and Griffiths, D.F., 1981, The finite difference method in partial differential equations,Wiley, N.Y.

Muller, G., 1983, Rheological properties and velocity dispersion of a medium with power-law dependence of Q on frequency, J.Geoph., v. 54, 20-29.

Nur, A., Walls, J.D., Winkler, K., and De Vilbiss, J., 1980, Effects of fluid saturation on waves in porous rock and relations to hydraulic permeability: SPEJ, v.

24,p. 450- 458.

Nyland, E., 1985, Seismic attenuation in oil sand, AOSTRA Journal of Research, v.2, p.47-51.

Santosa, F., and Pao, Y.H., 1986, Accuracy of a Lax-Wendroff scheme for the acoustic wave equation, J. Acoust. Soc. Am., v. 80, n. 5, p. 1429-1437.

Savage, J.C. and O'Neill, M.E., 1975, The relation between the Lomnitz and Futterman theories of internal friction, J. of Geoph. Res., v. 80, n.2, p. 249- 251.

Shanks, J.L., 1967, Recursion filters for digital processing: Geophysics, v. 32, n. 1, p. 33- 51.

Silva, W., 1976, Body waves in a layered anelastic solid: SSA Bull., v. 66, p. 1539-1554.

Singh, R.P., and Nyland, E., 1988, Ray bending in tomography of strong anomalies, Geophysics, preprint.

Smith, W.D., 1974, A nonreflecting plane boundary for wave propagation problems, J. Comp. Phys., v.15, 492-508.

Stephen, R., 1983, A comparison of finite difference and reflectivity seismograms for marine models, Geophys. J. R. Astr. Soc., v. 72, p. 39-58.

Strang, G., 1968, On the construction and comparison of difference schemes: SIAM J. Num. Anal., 5, 506-517.

Tarantola, A., 1984, Linearized inversion of seismic reflection data, Geoph. Prosp., v.32, p.998-1015.

Tosaya, C.A., Nur, A.M., and Da Prat, G., 1984, Monitoring of Thermal EOR Fronts by seismic methods: SPE 12744, 179-186.

Treitel, S., Shanks, J.L., and Frasier, C.W., 1967, Some aspects of fan filtering, Geophysics, v. 32, n. 5, p. 789-800.

Trorey, A. W., 1962, Theoretical seismograms with frequency and depth dependent

absorption: Geophysics, v.27, n. 6, p. 766-785.

Turkel, E., 1974, Phase error and stability of second order methods for hyperbolic problems, J. Comp. Phys., v.15, 226-250.

Turkel, E., 1980, On the practical use of high order methods for hyperbolic systems, J. Comp. Phys., v. 35, p. 319-340.

Vafidis A., Abramovici F, and E.R. Kanasewich, 1987 , Supercomputer finite difference algorithms for use in seismic tomography as applied to oil sands projects, Extended Abstracts, SEG Fifty-Seventh Annual International Meeting and Exposition 1987 National Convention, October 11-15, 1987, New Orleans, Louisiana.

Virieux, J., 1984, SH-wave propagation in heterogeneous media: Velocity-stress finite-difference method: Geophysics, **49**, 1933-1957.

Virieux, J., 1986, PSV-wave propagation in heterogeneous media: Velocity-stress finite-difference method: Geophysics, **51**, 889-901.

Appendix A

A.1 Derivation of formula (2.2.10)

Gottlieb and Turkel (1976) proposed two-step schemes similar to the original MacCormack scheme for a non-linear system in one dimension

$$\partial_t w + \partial_x f = 0 \tag{A-1}$$

where $f=f(w)$ is a non linear function of the vector w. In one of those schemes we compute a 'predictor' equation

$$w_j^{(1)} = w_j^n + a\,p\,\Delta_x f_j^n + b\,p\,\Delta_x(\Delta_x f_j^n) \tag{A-2}$$

which evaluates the vector $w^{(1)}$ at an indermediate time step using forward difference operators. Then we compute the 'corrector' equation,

$$w_j^{n+1} = \frac{1}{2}(w_j^n + w_j^{(1)}) + c\,\frac{p}{2}\,\nabla_x f_j^{(1)} + d\,\frac{p}{2}\,\nabla_x(\nabla_x f_j^{(1)}) \tag{A-3}$$

which evaluates the vector w^{n+1} at the next time step using backward difference operators with the operators defined by $\Delta_x f_j = f_{j+1} - f_j$, $\nabla_x f_j = f_j - f_{j-1}$ and p being the mesh ratio. For $a = b = -1$ and $c = -d = 1/6$ it can be proven (see section A.2) that the local error is second order both in time and space. Then, the predictor can be written as

$$w_j^{(1)} = w_j^n + \frac{p}{6}(7f_j^n - 8f_{j+1}^n + f_{j+2}^n) \qquad n = 0, 2, 4, \ldots \tag{A-4}$$

and the corrector, as

$$w_j^{n+1} = \frac{1}{2}(w_j^{(1)} + w_j^n) - \frac{p}{12}(7f_j^{(1)} - 8f_{j-1}^{(1)} + f_{j-2}^{(1)}) \qquad n = 0, 2, 4, \ldots \tag{A-5}.$$

In order to achieve fourth order accuracy in space an alternate scheme can be similarly derived with the differences in reverse order

$$w_j^{(1)} = w_j^n - \frac{p}{6}\left(7f_j^n - 8f_{j-1}^n + f_{j-2}^n\right) \qquad n = 1, 3, 5, \ldots$$

(A-6)

$$w_j^{n+1} = \frac{1}{2}\left(w_j^{(1)} + w_j^n\right) + \frac{p}{12}\left(7f_j^{(1)} - 8f_{j+1}^{(1)} + f_{j+2}^{(1)}\right) \qquad n = 1, 3, 5, \ldots$$

(A-7).

Later (eq. 2.18) these are combined to obtain a final solution (A-4, A-5) and (A-6, A-7). By applying dimensional splitting (Strang, 1968) in the SH-wave equation (3.2.4), the x-direction propagation is described by

$$\partial_t \mathbf{U} = \mathbf{A}\, \partial_x \mathbf{U}$$

(A-8)

where $\mathbf{A} = \begin{bmatrix} 0 & \rho^{-1} & 0 \\ \mu & 0 & 0 \\ 0 & 0 & 0 \end{bmatrix}$ and $\mathbf{U} = \begin{bmatrix} \dot{v} \\ \sigma_{xy} \\ \sigma_{zy} \end{bmatrix}$.

Let

$$\mathbf{E}_0\, \partial_t \mathbf{U} = \mathbf{A}_0\, \partial_x \mathbf{U}$$

(A-9)

where $\mathbf{E}_0$ is a time independent real symmetric matrix (3.2.5) and $\mathbf{A}_0$ is a constant matrix described by

$$\mathbf{E}_0 = \begin{bmatrix} \rho & 0 & 0 \\ 0 & \mu^{-1} & 0 \\ 0 & 0 & \mu^{-1} \end{bmatrix} \qquad \mathbf{A}_0 = \begin{bmatrix} 0 & 1 & 0 \\ 1 & 0 & 0 \\ 0 & 0 & 0 \end{bmatrix}.$$

Equations (A-1) and (A-9) are equivalent after substituting

$$E_0 U = w \quad \text{and} \quad -A_0 U = f$$

(A-10).

The equation A-9 (see 3.2.5) is then in a divergence free form. Applying these substitutions to equations (A-4) and (A-5), one can get

$$E_0\, U^{(1)}_{j,m} = E_0\, U^n_{j,m} - \frac{p}{6} A_0 \left(7U^n_{j,m} - 8U^n_{j+1,m} + U^n_{j+2,m} \right)$$

$$E_0\, U^n_{j,m} = \frac{1}{2} E_0 \left(U^n_{j,m} + U^{(1)}_{j,m} \right) + \frac{p}{12} A_0 \left(7U^{(1)}_{j,m} - 8U^{(1)}_{j-1,m} + U^{(1)}_{j-2,m} \right)$$

(A-11).

It is known that

$$A = E_0^{-1} A_0$$

(A-12)

so multiplying both sides of equation (A-11) by E_0^{-1} results in

$$U^{(1)}_{j,m} = U^n_{j,m} - \frac{p}{6} A_{j,m} (7U^n_{j,m} - 8U^n_{j+1,m} + U^n_{j+2,m})$$

$$U^{n+1}_{j,m} = \frac{1}{2} (U^{(1)}_{j,m} + U^n_{j,m}) + \frac{p}{12} A_{j,m} (7U^{(1)}_{j,m} - 8U^{(1)}_{j-1,m} + U^{(1)}_{j-2,m})$$

(A-13).

Similar expressions can be derived for equations (A-6) and (A-7).

From (3.24) the system that describes propagation in the z-direction is

$$\partial_t U = B\, \partial_z U$$

(A-14).

The corresponding difference equations become

$$U^{(1)}_{j,m} = U^n_{j,m} - \frac{p}{6} B_{j,m} (7U^n_{j,m} - 8U^n_{j,m+1} + U^n_{j,m+2})$$

$$U_{j,m}^{n+1} = \frac{1}{2}(U_{j,m}^{(1)} + U_{j,m}^{n}) + \frac{p}{12} B_{j,m} (7U_{j,m}^{(1)} - 8U_{j,m-1}^{(1)} + U_{j,m-2}^{(1)})$$

(A-15).

A.2 Derivation of formula (2.3.6)

In order to calculate the truncation error, the difference operators in (A-2) are expanded in Taylor series :

$$\Delta_x f_j = f_{j+1} - f_j = h f_x + \frac{h^2}{2} f_{xx} + \frac{h^3}{6} f_{xxx} + \frac{h^4}{24} f_{xxxx} + O(h^5)$$

(A-16)

and

$$\Delta_x (\Delta_x f_j) = h^2 f_{xx} + h^3 f_{xxx} + \frac{7}{12} h^4 f_{xxxx} + O(h^5)$$

(A-17)

where h is the grid size and the subscripts on the right hand sides denote partial derivatives with respect to space, the order of differentiation being equal to the number of repetitions of the subscript x. To simplify the notation the time index n is omitted in f. Also, in those cases where any of the space indices are missing, U or f is defined at location j,m. Equation (A-2) can be written as

$$E_0^j U_j^{(1)} = E_0^j U_j^n - \kappa f_x - \kappa \frac{h}{3} f_{xx} + \kappa \frac{h^3}{18} f_{xxxx} + O(h^5)$$

(A-18)

$f^{(1)}$ can also be expanded in Taylor series around $U^{(1)}$

$$f^{(1)} = f(U^{(1)}) = f + f_U (U^{(1)} - U) + \frac{1}{2} f_{UU} (U^{(1)} - U)^2 + O((U^{(1)} - U)^3)$$

(A-19)

but from (A-10), $f_{UU} = f_{UUU} = 0$. Therefore, equation (A-19) after (A-18) becomes

$$f^{(1)} = f - \frac{A_0}{E_0}\left(- \kappa f_x - \kappa \frac{h}{3} f_{xx} + \kappa \frac{h^3}{18} f_{xxxx} + O(h^5)\right)$$

(A-20).

Expanding similarly, the difference operators in equation (A-3) are given by

$$\nabla_x f_j = f_j - f_{j-1} = h f_x - \frac{h^2}{2} f_{xx} + \frac{h^3}{6} f_{xxx} - \frac{h^4}{24} f_{xxxx} + O(h^5)$$

(A-21)

and

$$\nabla_x (\nabla_x f_j) = h^2 f_{xx} - h^3 f_{xxx} + \frac{7}{12} h^4 f_{xxxx} + O(h^5)$$

(A-22).

Then equation (A-3) can be written as

$$E_0^j U_j^{n+1} = \frac{1}{2} E_0^j (U_j^n + U_j^{(1)}) - \frac{1}{2} \kappa f_x^{(1)} + \kappa \frac{h}{6} f_{xx}^{(1)} - \kappa \frac{h^3}{36} f_{xxxx}^{(1)} + O(h^5)$$

(A-23).

By substituting $f^{(1)}$ from (A-20) and $U^{(1)}$ from (A-18) and using (A-10), equation (A-21) can be written as

$$E_0^j U_j^{n+1} = E_0^j U_j^n - \kappa f_x - \frac{1}{2}\kappa^2 [A f_{xx} + A_x f_x] + \kappa^2 \frac{h}{6} [A_{xx} f_x + A_x f_{xx}] + O(h^2\kappa^2) + O(h^5)$$

(A-24).

Multiplying both sides of the Taylor expansion of U at time n+1

$$U_j^{n+1} = U_j^n + \kappa (U_j^n)_t + \frac{1}{2}\kappa^2 (U_j^n)_{tt} + O(\kappa^3)$$

(A-25)

with E_0 and comparing the result with equation (A-24) by taking into account

$$E_0 U_t = - f_x, \quad E_0 U_{tt} = (- f_x)_t = - (f_t)_x = - [(-A_0 U)_t]_x = (- \frac{A_0}{E_0} f_x)_x = - (A f_x)_x$$

(A-26)

and

$$(A_x f_x)_x = A_{xx} f_x + A_x f_{xx}$$

(A-27)

the error of the numerical scheme described by (A-4) and (A-5) is given by

$$E = \kappa [- \frac{1}{6} A_0 \ (A_x U_x)_x \kappa h + O(h^4) + O(\kappa h^2) + O(\kappa^2) \ ]$$

(A-28).

Similarly for equations (A-6) and (A-7) the error is given by

$$E = \kappa [+ \frac{1}{6} A_0 \ (A_x U_x)_x \kappa h + O(h^4) + O(\kappa h^2) + O(\kappa^2) \ ]$$

(A-29).

A.3 Derivation of formula (2.3.17)

The amplification matrix for the Lax-Wendroff scheme with constant **A**, **B** is given by equation

$$G = I - p^2[A^2(1-\cos\xi)+B^2(1-\cos\eta)+\frac{1}{2}(AB+BA)\sin\xi\sin\eta]+ip[A\sin\xi+B\sin\eta]$$

(A-30)

or in terms of sines only

$$G = I - p^2[2A^2\sin^2(\frac{\xi}{2})+2B^2\sin^2(\frac{\eta}{2})+\frac{1}{2}(AB+BA)\sin\xi\sin\eta]+ip[A\sin\xi+B\sin\eta]$$

(A-31)

Expanding the sine functions in Taylor series up to 3rd order in ξ, η, (A-31) becomes

$$G \approx I - p^2[2A^2(\frac{\xi}{2})^2+2B^2(\frac{\eta}{2})^2+\frac{1}{2}(AB+BA)\xi\eta]+ip(A\xi+B\eta)-i\frac{p^3}{6}(A\xi^3+B\eta^3)$$

(A-32)

and for **A**, **B** commuting the amplification matrix becomes

$$G = I - \frac{p^2}{2}(A\xi+B\eta)^2 + ip(A\xi+B\eta) - i\frac{p^3}{6}(A\xi^3+B\eta^3)$$

(A-33).

The numerical phase, given by equation (2.3.14), becomes

$$\tan P(\xi,\eta) = \frac{p(A\xi+B\eta) - \frac{p^3}{6}(A\xi^3+B\eta^3)}{I - \frac{p^2}{2}(A\xi+B\eta)^2}$$

(A-34).

Expanding the denominator in a Neumann series

$$\tan P(\xi,\eta) = p(A\xi+B\eta) - \frac{p^3}{6}(A\xi^3+B\eta^3) + \frac{p^3}{2}(A\xi+B\eta)^3$$

(A-35)

and the arctangent function in a Taylor series, the phase error becomes

$$P_e(\xi,\eta) = p(A\xi+B\eta) - \frac{p^3}{6}(A\xi^3+B\eta^3) + \frac{p^3}{2}(A\xi+B\eta)^3 \quad \frac{p^3}{3}(A\xi+B\eta)^3 - p(A\xi+B\eta)$$

(A-36)

or

$$P_e(\xi,\eta) = -\frac{1}{6}[pA\xi^3+pB\eta^3-(pA\xi+pB\eta)^3] + O(\xi^4+\eta^4)$$

(2.3.17).

Appendix B

B.1 A note on supercomputers

Supercomputers are fast (of the order of tens of MFLOPs), large-scale numerical processing machines consisting of one or more cpu's with separate scalar and vector processors and a central memory of at least two million 64-bit words. The understanding of how a supercomputer differs from a conventional computer is essential in order to exploiti the benefits of such a machine. A vector computer gives the opportunity for advances in applications previously too large and too expensive to try on conventional computers.

Vector computers are vector architecture computers while the conventional computers are scalar architecture computers. A scalar architecture has instructions for moving a single datum (a scalar) between the processor and the memory. By contrast, a vector architecture has instructions for moving a selected set of data (a vector) between the processor and the memory. For example, the addition of two arrays described by the code

```
      DO  10  I=1,N
10    X(I) = Y(I) + Z(I)
```

in a scalar processor consists of two loads, an add, a store and an increment instruction per element. So assuming that every instruction above is completed in one cycle the scalar addition (called ADD) requires at least five cycles. The total time consumed by a scalar computer would be N times that required for one element.

In a one-pipe vector computer a vector addition consists of a couple of vector loads, a vector add and a vector store. A vector processor can accomplish two loads, an add,a store and an increment instruction for a vector element (the equivalent of an ADD) in one cycle. Thus this computer is five times faster than the scalar one in this case. The speed of the machine is doubled if there are two vector pipes.

In order to achieve high performance levels a supercomputer must have a large

memory with fast access. The performance of an application depends on the level of vectorization. If an application cannot be vectorized, a vector computer performs as a scalar one. There are two important conditions in order to achieve high levels of performance: the application must allow the corresponding computations to be vectorized and must be coded so that the compiler can recognize and compile vector operations.

Vectorization is a concept which has to be taken into account not only when programming but also when designing the algorithms. Vectorization is not achieved as an afterthought, and vectorizing compilers cannot necessarily overcome a poor algorithm.

FORTRAN 200 is a FORTRAN 77 compiler with extensions to allow for vectorization of appropriate DO loops. The compiler attempts to vectorize all DO loops (automatic vectorization) but only a very limited number are usually vectorizable. Loops with recursive logic or loops which contain IF and/or I/O statements are examples of non-vectorizable ones.

B.2 On vectorization of a program

When writing a program there are three wide options in order to take advantage of vector speeds. The easiest option is to compile the program with the vector optimization parameter on. In this option the constraints placed on DO-loops in order for them to vectorize are stringent. Semantic vectorization requires a fundamental structuring of the algorithms in order to suit the architecture of the computer. Finally syntactic vectorization employs the vector programming features of the FORTRAN 200 language such as vector syntax and vector intrinsic functions.

In order to optimize the program we can use either or all of the three options. Since most of the execution time is usually consumed in a small portion of the code the first optimization efforts must be concentrated on that part.

One of the constructs available in vector syntax notation is the semicolon notation for

describing a vector. Vectors reside in contiguous memory locations and they exhibit a one-dimensional nature. Parts of FORTRAN arrays may or may not reside in contiguous locations. For example, since two-dimensional arrays are stored by columns, the elements of a row of such an array do not reside in contiguous locations. However a particular column of the array is stored in contiguous locations. A(I;N), an example of the semicolon notation for a one-dimensional array represents a vector of N contiguous elements beginning at A(I).

The FORTRAN 200 compiler provides a set of intrinsic functions called vector intrinsic functions that can perform vector manipulations. A list of the vector intrinsic functions is given in chapter 10 of the FORTRAN 200 reference manual. Apart from the ones that are the vector equivalents of the scalar intrinsic functions, there are some that perform more complicated manipulations between vectors.

A special operation called a *linked triad* involves exactly three operands: two vectors and one scalar. The three operands are linked by exactly one ADD and one MULTIPLY. Since each vector pipeline consists of an adder and a multiplier, the linked triad is able to perform the ADD and the MULTIPLY simultaneously in one cycle.

B.3 Vectorizing the finite differences wave propagation code

Following semantic vectorization, most of our effort was spent in restructuring the finite difference algorithm. Expressing the finite difference equations in matrix formulation (see chapter 3), the algorithm turns out to be fully vectorized when the matrix by vector multiplication operation is performed by diagonals (see chapter 2).

Then the syntactic vectorization is used in order to take into advantage the vector syntax as well as the fast vector manipulation ability of the compiler through its built-in vector functions. Here we describe parts of the code where syntactic vectorization has been applied.

Looking at equation (3.3.2) the particle velocity at the next time step is calculated after performing three matrix by vector multiplications and two vector additions. Since the matrices do not depend on time and are sparse banded, their diagonals are constructed and stored in vectors. For instance, in order to construct the diagonals of A described by equations (3.3.4), (3.3.5), (3.3.6), (3.3.9) and (3.3.10), we used three vector intrinsic functions. The first, called Q8VADJM returns the averages of adjacent elements of the rigidity vector. The second, called Q8VGATHR creates intermediate vectors consisting of a gather of selected elements which will later be used for the main diagonal. This vector intrinsic function corresponds to an array that appears on the right hand of an assignment statement whose indices are arrays themselves. If the same array occurs on the left side of an assignment statement then Q8VSCATR performs vectorized scattering. Finally, the third, called Q8VCTRL replaces selected elements of the output argument with the corresponding elements of the input argument. Similarly all the diagonals of the matrices are constructed and stored in vectors.

Matrix by vector multiplication by diagonals involves a number of vector by diagonal multiplications and vector additions. In performing these operations two points are worth noting, the first being the effort in expressing all operations in terms of linked triads. The second point is the extensive use of the block WHERE statement especially for the operation that involved the matrices described in equations (3.3.9) to (3.3.12). The vector form of the block WHERE statement uses a bit vector to control whether the values are stored into a vector or not.

Appendix C

C.1 MacCormack type of scheme for the SH wave equation

The MacCormack type of scheme in the x-direction given by equation (2.2.10) when applied to the SH wave equation (3.2.4) results in

$$\dot{v}^{(1)}_{j,m} = \dot{v}^{n}_{j,m} - \frac{p}{6}\,\rho^{-1}_{j,m}\,(7\,(\sigma_{xy})^{n}_{j,m} - 8\,(\sigma_{xy})^{n}_{j+1,m} + (\sigma_{xy})^{n}_{j+2,m})$$

$$\dot{v}^{n+1}_{j,m} = \frac{1}{2}(\dot{v}^{(1)}_{j,m} + \dot{v}^{n}_{j,m}) + \frac{p}{12}\,\rho^{-1}_{j,m}\,(7\,(\sigma_{xy})^{(1)}_{j,m} - 8\,(\sigma_{xy})^{(1)}_{j-1,m} + (\sigma_{xy})^{(1)}_{j-2,m})$$

$$(\sigma_{xy})^{(1)}_{j,m} = (\sigma_{xy})^{n}_{j,m} - \frac{p}{6}\,\mu_{j,m}\,(7\,\dot{v}^{n}_{j,m} - 8\,\dot{v}^{n}_{j+1,m} + \dot{v}^{n}_{j+2,m})$$

$$(\sigma_{xy})^{n+1}_{j,m} = \frac{1}{2}\,((\sigma_{xy})^{(1)}_{j,m} + (\sigma_{xy})^{n}_{j,m}) + \frac{p}{12}\,\mu_{j,m}\,(7\,\dot{v}^{(1)}_{j,m} - 8\,\dot{v}^{(1)}_{j-1,m} + \dot{v}^{(1)}_{j-2,m})$$

Those difference equations are employed in alternate time steps with the following ones (resulting from equation 2.2.10)

$$\dot{v}^{(1)}_{j,m} = \dot{v}^{n}_{j,m} + \frac{p}{6}\,\rho^{-1}_{j,m}\,(7\,(\sigma_{xy})^{n}_{j,m} - 8\,(\sigma_{xy})^{n}_{j-1,m} + (\sigma_{xy})^{n}_{j-2,m})$$

$$\dot{v}^{n+1}_{j,m} = \frac{1}{2}(\dot{v}^{(1)}_{j,m} + \dot{v}^{n}_{j,m}) - \frac{p}{12}\,\rho^{-1}_{j,m}\,(7\,(\sigma_{xy})^{(1)}_{j,m} - 8\,(\sigma_{xy})^{(1)}_{j+1,m} + (\sigma_{xy})^{(1)}_{j+2,m})$$

$$(\sigma_{xy})^{(1)}_{j,m} = (\sigma_{xy})^{n}_{j,m} + \frac{p}{6}\,\mu_{j,m}\,(7\,\dot{v}^{n}_{j,m} - 8\,\dot{v}^{n}_{j-1,m} + \dot{v}^{n}_{j-2,m})$$

$$(\sigma_{xy})^{n+1}_{j,m} = \frac{1}{2}\left((\sigma_{xy})^{(1)}_{j,m} + (\sigma_{xy})^{n}_{j,m}\right) - \frac{p}{12}\mu_{j,m}\left(7\,\dot{v}^{(1)}_{j,m} - 8\,\dot{v}^{(1)}_{j+1,m} + \dot{v}^{(1)}_{j+2,m}\right)$$

Similarly in the z-direction (see equation A-15) after substituting **B** from (3.2.4) we get

$$\dot{v}^{(1)}_{j,m} = \dot{v}^{n}_{j,m} - \frac{p}{6}\,\rho^{-1}_{j,m}\left(7\,(\sigma_{zy})^{n}_{j,m} - 8\,(\sigma_{zy})^{n}_{j,m+1} + (\sigma_{zy})^{n}_{j,m+2}\right)$$

$$\dot{v}^{n+1}_{j,m} = \frac{1}{2}\left(\dot{v}^{(1)}_{j,m} + \dot{v}^{n}_{j,m}\right) + \frac{p}{12}\,\rho^{-1}_{j,m}\left(7\,(\sigma_{zy})^{(1)}_{j,m} - 8\,(\sigma_{zy})^{(1)}_{j,m-1} + (\sigma_{zy})^{(1)}_{j,m-2}\right)$$

$$(\sigma_{zy})^{(1)}_{j,m} = (\sigma_{zy})^{n}_{j,m} - \frac{p}{6}\,\mu_{j,m}\left(7\,\dot{v}^{n}_{j,m} - 8\,\dot{v}^{n}_{j,m+1} + \dot{v}^{n}_{j,m+2}\right)$$

$$(\sigma_{zy})^{n+1}_{j,m} = \frac{1}{2}\left((\sigma_{zy})^{(1)}_{j,m} + (\sigma_{zy})^{n}_{j,m}\right) + \frac{p}{12}\mu_{j,m}\left(7\,\dot{v}^{(1)}_{j,m} - 8\,\dot{v}^{(1)}_{j,m-1} + \dot{v}^{(1)}_{j,m-2}\right)$$

which are employed in alternate steps with,

$$\dot{v}^{(1)}_{j,m} = \dot{v}^{n}_{j,m} + \frac{p}{6}\,\rho^{-1}_{j,m}\left(7\,(\sigma_{zy})^{n}_{j,m} - 8\,(\sigma_{zy})^{n}_{j,m-1} + (\sigma_{zy})^{n}_{j,m-2}\right)$$

$$\dot{v}^{n+1}_{j,m} = \frac{1}{2}\left(\dot{v}^{(1)}_{j,m} + \dot{v}^{n}_{j,m}\right) - \frac{p}{12}\,\rho^{-1}_{j,m}\left(7\,(\sigma_{zy})^{(1)}_{j,m} - 8\,(\sigma_{zy})^{(1)}_{j,m+1} + (\sigma_{zy})^{(1)}_{j,m+2}\right)$$

$$(\sigma_{zy})^{(1)}_{j,m} = (\sigma_{zy})^{n}_{j,m} + \frac{p}{6}\,\mu_{j,m}\left(7\,\dot{v}^{n}_{j,m} - 8\,\dot{v}^{n}_{j,m-1} + \dot{v}^{n}_{j,m-2}\right)$$

$$(\sigma_{zy})^{n+1}_{j,m} = \frac{1}{2}\left((\sigma_{zy})^{(1)}_{j,m} + (\sigma_{zy})^{n}_{j,m}\right) - \frac{p}{12}\mu_{j,m}\left(7\,\dot{v}^{(1)}_{j,m} - 8\,\dot{v}^{(1)}_{j,m+1} + \dot{v}^{(1)}_{j,m+2}\right)$$

C.2 MacCormack type of scheme for the elastic wave equation

The MacCormack type of schemes in the x-direction given by equations (2.2.10) or (2.2.11) when applied to the elastic wave equation (4.2.5) result in:

a) for n = 2k, k=0, 1, 2, . . .

$$\dot{u}^{(1)}_{j,m} = \dot{u}^{n}_{j,m} - \frac{p}{6}\,\rho^{-1}_{j,m}\,(7\,(\sigma_{xx})^{n}_{j,m} - 8\,(\sigma_{xx})^{n}_{j+1,m} + (\sigma_{xx})^{n}_{j+2,m})$$

$$\dot{u}^{n+1}_{j,m} = \frac{1}{2}(\dot{u}^{(1)}_{j,m} + \dot{u}^{n}_{j,m}) + \frac{p}{12}\,\rho^{-1}_{j,m}\,(7\,(\sigma_{xx})^{(1)}_{j,m} - 8\,(\sigma_{xx})^{(1)}_{j-1,m} + (\sigma_{xx})^{(1)}_{j-2,m})$$

$$\dot{w}^{(1)}_{j,m} = \dot{w}^{n}_{j,m} - \frac{p}{6}\,\rho^{-1}_{j,m}\,(7\,(\sigma_{xz})^{n}_{j,m} - 8\,(\sigma_{xz})^{n}_{j+1,m} + (\sigma_{xz})^{n}_{j+2,m})$$

$$\dot{w}^{n+1}_{j,m} = \frac{1}{2}(\dot{w}^{(1)}_{j,m} + \dot{w}^{n}_{j,m}) + \frac{p}{12}\,\rho^{-1}_{j,m}\,(7\,(\sigma_{xz})^{(1)}_{j,m} - 8\,(\sigma_{xz})^{(1)}_{j-1,m} + (\sigma_{xz})^{(1)}_{j-2,m})$$

$$(\sigma_{xx})^{(1)}_{j,m} = (\sigma_{xx})^{n}_{j,m} - \frac{p}{6}\,(\lambda+2\mu)_{j,m}\,(7\,\dot{u}^{n}_{j,m} - 8\,\dot{u}^{n}_{j+1,m} + \dot{u}^{n}_{j+2,m})$$

$$(\sigma_{xx})^{n+1}_{j,m} = \frac{1}{2}((\sigma_{xx})^{(1)}_{j,m} + (\sigma_{xx})^{n}_{j,m}) + \frac{p}{12}\,(\lambda+2\mu)_{j,m}\,(7\,\dot{u}^{(1)}_{j,m} - 8\,\dot{u}^{(1)}_{j-1,m} + \dot{u}^{(1)}_{j-2,m})$$

$$(\sigma_{zz})^{(1)}_{j,m} = (\sigma_{zz})^{n}_{j,m} - \frac{p}{6}\,\lambda_{j,m}\,(7\,\dot{u}^{n}_{j,m} - 8\,\dot{u}^{n}_{j+1,m} + \dot{u}^{n}_{j+2,m})$$

$$(\sigma_{zz})^{n+1}_{j,m} = \frac{1}{2}((\sigma_{zz})^{(1)}_{j,m} + (\sigma_{zz})^{n}_{j,m}) + \frac{p}{12}\,\lambda_{j,m}\,(7\,\dot{u}^{(1)}_{j,m} - 8\,\dot{u}^{(1)}_{j-1,m} + \dot{u}^{(1)}_{j-2,m})$$

$$(\sigma_{xz})^{(1)}_{j,m} = (\sigma_{xz})^{n}_{j,m} - \frac{p}{6}\,\mu_{j,m}\,(7\,\dot{w}^{n}_{j,m} - 8\,\dot{w}^{n}_{j+1,m} + \dot{w}^{n}_{j+2,m})$$

$$(\sigma_{xz})^{n+1}_{j,m} = \frac{1}{2}\,((\sigma_{xz})^{(1)}_{j,m} + (\sigma_{xz})^{n}_{j,m}) + \frac{p}{12}\,\mu_{j,m}\,(7\,\dot{w}^{(1)}_{j,m} - 8\,\dot{w}^{(1)}_{j-1,m} + \dot{w}^{(1)}_{j-2,m})$$

b) for n = 2k+1, k=0, 1, 2, . . .

$$\dot{u}^{(1)}_{j,m} = \dot{u}^{n}_{j,m} + \frac{p}{6}\,\rho^{-1}_{j,m}\,(7\,(\sigma_{xx})^{n}_{j,m} - 8\,(\sigma_{xx})^{n}_{j-1,m} + (\sigma_{xx})^{n}_{j-2,m})$$

$$\dot{u}^{n+1}_{j,m} = \frac{1}{2}\,(\dot{u}^{(1)}_{j,m} + \dot{u}^{n}_{j,m}) - \frac{p}{12}\,\rho^{-1}_{j,m}\,(7\,(\sigma_{xx})^{(1)}_{j,m} - 8\,(\sigma_{xx})^{(1)}_{j+1,m} + (\sigma_{xx})^{(1)}_{j+2,m})$$

$$\dot{w}^{(1)}_{j,m} = \dot{w}^{n}_{j,m} + \frac{p}{6}\,\rho^{-1}_{j,m}\,(7\,(\sigma_{xz})^{n}_{j,m} - 8\,(\sigma_{xz})^{n}_{j-1,m} + (\sigma_{xz})^{n}_{j-2,m})$$

$$\dot{w}^{n+1}_{j,m} = \frac{1}{2}\,(\dot{w}^{(1)}_{j,m} + \dot{w}^{n}_{j,m}) - \frac{p}{12}\,\rho^{-1}_{j,m}\,(7\,(\sigma_{xz})^{(1)}_{j,m} - 8\,(\sigma_{xz})^{(1)}_{j+1,m} + (\sigma_{xz})^{(1)}_{j+2,m})$$

$$(\sigma_{xx})^{(1)}_{j,m} = (\sigma_{xx})^{n}_{j,m} + \frac{p}{6}\,(\lambda+2\mu)_{j,m}\,(7\,\dot{u}^{n}_{j,m} - 8\,\dot{u}^{n}_{j-1,m} + \dot{u}^{n}_{j-2,m})$$

$$(\sigma_{xx})^{n+1}_{j,m} = \frac{1}{2}\,((\sigma_{xx})^{(1)}_{j,m} + (\sigma_{xx})^{n}_{j,m}) - \frac{p}{12}\,(\lambda+2\mu)_{j,m}\,(7\,\dot{u}^{(1)}_{j,m} - 8\,\dot{u}^{(1)}_{j+1,m} + \dot{u}^{(1)}_{j+2,m})$$

$$(\sigma_{zz})^{(1)}_{j,m} = (\sigma_{zz})^{n}_{j,m} + \frac{p}{6}\,\lambda_{j,m}\,(7\,\dot{u}^{n}_{j,m} - 8\,\dot{u}^{n}_{j-1,m} + \dot{u}^{n}_{j-2,m})$$

$$(\sigma_{zz})^{n+1}_{j,m} = \frac{1}{2}\,((\sigma_{zz})^{(1)}_{j,m} + (\sigma_{zz})^{n}_{j,m}) - \frac{p}{12}\,\lambda_{j,m}\,(7\,\dot{u}^{(1)}_{j,m} - 8\,\dot{u}^{(1)}_{j+1,m} + \dot{u}^{(1)}_{j+2,m})$$

$$(\sigma_{xz})^{(1)}_{j,m} = (\sigma_{xz})^{n}_{j,m} + \frac{p}{6}\,\mu_{j,m}\,(7\,\dot{w}^{n}_{j,m} - 8\,\dot{w}^{n}_{j-1,m} + \dot{w}^{n}_{j-2,m})$$

$$(\sigma_{xz})^{n+1}_{j,m} = \frac{1}{2}\,((\sigma_{xz})^{(1)}_{j,m} + (\sigma_{xz})^{n}_{j,m}) - \frac{p}{12}\,\mu_{j,m}\,(7\,\dot{w}^{(1)}_{j,m} - 8\,\dot{w}^{(1)}_{j+1,m} + \dot{w}^{(1)}_{j+2,m})$$

Similarly in the z-direction we get :

a) for n = 2k, k=0, 1, 2, . . .

$$\dot{u}^{(1)}_{j,m} = \dot{u}^{n}_{j,m} - \frac{p}{6}\,\rho^{-1}_{j,m}\,(7\,(\sigma_{xz})^{n}_{j,m} - 8\,(\sigma_{xz})^{n}_{j,m+1} + (\sigma_{xz})^{n}_{j,m+2})$$

$$\dot{u}^{n+1}_{j,m} = \frac{1}{2}\,(\dot{u}^{(1)}_{j,m} + \dot{u}^{n}_{j,m}) + \frac{p}{12}\,\rho^{-1}_{j,m}\,(7\,(\sigma_{xz})^{(1)}_{j,m} - 8\,(\sigma_{xz})^{(1)}_{j,m-1} + (\sigma_{xz})^{(1)}_{j,m-2})$$

$$\dot{w}^{(1)}_{j,m} = \dot{w}^{n}_{j,m} - \frac{p}{6}\,\rho^{-1}_{j,m}\,(7\,(\sigma_{zz})^{n}_{j,m} - 8\,(\sigma_{zz})^{n}_{j,m+1} + (\sigma_{zz})^{n}_{j,m+2})$$

$$\dot{w}^{n+1}_{j,m} = \frac{1}{2}\,(\dot{w}^{(1)}_{j,m} + \dot{w}^{n}_{j,m}) + \frac{p}{12}\,\rho^{-1}_{j,m}\,(7\,(\sigma_{zz})^{(1)}_{j,m} - 8\,(\sigma_{zz})^{(1)}_{j,m-1} + (\sigma_{zz})^{(1)}_{j,m-2})$$

$$(\sigma_{xx})^{(1)}_{j,m} = (\sigma_{xx})^{n}_{j,m} - \frac{p}{6}\,\lambda_{j,m}\,(7\,\dot{w}^{n}_{j,m} - 8\,\dot{w}^{n}_{j,m+1} + \dot{w}^{n}_{j,m+2})$$

$$(\sigma_{xx})^{n+1}_{j,m} = \frac{1}{2}\,((\sigma_{xx})^{(1)}_{j,m} + (\sigma_{xx})^{n}_{j,m}) + \frac{p}{12}\,\lambda_{j,m}\,(7\,\dot{w}^{(1)}_{j,m} - 8\,\dot{w}^{(1)}_{j,m-1} + \dot{w}^{(1)}_{j,m-2})$$

$$(\sigma_{zz})^{(1)}_{j,m} = (\sigma_{zz})^{n}_{j,m} - \frac{p}{6}\,(\lambda+2\mu)_{j,m}\,(7\,\dot{w}^{n}_{j,m} - 8\,\dot{w}^{n}_{j,m+1} + \dot{w}^{n}_{j,m+2})$$

$$(\sigma_{zz})^{n+1}_{j,m} = \frac{1}{2}\,((\sigma_{zz})^{(1)}_{j,m} + (\sigma_{zz})^{n}_{j,m}) + \frac{p}{12}\,(\lambda+2\mu)_{j,m}\,(7\,\dot{w}^{(1)}_{j,m} - 8\,\dot{w}^{(1)}_{j,m-1} + \dot{w}^{(1)}_{j,m-2})$$

$$(\sigma_{xz})^{(1)}_{j,m} = (\sigma_{xz})^{n}_{j,m} - \frac{p}{6}\,\mu_{j,m}\,(7\,\dot{u}^{n}_{j,m} - 8\,\dot{u}^{n}_{j,m+1} + \dot{u}^{n}_{j,m+2})$$

$$(\sigma_{xz})^{n+1}_{j,m} = \frac{1}{2}\,((\sigma_{xz})^{(1)}_{j,m} + (\sigma_{xz})^{n}_{j,m}) + \frac{p}{12}\,\mu_{j,m}\,(7\,\dot{u}^{(1)}_{j,m} - 8\,\dot{u}^{(1)}_{j,m-1} + \dot{u}^{(1)}_{j,m-2})$$

b) for $n = 2k+1$, $k=0, 1, 2, \ldots$

$$\dot{u}^{(1)}_{j,m} = \dot{u}^{n}_{j,m} + \frac{p}{6}\,\rho^{-1}_{j,m}\,(7\,(\sigma_{xz})^{n}_{j,m} - 8\,(\sigma_{xz})^{n}_{j,m-1} + (\sigma_{xz})^{n}_{j,m-2})$$

$$\dot{u}^{n+1}_{j,m} = \frac{1}{2}\,(\dot{u}^{(1)}_{j,m} + \dot{u}^{n}_{j,m}) - \frac{p}{12}\,\rho^{-1}_{j,m}\,(7\,(\sigma_{xz})^{(1)}_{j,m} - 8\,(\sigma_{xz})^{(1)}_{j,m+1} + (\sigma_{xz})^{(1)}_{j,m+2})$$

$$\dot{w}^{(1)}_{j,m} = \dot{w}^{n}_{j,m} + \frac{p}{6}\,\rho^{-1}_{j,m}\,(7\,(\sigma_{zz})^{n}_{j,m} - 8\,(\sigma_{zz})^{n}_{j,m-1} + (\sigma_{zz})^{n}_{j,m-2})$$

$$\dot{w}^{n+1}_{j,m} = \frac{1}{2}\,(\dot{w}^{(1)}_{j,m} + \dot{w}^{n}_{j,m}) - \frac{p}{12}\,\rho^{-1}_{j,m}\,(7\,(\sigma_{zz})^{(1)}_{j,m} - 8\,(\sigma_{zz})^{(1)}_{j,m+1} + (\sigma_{zz})^{(1)}_{j,m+2})$$

$$(\sigma_{xx})^{(1)}_{j,m} = (\sigma_{xx})^{n}_{j,m} + \frac{p}{6}\,\lambda_{j,m}\,(7\,\dot{w}^{n}_{j,m} - 8\,\dot{w}^{n}_{j,m-1} + \dot{w}^{n}_{j,m-2})$$

$$(\sigma_{xx})^{n+1}_{j,m} = \frac{1}{2}\,((\sigma_{xx})^{(1)}_{j,m} + (\sigma_{xx})^{n}_{j,m}) - \frac{p}{12}\,\lambda_{j,m}\,(7\,\dot{w}^{(1)}_{j,m} - 8\,\dot{w}^{(1)}_{j,m+1} + \dot{w}^{(1)}_{j,m+2})$$

$$(\sigma_{zz})^{(1)}_{j,m} = (\sigma_{zz})^{n}_{j,m} + \frac{p}{6}\,(\lambda+2\mu)_{j,m}\,(7\,\dot{w}^{n}_{j,m} - 8\,\dot{w}^{n}_{j,m-1} + \dot{w}^{n}_{j,m-2})$$

$$(\sigma_{zz})^{n+1}_{j,m} = \frac{1}{2}\,((\sigma_{zz})^{(1)}_{j,m} + (\sigma_{zz})^{n}_{j,m}) - \frac{p}{12}\,(\lambda+2\mu)_{j,m}\,(7\,\dot{w}^{(1)}_{j,m} - 8\,\dot{w}^{(1)}_{j,m+1} + \dot{w}^{(1)}_{j,m+2})$$

$$(\sigma_{xz})^{(1)}_{j,m} = (\sigma_{xz})^{n}_{j,m} + \frac{p}{6}\,\mu_{j,m}\,(7\,\dot{u}^{n}_{j,m} - 8\,\dot{u}^{n}_{j,m-1} + \dot{u}^{n}_{j,m-2})$$

$$(\sigma_{xz})^{n+1}_{j,m} = \frac{1}{2}\,((\sigma_{xz})^{(1)}_{j,m} + (\sigma_{xz})^{n}_{j,m}) - \frac{p}{12}\,\mu_{j,m}\,(7\,\dot{u}^{(1)}_{j,m} - 8\,\dot{u}^{(1)}_{j,m+1} + \dot{u}^{(1)}_{j,m+2})$$